GIMA
Geographical Information Management and Applications

Comparing high quality digital elevation models to estimate ponding in urban systems

MSc Thesis report

Jeroen Muller
jeroenfm@gmail.com

November, 2015

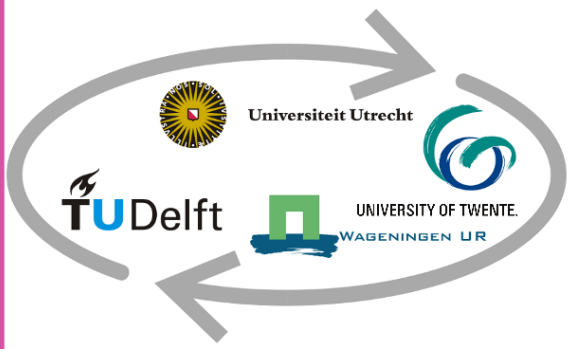

Comparing high quality digital elevation models to estimate ponding in urban systems

MSc Thesis report

Jeroen Muller

Amsterdam, the Netherlands, November 2015

SUPERVISORS:

Dr. D. Karssenberg
Drs. M. J. Zeylmans Van Emmichoven

PROFESSOR:

Prof. Dr. S.M. de Jong

“ …essentially, all models are wrong, but some are useful.”

(George E. P. Box)

ACKNOWLEDGEMENTS

Before you lies my master thesis written for the master Geographical Information Management and Applications (GIMA). The research was conducted at Gemeente Amsterdam Ingenieursbureau (formerly IBA) of the municipality of Amsterdam. At the organization and within the municipality quite some people have helped me with my research. I'd like to thank all of them for all their time, advice, support and the data they gave me without hesitation.

Some people I'd like to mention personally: Michael and Teun from the Ingenieursbureau for all their time, ideas and feedback. You were always supportive of my research and helped me with new insights into the world of photogrammetry and urban water management. Also thank you for making me feel welcome within the Water team. Also I would like to thank Ries Visser from Dienst Basis Informatie who provided me with the aerial photographs and was very supportive in my research.

I would like to thank Derek Karssenberg and Maarten Zeylmans van Emmichoven, my supervisors at Utrecht University, for their constructive feedback, advice, patience and guidance. I'd also like to thank them for always making time when needed and helping me through the sometimes difficult steps of writing a thesis. I also want to the people from Imagem by providing me with access to their software. This made it possible to pursue my interest in the field of digital photogrammetry.

Further, I would like to thank my GIMA buddies Cecile, Nikki, and Nikkie who have always believed in me and supported me in every way needed. Thanks for the chats, dinner, and drinks. It helped to keep up my positivity and succeeding in the research.

Finally, I'd like to thank my family (especially my mother) and my friends who have always believed in me and supported me in every way needed. Without your support I wouldn't be where I am now.

Jeroen Muller

Amsterdam, 2015

SUMMARY

Urbanization and climate change are two (interlinked) problems for the urban (water) system. Urbanization is a major 21st century problem. Cities are becoming bigger changing the (urban) landscape in the process. This can affect the flow of water, as due to urbanization vegetation and other unpaved area is lost. Loss of unpaved area decreases the infiltration capacity. Climate change is the other problem. According to the Royal Netherlands Meteorological Institute (KNMI) the frequency of intense rainfall events will increase in the coming years due to climate change. Meaning that in less time, more precipitation will fall down. More rainfall events and less unpaved areas increases the need for understanding the urban (hydrological) environment.

Hydrological models can be used to simulate the water flow in urban systems. An important input for these models is a digital elevation model (DEM). In the Netherlands the Actueel Hoogtebestand Nederland (AHN2) is an example of a freely available DEM. The AHN2 is derived from Lidar data, which is highly detailed and accurate. Only it is also a costly remote sensing technique and as such the AHN is only updated every 5 years. For the urban landscape this can be problematic, as areas can change a lot in 5 years. This can be seen in the Zuidas area, a business area in the city of Amsterdam, here many projects are simultaneously undertaken which rapidly changes the landscape.

Lidar technology is one technique to acquire elevation data. A different method to obtain elevation values can be found in the photogrammetry sector. The semi-global matching (SGM) method uses overlapping aerial photographs. From these images it is possible to derive a point cloud. A point cloud contains data points with known coordinates including the elevation value. Lidar technology also uses point clouds to store the elevation values. As aerial photographs are annually taken for topographical maps there is no added cost (in the data collection) to obtain the elevation values.

In this study SGM DEMs were tested against the AHN2 DEM. This was done for the Amsterdam area, were water problems exist due to urbanization and an increase of heavy rain events. During a rain event in the summer of 2014 roads and train stations were flooded. Many basements in residences and shops experienced water problems. This raised the need for up-to-date information of height data in the Amsterdam area. The study sites are the Rivierenbuurt and the Zuidas area, which are both in the municipality of Amsterdam. The Rivierenbuurt is a residential area with wide streets and large patches of vegetation. While the Zuidas is a business area and contains water bodies, high rises and mostly paved area. Both of these areas had problems with excessive runoff during the large rain event of July 28th.

The accuracy of the SGM and AHN was tested against land survey measurements. Another question in the research was the usability of the SGM DEMs in a hydrological model that predicts water risk in a small scale (urban) area. The DEMs resolution was tested to understand the influence of grid size on the hydrological model. A second SGM dataset was created by lowering the number of points per square meter of the original SGM point cloud, so called thinning. This was done to test needed resolution of the point cloud. Less points reduces the size of the files, and decreases the time when working with the point cloud.

To create a DEM from the SGM point cloud it was classified and filtered to obtain the 'bare earth' data. Only the surface points and points belonging to spatial objects which could limit the flow of water remained. Using a topographical map the points in the cloud were classified on type of land cover. The point cloud was then split on attribute type (ground or spatial objects) and each splitted point cloud was then converted to a single grid. These grids were then merged to construct a DEM grid consisting of spatial objects (i.e. houses, walls) and the ground level.

The result of the DEM accuracy test was positive for the AHN Lidar DEM. The coefficient of determination (R^2), RMSE, and mean absolute error showed the best outcome for the Lidar DEM when compared with the land survey measurements. The SGM DEMs showed less similarity with the land survey measurement. There was no significant difference between the thinned (SGM 10) and unthinned (SGM 80) DEMs. Each DEM source consisted of four different grid sizes (25, 50, 100 and 200 cm). These 12 DEMs were all tested in the hydrological model.

A hydrological model was constructed with the environmental modeling software PCRaster to simulate the water level and ponded area in an urban area. The model simulates overland flow with the Manning's formula for flow in combination with the kinematic wave function. It contains Manning's n which represents surface roughness. The infiltration was constant, and was only dependent on water bodies, paved or unpaved land cover. A scenario similar to the rain event of July 28th was simulated in the model (60 mm/hour precipitation). No gauged data is available for the study sites.

The hydrological model showed a different outcome of average water level and ponded for the SGM AHN DEMs. The AHN performs as expected with water flowing on the sides of the roads and along the pavement. Water flows from uphill areas down and gathers (ponds) in lower situated areas. The SGM DEMs does the same, only here streams are not strict to the side of road and along the pavements. Water flows more freely as the surface in the SGM DEMs was less smooth than the AHN DEMs. Choosing the correct grid size of the DEM for use in a hydrologic model depends on the objective of the researcher. Some ponded areas did not show in the larger grid sizes (1 and 2 m). So if even the smallest areas must be noticed, than a smaller cell size (25 or 50 cm) is warranted. Only modeling time increases exponentially when dealing with smaller grid cells.

This research showed that in the case of Amsterdam the SGM DEMs cannot match the AHN Lidar DEM. This can be attributed to the lack of detail in the aerial photographs, because of the proximity to Schiphol it is not allowed to fly on the standard flying height to take aerial photographs. Flying higher led to less detail in the photographs, which resulted in a noise ridden SGM point cloud. Filtering the point cloud did not help in achieving a smooth surface. Thus the AHN Lidar dataset, although outdated, proved to be the more realistic and useful DEM in the end.

CONTENT

1 INTRODUCTION

1.1 Context and background

Urbanization is one of the major challenges of the 21st century. Cities are becoming bigger, while the change in urban landscape is happening rapidly, and both these developments can create problems for the urban water system (Blanc et al., 2010; Schubert et al., 2008). By changing the urban landscape, rainfall water has to find new routes and this can lead to problems (Chocat, 2010). Problems occur if the sewage or drainage system is not able to deal with the excess of water during a storm event. Water will accumulate on the streets and pavements. This effect is called ponding or pluvial flooding, which can cause economic damage and disruptions to the urban infrastructure system (Blanc et al., 2012; Mark, 2004). Ponding occurs when water from a storm event encounters runoff problems (Dottori et al., 2013; Mark, 2004). Passages close to the sewage or drainage system inlet may be blocked or insufficiently sized, or the sewage system itself is insufficiently sized for the influx of runoff. This results in ponding of the water at the inlets or flowing further down the street.

Not only urbanization increases the chance of problems in the urban water system. Another influence is climate change. The Royal Netherlands Meteorological Institute (KNMI) already stated that in the coming decades rain events will be more frequent and more intense (KNMI, 2015). In August 2014 and 2015 this could already be noticed with 2 separate rain events which disrupted city life in Amsterdam. Especially the 2014 rain event, in which 90 to a 110 mm of rain fell within 24 hours, caused tunnels and other low lying areas to overflow and disrupted city traffic.

Helpful in predicting the before mentioned urban water problems are hydrological models. Modeling can help predict how (urban) areas react to surface flooding and ponding. It is predicted by Mason (2007) and Chen et al. (2012) that the coming years the hydrological understanding of the urban environment will increase. This is achieved due to the advances in technology and the increasing availability of high resolution data (Dottori et al, 2013; Wilson, 2012). A problem arises how to benefit from these advances and whether these advances will indeed result in better hydrological models.

Hydrological models can be evaluated by two major indicators: accuracy and efficiency (Chen et al., 2012). Higher accuracy can be obtained by (1) changing the detail in the explaining equations by using more terms, and/or (2) providing more detail in the spatial and temporal resolution, and/or (3) calibrating the model against gauged outputs (e.g. water depth or discharge). Increasing efficiency is related to (1) using simpler equations to reduce complexity, (2) reducing the size or scale of the case site to the essential area and objective, and/or (3) use of better hardware to fasten the model run. Understanding efficiency and accuracy is helpful in determining the needed models resolution, and thus the needed hardware and computation time to process the model. Next to these factors use of observational data is important to validate the models outcome.

An important input of a hydrological model is the digital elevation model (DEM). One of the features of a DEM is that it is beneficial in determining the flow of water within an area. In the Netherlands the AHN2 (Actueel Hoogtebestand Nederland) is a freely available DEM of the whole country (Van Der Zon, 2013). It is derived with Lidar technology and is available in resolutions of 50 centimeters and up. A problem with the AHN2 is that it is only updated every 5 years. Especially for urban areas this can make a difference for the elevation values in the DEM, as change can happen quite rapidly.

This can be seen in the Zuidas area in Amsterdam, where many construction projects are planned or are already undertaken changing the dynamics of the system.

A DEMs elevation values can be determined through several techniques: e.g. field measurements, contour maps, Lidar technology, or aerial (digital) photogrammetry. Thanks to Lidar technology and advances in digital photogrammetry it is possible to construct high-resolution DEMs (1 and 2 m resolution or finer). Hirschmüller (2005, 2008) designed the semi-global matching (SGM) method which uses digital aerial photographs to derive point clouds. Point clouds are a product of both digital photogrammetry and Lidar before a DEM is constructed. In essence it is a spatial dataset which includes the elevation. SGM is especially useful for urban areas as it specifically looks at an object boundary, providing a clearer identification of manmade objects then previous photogrammetry methods.

Not only has the resolution of DEMs increased, but the accuracy as well, resulting in vertical errors of 5-20 cm (Chen et al., 2012; Dottori et al., 2013). A problem that occurs due to the increase in spatial resolution is that it has the potential to magnify errors in (hydrological) models instead of removing them (Beven, 2000).

Optimum grid scale of hydrological models is still under discussion (Dottori et al., 2013). Shubert et al. (2008) and Fewtrell et al. (2008, 2011) have performed research related to the urban setting. Clear is that optimum grid size of an urban hydrological model is related to the dimension of the streets and the buildings of the study site, although it is dependent on the objective of modeling (Dottori et al, 2013; Fewtrell et al. 2008). This research will focus on the spatial resolution, and mainly the accuracy and necessity of high-resolution digital elevation models (DEMs) in urban rainfall-runoff models.

1.2 Problem statement and research objective

1.2.1 Problem statement

High resolution, up to date DEMs can be derived with the Lidar or SGM method. However, the currently available Lidar DEM is not up to date. Updating a Lidar DEM annually is a costly affair. The other, newer, technique SGM uses high resolution digital aerial photographs. As in the Netherlands aerial photographs are taken annually for topographic mapping it is not necessary to collect new data. A new DEM can be constructed annually with digital photogrammetry without too much added cost. Thus far, however, the SGM derived DEM has not been tested for use in a hydrological model. Furthermore not much is known about the SGM DEM accuracy as it has only been implemented in software since 2013 (Hexagon Geospatial, 2013).

Another part of the research is identifying the usefulness of high resolution DEM (i.e. smaller than 1 or 2 meters) for use in hydrological models (Dottori et al., 2013). It is stated by Fewtrell et al. (2008) that in an urban river flooding model grid size is more important than the equations used. Thus a simple model with a high resolution DEM can be more precise than a coarse grid model with elaborate flow equations. Gallegos et al. (2009) states that 3 model cells for street width are the optimal resolution to simulate river flooding in urban areas. While Fewtrell et al. (2008) looks at the minimum distance between buildings as the optimal model resolution.

Many of the currently used urban hydrological models focus on river flooding. Rainfall flooding (runoff and ponding effect) however is in the Dutch case (more) interesting. This is seen in the storm event of July 28th 2014 when precipitation caused huge problems in the city of Amsterdam, while surface water barely caused flooding problems.

1.2.2 Research objective

Lidar DEMs are costly to keep up to date, while the SGM DEM deriving method is quite new and has not been tested for use in a hydrological model. Furthermore the optimal resolution for an urban hydrological model that deals with precipitation and ponding is not known. There has been research towards the optimal resolution to simulate river flooding in urban areas, the researchers however used DEMs derived from Lidar and only some have looked at the influence of precipitation on flooding. High density points clouds are resource intensive (i.e. big data files and long computation times), thus it must be known what the optimum point cloud density is for a rainfall runoff model. Understanding the necessary model resolution for a rainfall-runoff model will help determine the needed point cloud density, as the DEMs are constructed from the point clouds.

1.3 Research questions

From the problem statement the following research question can be formulated:

> "How does the SGM derived DEM perform against a Lidar derived DEM when comparing accuracy in absolute height and use in a rainfall-runoff model, for various raster resolutions?"

The following sub-questions are answered to understand the influence of the (SGM and AHN) DEMs (source, resolution and construction method) on land survey measurements, the DEM derivatives, and the hydrological model:

1. What is the accuracy of the DEMs when the elevation values are tested against land survey measurements?
    a. Does the DEM construction method influence the DEM performance?
    b. Does raster resolution influence the DEM performance?

2. What are the changes between the SGM and Lidar derived DEM regarding the DEM derivatives (slope and catchment area)?
    a. Does the raster resolution influence the DEM derivatives (slope and catchment area)?

3. What is the quality of the SGM and Lidar derived DEM and raster resolution on the urban rainfall-runoff model?
    a. Does the DEM sources and resolution influence the water level?
    b. Do the DEM sources and resolution influence the ponded area?

1.4 Research design

In this thesis research the AHN2 Lidar derived DEM is compared to a SGM derived DEM. Not only DEM source, but also DEM construction method, point cloud resolution, and DEM grid size are tested against each other and against land survey measurements. The research is conducted by testing two study sites in the city of Amsterdam. Amsterdam underwent many problems during the storm event of July 28th 2014. Train stations were flooded and many roads and tunnels became inaccessible during the rain event.

To understand the risk and excess of water problems it is possible to simulate the urban system in a model. A hydrological computer model is one method to simulate the effects of precipitation in urban areas. The model used in this research is a distributed temporal hydrological model. Spatial variability of the study site is taken into account such as elevation and the surface roughness. The distributed model is grid-based with runoff transported over the grid using the local drain direction of each cell.

Citywide models can be resource intensive, both time-consuming and hardware demanding. Interesting here is to focus on small-scale study sites, areas around 1 km^2. Using a small-scale study site limits the modeling time in such a way that it is possible to do many simulations, but the site still remains large enough to have enough spatial variability. Further the modeler can still have attention to the detail of the data input.

The research consists of 3 stages: (1) DEM construction, accuracy testing, and DEM choice, (2) model construction and testing, and (3) the actual running of the model (fig. 1).

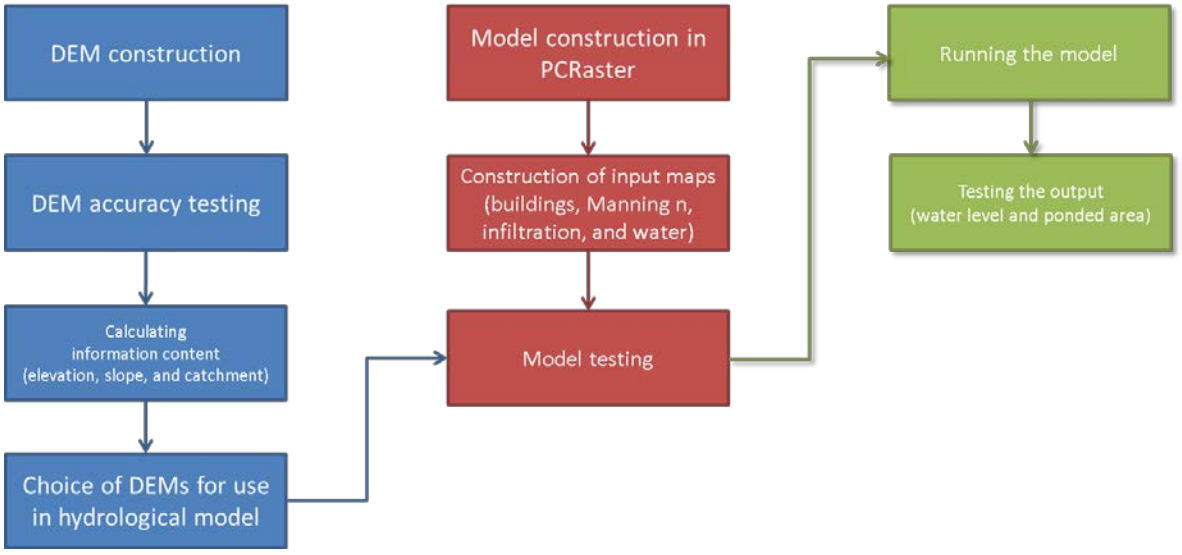

Figure 1: Overview of the three stages of the research

1.5 Chapter outline

The second chapter discusses the theoretical background of the research. The main terms and concepts such as DEM, digital photogrammetry, and current trends in (urban) hydrological models are described in detail. It further explains the data necessity for hydrological models and the importance of DEMs in such models. After the theoretical background, chapter three explains the

methodology used to help answer the research questions. It provides explanation on how point clouds are extracted from digital aerial photographs. Further giving insight in the equations used to test DEMs accuracy and the hydrological model. The working of the hydrological is explained in great detail. Further the used data, software applications, and study sites are addressed. Chapter four shows the results of the thesis research. First the outcome of the DEM accuracy test is shown, and the choices which were made which constructed DEMs were used in the distributed hydrological model. The second part of chapter four shows the average water level and ponded area taken from the hydrological models outcome. Chapter five discusses the results of the research and its connection to the scientific literature used in the theoretical background. After which, chapter six answers the research questions. Chapter seven concludes the research by giving recommendations for further study.

2 THEORETICAL BACKGROUND

The effects of precipitation and pluvial flooding are currently evolving topics in (urban) hydrology. This can be attributed to the more than likely increase of intense rainfall events in the future due to climate change, and reduction of infiltration in urban areas (Blanc et al., 2012; Climate Scenarios, 2014; Krebs, 2014). The effects of precipitation in urban areas can be understood by using hydrological models which simulate rainfall and runoff (Fewtrell et al, 2008; Fewtrell et al. 2011; Schubert et al., 2012). Thanks to advances in technology more data is available to help simulate the urban environment. These advances are high resolution cameras, introduction of fast graphics processing units, a decrease in computer hardware cost, and improved computer algorithms (Chen et al., 2013; Dottori et al., 2012).

2.1 Digital Elevation Models

There are several descriptions of what a digital elevation model (DEM) is. One of them is a two dimensional (regular) grid that represents the spatial distribution of elevation (Walker & Willgoose, 1999). DEMs are important for use in the environmental sciences (Li & Wong, 2010; Walker & Willgoose, 1999; Wilson, 2012). This can be seen in the field of hydrology, hydrological models are dependent on high quality spatially distributed elevation data (Ludwig et al., 2006; Liu et al., 2005). DEMs are needed to understand the direction of stream flow, the size of catchment areas, and the location of river networks. Further they are used to determine slope, watershed extent and hydrological indices (Valeo & Moin, 2000). Urban areas are complex areas for generation of DEMs because of the diversity and density of surface features.

A definition of what exactly is a high resolution DEM is proposed by Dottori et al. (2013). Categorizing the differences in DEM resolution: very fine or high < 2 m, fine or high 2 to 5 m, low/coarse > 20 m. Most researchers consider DEMs until 2 meter resolution as high-resolution DEMs (Blanc et al, 2012; Chen et al., 2012; Fewtrell et al., 2011), but some extent this to 5 m (Gallegos et al., 2009).

2.1.1 DEM sources

DEMs can be created from several sources. In the past they were mostly constructed from spot heights or the elevation data was taken from aerial photographs or topographic maps. A problem with these maps was that the resolution was quite low (90-250 m) and also that the maps had low accuracy (1-10 m) (Rayburg et al., 2009). It is also possible to scan large areas with satellites to offer images for constructing DEMs. For urban areas however they no do not (yet) offer enough detail. Ground-based surveys with GPS can offer higher accuracy, but are time consuming and difficult to undertake in inaccessible terrain (Rayburg et al., 2009). Two approaches that do not encounter these problems are Lidar technology and digital photogrammetry.

Lidar technology is a remote sensing technique which uses laser scanning (Haala & Rothermel, 2012). It is an acronym for Light Detection and Ranging and can be compared to radar technology, using light instead of radio waves. For the creation of a DEM airplanes fly over areas and emit light pulses, these pulses bounce back from either the ground or objects (e.g. buildings, vegetation, roads). From the return signal a location can be derived and a point cloud can be created. A point

cloud is a 3D set of data points which contain X, Y, and Z coordinates. Lidar has an added benefit that it can 'see' through vegetation. This results in a first and last return of the light pulse (e.g. first return being the leaves of a tree, and the last return the ground level). Thus it is possible to create a 'bare earth' model without the vegetation. A problem with Lidar is how it reacts to water. A light pulse goes through water and (depending on the depth) will not give a return. This is not necessarily a problem for waterways or a lake, but it is when water is ponded on a rooftop or on a road it will not result in a data point. In the last decade Lidar has become the main method of constructing high quality DEMs, as other technologies could not compete with the quality of a Lidar DEM (Haala & Rothermel, 2012). In the Netherlands the AHN2 (Dutch elevation map) is created with Lidar (Van der Zon, 2013). Also for use in hydrological models Lidar data is popular method for DEM construction (Ozdemir et al., 2013).

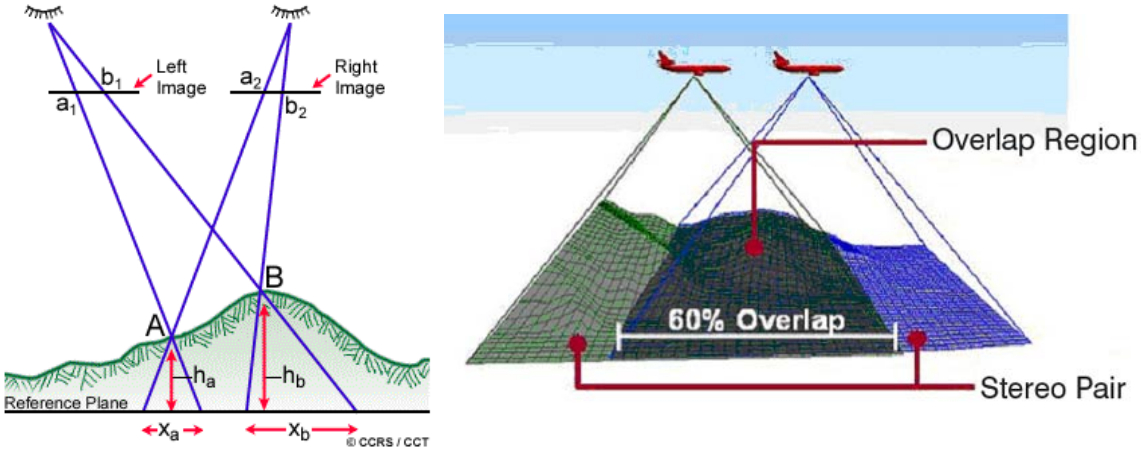

Figure 2: Example of digital photogrammetry. The left image shows that the direction and angles are needed to determine the elevation values on the ground. The right image show how stereo-photos are taken. Knowing the exact location (i.e. coordinates) of both images makes it possible to derive a digital elevation model.

Digital aerial photogrammetry uses stereoscopic photos to create a DEM (fig. 2). Stereoscopic photos are photos which overlap with each other, and are taken at different locations. It is possible to derive a point cloud if the exact location (including flying height of the airplane) is known of the photos. In the past urban structures could not adequately be reconstructed from aerial photographs. Only recently an algorithm was introduced in the computer vision sector by Hirschmüller (2005, 2008). This algorithm is known as the semi-global matching (SGM) method. It relies on new technologies (e.g. high quality photographs, graphics processing units that can deal with high resolution images, fast processors) to create dense point cloud data of aerial photographs. The SGM method consists of an algorithm which also takes the sub-pixel into account, something which other photogrammetry methods did not do. The sub-pixel can be seen as a lower level than the normally used pixel, a building block as such. By using the sub-pixel it is better possible to define an objects edge, something which is important for image-matching in urban areas. The algorithm searches for the shortest path of Mutual Information (MI) between two stereo images in its image matching technique. MI is a method to measure how much two variables, in this case two images, have in common. MI is used to match images with complex relationships to find relationships, even when the images are distorted (as stereo images) (Hirschmüller, 2008). In this case the exact same information stored in each (sub-)pixel of a different image is used. SGM has already been used to create 3D models of cities from a digital surface model (DSM) and its point clouds are already proven

to be of a higher quality and density than past digital photogrammetry methods (Gehrke et al., 2010).

DEM construction from point clouds can take place in any GIS program that is capable of handling the point cloud data format. Both ArcGIS as ERDAS IMAGINE have this functionality. ArcGIS has more functions for interpolation, the most interesting to use are the IDW (inverse distance weighting) and averaging in grid cells. ERDAS only supports linear interpolation in raster construction. Inverse distance weighting is a method to statistically determine a value from a certain number of scattered points. It takes into account Tobler's first law of geography "everything is related to everything, but near things are more related than distant things" (Heywood et al., 2011).

2.1.2 Point cloud classification and filtering

Point clouds are a set of data points before a DEM raster is constructed. The two standard formats of a DEM are the Cartesian grid or the triangulated irregular network (TIN) (Walker & Willgoose, 1999). A Cartesian grid is a regularly sized grid and is the one most often used. A TIN has the benefit of (usually) being less resource intensive as less points and cells are saved to represent the landscape.

The objective of the model should always be kept in mind when a DEM is constructed. Depending on which spatial features are important a scale must be chosen. Otherwise features which could be important (e.g. ridgelines, curbs, sidewalks) could be lost (Wilson, 2012). These features can determine how and where the water flows to.

The most commonly used inclusion of a DEM in environmental modeling is the digital terrain model (DTM), a 'bare earth' model with no vegetation and man-made buildings (fig. 3). To achieve a DTM from a SGM point cloud filtering must take place to 'remove' the unwanted features. Lidar point clouds do not need filtering to obtain a DTM, as it already can filter out the vegetation during the remote sensing process. For an urban hydrological model it is not enough to have a DTM as the buildings are needed as they will influence the stream flow (Fewtrell et al, 2011). Depending on the wanted model complexity a digital surface model (DSM) without vegetation is adequate for an urban hydrological model. Adding the vegetation will make it more complex, while a friction factor like Manning's n is enough to simulate the vegetation cover (Schubert et al., 2008).

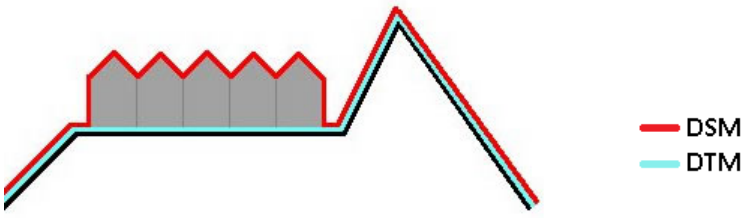

Figure 3: Differences in a digital elevation model (DEM) between a digital surface model (DSM) and digital terrain model (DTM)

Depending on the use of the DEM, filtering can take place to the fit the DEM to the specific need. For construction of a 3D model of a city it is not necessary to filter the DEM as all of the aspects of it are likely to be used. When used in a hydrological model the ground level is important as water flows over and infiltrates into the ground.

Point clouds can be used to create a DTM or DSM. To create a DTM it is necessary to know what land cover class (e.g. water, vegetation, buildings) each point belongs to. Lidar point clouds have the advantage over digital photogrammetry point clouds that it can automatically classify the vegetation with its laser system (e.g. first return is canopy, last return is the ground level) (ESRI, 2014). A DTM can thus be constructed from the last return laser pulse. SGM point clouds have to be manually classified. Classification in the SGM point clouds can be based on RGB encoding (Hexagon Geospatial, 2013). Unlike Lidar point clouds, SGM point cloud data can contain their original color value (RGB) as an attribute, thus making it possible to use the original color of the aerial photos in the classification process of the point cloud. Currently the classification process can only be done manually, as the automated process is not foolproof.

2.2 Urban hydrological models

A hydrological model simulates the interaction of water with the environment. It is dependent on the research objective what interactions will be simulated in the model. A research objective can be to investigate which areas will flood when a dike breaks, or understanding the influence of green roofs on infiltration, or whether a new sewage system fits the need of the neighborhood. There are several ways to construct a hydrological model. Some models already prebuilt and can be adapted for different situations (e.g. SWMM or Lisflood), or a model can be built from scratch (or adapted from a pre-existing model) within modeling tools and languages (e.g. Matlab, Python or PCRaster). All software programs are based on a programming languages (e.g. C or PCRaster) making the program adaptable for different situations and research objectives. A rainfall-runoff model is a specific type of hydrological model.

The urban situation differs from natural areas with the inclusion of man-made objects (e.g. buildings, sewage systems, paved roads). Flow paths of water in natural areas are determined by slope and aspect. While this still applies to the urban situation other factors also determine flow paths. These effects include the man-made objects and the possible hindrance of objects in the flow paths which forces the water to find a new path (Blanc et al, 2013). Possible obstructions can be the accumulation of dirt in a sewage inlet or incorrect placement of the inlet at an elevated point in the street (Dottori et al., 2013; Mark, 2004). This leads to a higher complexity when simulating the urban area.

2.2.1 Trends and problems

An overview of the current research towards urban hydrological models is given in table 1. Much emphasis in research is placed on pluvial flooding due to the occurrence of high-profile flood events in the last decade. Think about the flood events in the UK in 2007 (Fewtrell et al., 2008; Fewtrell et al., 2011; Sampson et al., 2013; Ozdemir, 2013) which caused over 4 billion euros in damages (Blanc et al., 2012).

A trend in the research is the focus on high resolution data. High resolution (smaller than 1 m) digital elevation models (DEMs) are constructed from new remote sensing techniques (e.g. Lidar and digital photogrammetry) to simulate the landscape. New techniques made it possible to simulate the urban environment, which was difficult in the past due to the complexity. Not all researchers are sure if small scale equals a better hydrological model (Dottori et al, 2013). As can be seen from other research it must depend on the complexity of the urban situation and the objective of the model (Fewtrell et al., 2008; Gallegos et al., 2009; Fewtrell et al., 2011). High resolution data can raise false

confidence in the results, meaning that dealing with gauged and validated data will not necessarily mean that the out coming research will be good. An analysis of the output is still needed. Still lacking in many cases is the availability of high quality datasets for validation of the before mentioned models.

A problem that has not changed despite technological advances is the computing time when using high resolution data (Blanc et al, 2012; Chen et al., 2012; Dottori et al., 2013; Fewtrell et al, 2011;). Fewtrell et al. (2011) even adapted their research objective as they were not able to simulate the landscape at the two smallest grid resolutions (10 and 25 cm). Ozdemir et al. (2013), using an improved model of Fewtrell, was able to use a smaller grid resolution (10 cm) but concluded that computation time still took too long to be usable. Hardware is thus still a restricting factor, as the increase and availability of high-resolution data goes faster than the advances in technology (Chen et al. 2012).

Adequately simulating the sewage system is also troublesome within an urban rainfall-runoff model. Dottori et al. (2013) state that a sewage system never works at optimum capacity and this should be represented in a model that implements sewage systems. In urban systems it is possible that sewage systems can overflow on the surface during a flood. Maksimovic et al. (2009) tried to simulate this effect in a 1D-1D model. Within 1D-1D modeling the surface flow paths are constructed beforehand in a 1D system and connected to a 1D sewage network for the routing of surface flow (Blanc et al, 2012). Although this is a very efficient method, it does not adequately describe the process as it does not describe the flooding and ponding of the surface level.

Table 1: Overview of urban hydrological modeling research and usability.

Author	Topic	Model	Keywords
Blanc et al. (2012)	River-rainfall flooding	Infoworks	High quality data, rain data; model limiting factors
Chen et al. (2012)	River flooding	Urban Inundation Model	Grid resampling; model limiting factors;
Dottori et al. (2013)	Urban hydrological model comparison	-	Sewage systems; drainage systems; model limiting factors; high resolution data; urban systems
Fewtrell et al. (2008)	River flooding	LISFLOOD-FP	High resolution data; model limiting factors; optimum grid cell size; grid resampling
Fewtrell et al. (2011)	River flooding	LISFLOOD-FP	High resolution data; optimum grid cell size
Gallegos et al. (2009)	Dam break flooding	BreZo – finite volume model	High resolution data; optimum grid cell size
Krebs et al. (2014)	Rainfall runoff - Impact of land surface change on water balance	SWMM	High resolution data; limiting model factors
Maksimovic et al. (2009)	Rainfall flooding	SIPSON 1D/1D	1D systems; drainage systems.
Mason et al.	River flooding	Horritt simple	Grid resamping; model efficiency testing

(2007)		finite volume (SFV) model	
Mitasova & Mitas (2001)	Soil erosion simulations	Grass (Qgis)	Non-urban system; GIS implementation
Ozdemir et al. (2013)	River Flooding	LISFLOOD-FP	Optimum grid cell size; high resolution data; model efficiency testing
Rumman et al. (2005)	Infiltration modeling	HEC-GeoHMS	High resolution data; drainage systems
Sampson et al. (2013)	Rainfall flooding	LISFLOOD-FP	High resolution data; ponding; model efficiency testing
Schubert et al. (2008)	River flooding	BreZo – finite volume model	Grid resampling; urban system
Skotnicki & Sowinski (2013)	Rainfall flooding	SWMM (v5)	Urban system
Yu & Lane (2006)	River flooding	Mesh grid diffusion-wave model	Model efficiency testing; grid resampling

2.2.2 Dutch water management

Many of the before mentioned scientific reports deal with river flooding in urban systems. In the Dutch case there is more interest in the influence of rainfall on the urban landscape, so called pluvial flooding. This can be attributed to several intense rainfall events which occurred in the last decade. One recent rainfall event is from July 28th 2014 which disrupted traffic and public life in Amsterdam (fig. 4). Not only Amsterdam was effected also other parts of the Netherlands (DUIC, 2014). According to the Dutch association of insurance companies the estimated damages were 10 million euros due to the precipitation (Verbond van Verzekeraars, 2014). While according the Royal Netherlands Meteorological Institute (KNMI) it was the third highest rainfall event ever recorded in the Netherlands (Van Oldenborgh & Lenderink, 2014). One year later on August 24th a similar rain event occurred, again causing disruption in Amsterdam (Parool, 2015).

In the Dutch water management sector there are consultancy companies who have developed (some in cooperation with research institutions) rainfall-runoff models which can simulate the effect of rainfall in an urban area and can predict where water problems will arise. All of them used the AHN2, which is the Dutch national elevation map. Consultancy company Neelen & Schuurmans works together with Deltares and TU Delft on 3Di (Van Wayenburg, 2014). Another consultancy company is Hydrologic they constructed their model, named PriceXD, together with the municipality of Amersfoort. It simulates the rainfall, runoff, and infiltration in urban systems (Spijker et al., 2012). PriceXD uses the AHN2, but it can be substituted with a locally derived Lidar dataset. Grontmij uses Wodan[123] (Grontmij, n.d.), Tauw has WOLK (Blok, 2010). All of these models work more or less alike, and all of them use the AHN2 as their base map for elevation height. Meaning that the highest resolution these models use is 50 cm.

Figure 4: Intense rainfall event on July 28th 2014 in Amsterdam

2.2.3 Flow routing and catchment areas

A flow direction map determines the route of the precipitation in a rainfall-runoff model. Understanding the flow direction helps knowing where the water could accumulate or pond. The flow direction can be taken from a DEM. In a hydrological model water will flow from cell to cell depending on the height in each neighboring cell, choosing the lowest cell as the pathway. If no neighboring cell is lower the cell will be determined as a 'no routing' cell and no flow will initially occur. It is possible to attach a threshold to a 'no routing' cell, if this threshold is exceeded it will enforce a flow to the neighboring cells despite the fact that it is lower in elevation. This flow is enforced until the water height is once again below the threshold.

In their research Sampson et al. (2013) used an automatic routing method to reduce computational cost. Instead of the model itself searching for the ideal route at each step, route is automated (calculated before) and the model only calculates water depth and velocity. The flow direction is taken from a DEM and follows the before mentioned method of flow. Catchment areas or watershed basins are an area where all the surface water from precipitation and other sources comes together at a single (lowest) point in the area, this can be a sink or an exit point where the water merges with other waterways. A catchment can consist of smaller sub catchments (fig. 5).

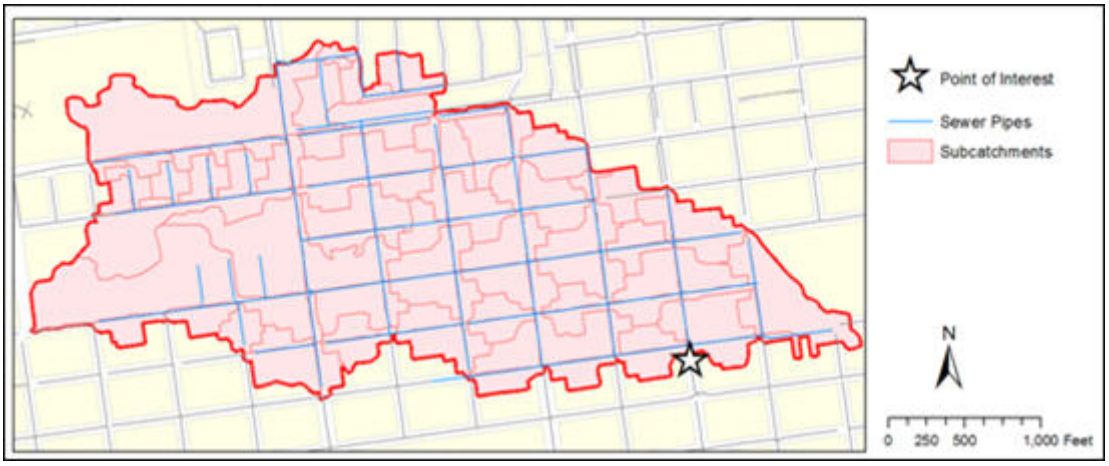

Figure 5: Example of an urban catchment area (including its sub catchments) in the city of San Francisco

2.2.4 Data necessity

To use a rainfall-runoff model input data is needed to run the model. To simulate precipitation climate data is used like a time-series of rainfall events. Such time-series can be gathered from meteorological stations, field measurements or from text books. In the Netherlands the KNMI have described rainfall events that can help researchers to simulate the environment (KNMI, 2014). They have gathered the rainfall events in a document that describes the intensity and the chance of such an event (e.g. once in 10 years or once in a 100 years). It can be used by engineers who design sewage systems to see if their design is up to the task or by consultancy companies to understand where in neighborhood water problems can occur.

The landscape must also be described in the model to understand water flow and infiltration. A digital elevation model (DEM) describes the elevation in an area. From the DEM the slope and aspect can be taken which are needed for the flow routes. Flow speed is partially determined by surface roughness (Manning's n) and the slope. Surface roughness depends on the type of surface (e.g. a paved or unpaved road).

Infiltration determines the amount of water that stays on the surface. There are several ways to simulate this effect. It depends if the groundwater is taken into account or not. It is possible to only use the surface type to determine the infiltration rate. Other factors that can determine the infiltration rate are the ground water level, porosity, Hydraulic conductivity (K-value), and Curve Number (CN) (Rossman, 2010).

3 METHODOLOGY

This chapter of the thesis report describes how the research questions are answered. The research consisted of three stages: (1) DEM construction, accuracy testing, and DEM choice, (2) model construction and testing, and (3) the model simulations and analyzing the results (fig. 6).

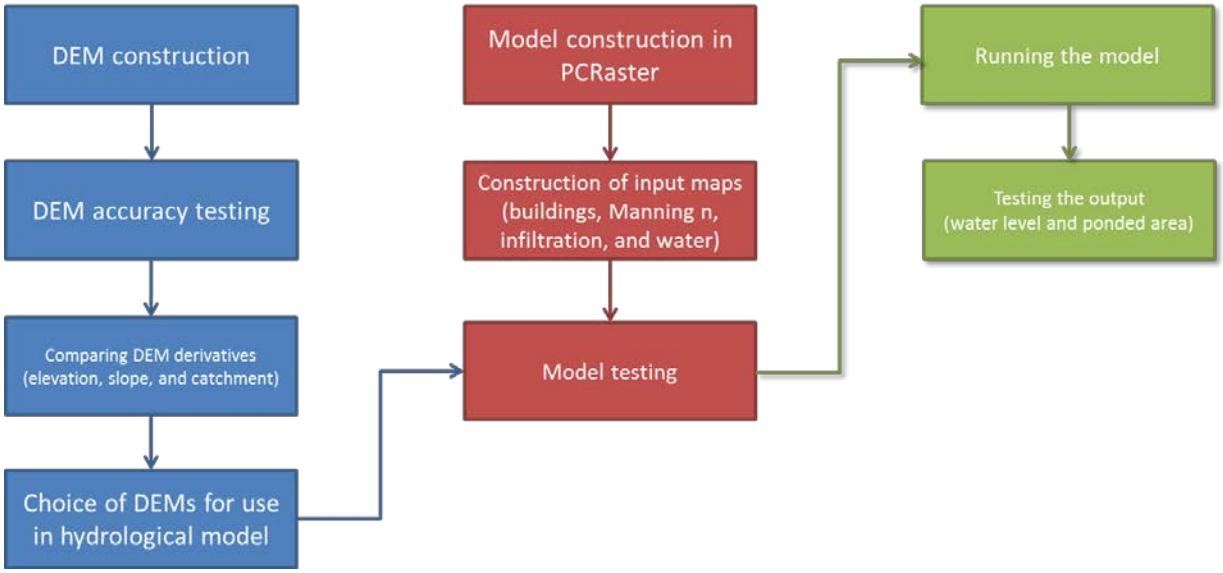

Figure 6: Overview of the three stages of the research

The first part of the research methodology 'DEM construction and accuracy testing' deals with research question one (section 3.1). The first part also answers research question two by comparing the DEM derivatives (slope and catchment area) based on grid cell size and DEM source. The model construction is explained in the second section (3.2). Research question three is answered in the last section 'Model simulations' (section 3.3).

3.1 DEM construction and accuracy testing

3.1.1 DEM construction from aerial photographs

Point clouds were used to create the digital elevation models (DEMs) (fig. 7). The point clouds were derived with the semi-global matching (SGM) method developed by Hirschmüller (2005, 2008). Using aerial stereo photographs (i.e. at least 2 images which overlap) it was possible to determine the height values. To use the SGM method the aerial photographs have to be digital, have at least 60% overlap with at least one other aerial photograph, and contain detailed metadata. The metadata includes the flying height were the photographs were taken, exact center point coordinates of each photograph (X_0, Y_0, Z_0), image pixel size, a camera report containing specific information about the used digital camera (e.g. the lens distortion, focal point), and which coordinate system was used.

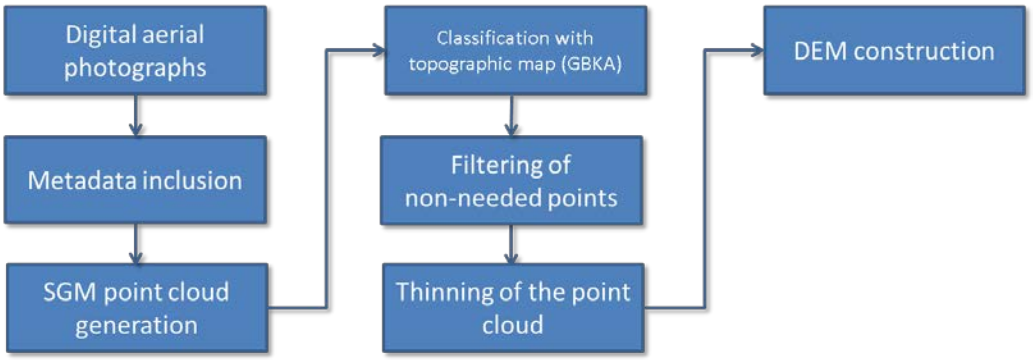

Figure 7: Workflow of DEM construction

Next to the digital camera specifications, the orientation of the camera sensor is an important factor. The inertial navigation system (INS) determines the exact camera position when each of the aerial photographs was taken. The orientation of the sensor is defined as the Heading (also known as Yaw), Pitch, and Roll (HPR) (fig. 8). Heading is related to the rotation of Z-axis, while Pitch is to the Y-axis and Roll to X-axis. It must be stated that pitch and roll are not fixed to the x and y axis, it can differ between software vendors, countries and different methodologies. In photogrammetry terms they can be translated to Omega (rotation to the x-axis), Phi (to the y-axis), and Kappa (to the z-axis). All this information was stored in a binary file (block file) for use within the software program ERDAS IMAGINE.

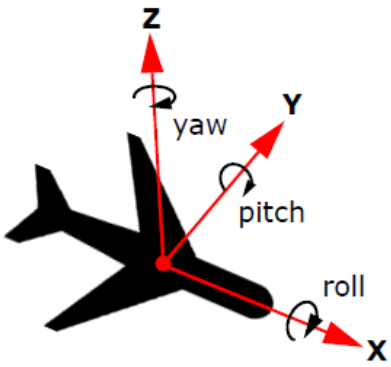

Figure 8: Camera positional angles yaw (or heading), pitch, and roll compared to the xyz direction

Direct geopositioning, instead of georeferencing with individual ground points, uses the exterior orientation parameters (i.e. the number of pixels, the cell length of each pixel, exact ground coordinates of the image center, the rotation angles of the camera) to position the image. The photogrammetry software then generated a mosaic that shows the position and overlap of the aerial photograph. The SGM process can only take place when the exact position is known of each image.

After point cloud generation, (manual) classification took place to distinguish building points and ground points in the SGM point cloud (fig. 7). Figures 9a and 9b show the result of the SGM process. Classification is the process of giving an attribute of land cover type to a point in the cloud. As the SGM method, unlike Lidar technology, cannot automatically classify the point cloud on land cover type classification had to be performed after the generation of the point cloud. The attributes in this

study was taken from the topographic map Grootschalige Basiskaart Amsterdam (GBKA) which is a continuously updated topographic map with e.g. roads, buildings, water ways, train tracks, and other spatial objects. The GBKA (Grootschalige Basiskaart Amsterdam) map is based on the digital aerial photographs and is also (continuously) updated with spatial plans. Some environmental models only want to use a 'bare earth' elevation model for analysis. The attributes then aid in the filtering process, by filtering out all none-ground points.

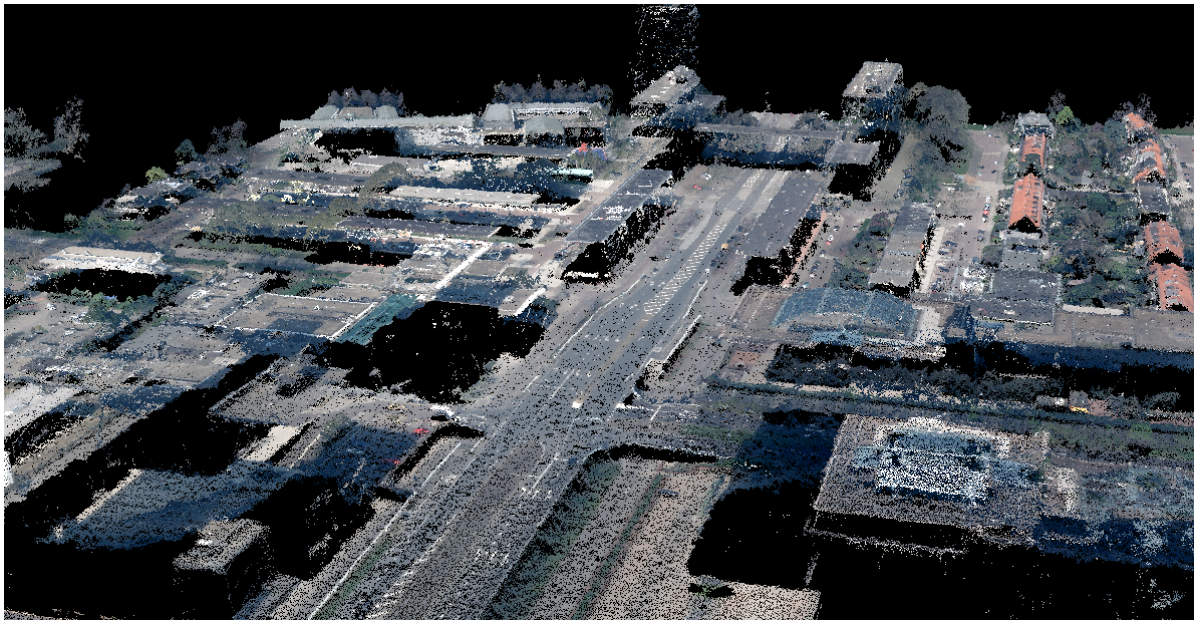

Figure 9a: Point cloud with RGB encoding, location shown is the Zuidas study site

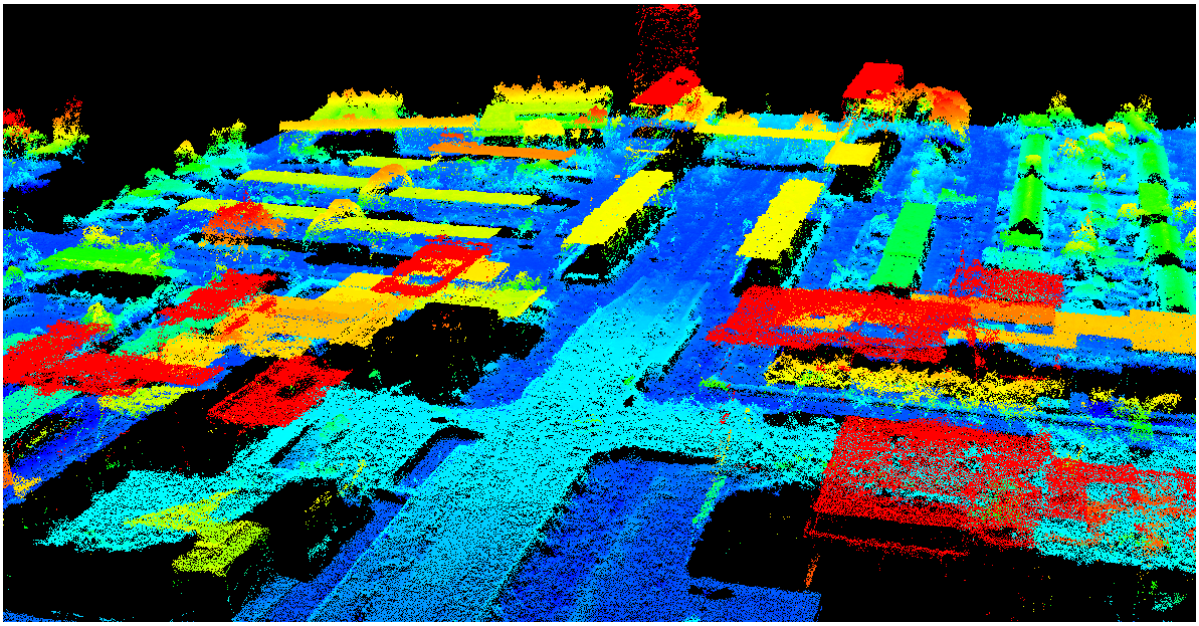

Figure 9b: Point cloud with elevation colors, location shown is the Zuidas study site

Some parts of the landscape could not adequately be transformed into a point cloud. These are non-needed points which had to be filtered. Water bodies in point clouds result in a large range of points, many outliers and not a clear pattern of elevation values. These water bodies were also filtered out

of the point cloud. This kind of filtering is considered ‘soft’ filtering. It is always needed to generate a useable point cloud.

A ‘bare earth’ model only contains the ground level data, without vegetation and objects like cars. For an urban rainfall runoff model it is necessary to include buildings and other large spatial objects that obstruct water flow. These objects can be separated from the non-needed points by filtering on the attribute data. The other manmade objects (e.g. pillars) which receive water must be tested in the model to understand how the model reacts to steep slopes. Filtering out spatial objects of the point cloud is considered ‘extreme’ filtering as it needed to create a ‘bare earth’ model. Not to make the point cloud useable.

After filtering the point cloud to create a ‘bare earth’ model a thinning process was performed to generate a second set of the SGM point cloud. From every 80 points in a square meter, 10 points were randomly chosen. The process was performed in the ERDAS IMAGINE software program. The first set was non-thinned and had a maximum of 80 points/m^2. The second, thinned, set was at most 10 points/m^2. The difference in data size was tenfold, also opening and viewing the non-thinned set took longer. A point cloud data set for the city of Amsterdam holds 350 gigabyte of data at 80 points/m^2. Point cloud data is usually separated in a mosaic dataset to ease the access. If thinning results in the same DEM accuracy and model output it would be possible to deliver the point cloud in smaller sized data sets, and increasing the size of individual areas in the mosaic. Although cost for storage has lowered in the last decade and internet speed has increased, it still can cause problems when exchanging large data files as point cloud data.

The point cloud itself was not usable in the intended modeling software. The software used for the hydrological model was PCRaster, which requires a Cartesian grid DEM. DEM grid construction from point clouds is possible in several GIS and Remote Sensing software programs. Many of the methods are the same in the software programs. Two options were compared to determine the influence of the construction method: the inverse distance weighting (IDW) and the averaging method. The IDW determines the cell value by using a linearly weighted algorithm on the point cloud data. It relies mainly on the power parameter, which controls the importance of the known points to the interpolated value. The power used here was the default value 2 within ArcGIS. Increasing the power value increases the importance of closer located points. Averaging is simply taking the mean of all known points within a certain chosen cell size resulting in block means (i.e. grid cells). This was different from IDW which uses point prediction (i.e. grid nodes).

The void fill method was used to make a ‘closed’ grid, because of filtering or a simple lack of data points gaps can exist in the point cloud. Void fill helps in filling these gaps, voids are larger areas than the typical space between points in a point cloud. Voids are larger areas, i.e. filtered water bodies, or missing buildings in the Lidar dataset. Two methods are used: linear and natural neighbor. Linear void fill uses linear interpolation to determine the cell value. Natural neighbor void fill is based on proximity of the other point values.

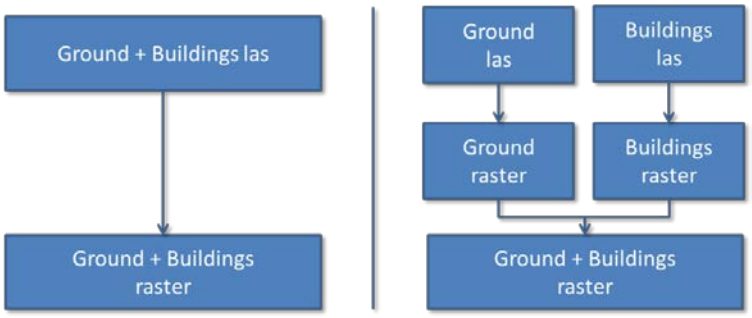

Figure 10: DEM construction from point cloud

For most rural areas it is possible to simply convert the point cloud to a grid with the above mentioned methods (fig. 10). Only in urban areas the (manmade) spatial objects usually are rectangle objects with strict 90 degree angles. Classification with the topographic map was used here to aid in the construction of the DEM. When using the single point cloud with the attributes ground and spatial objects a hill-like slope is created between buildings and the ground which does not exist in reality (fig. 11a). Thus it is needed to separate the different attributes and create grids for each attribute. After this it is possible to merge them to a new single DEM (fig. 11b).

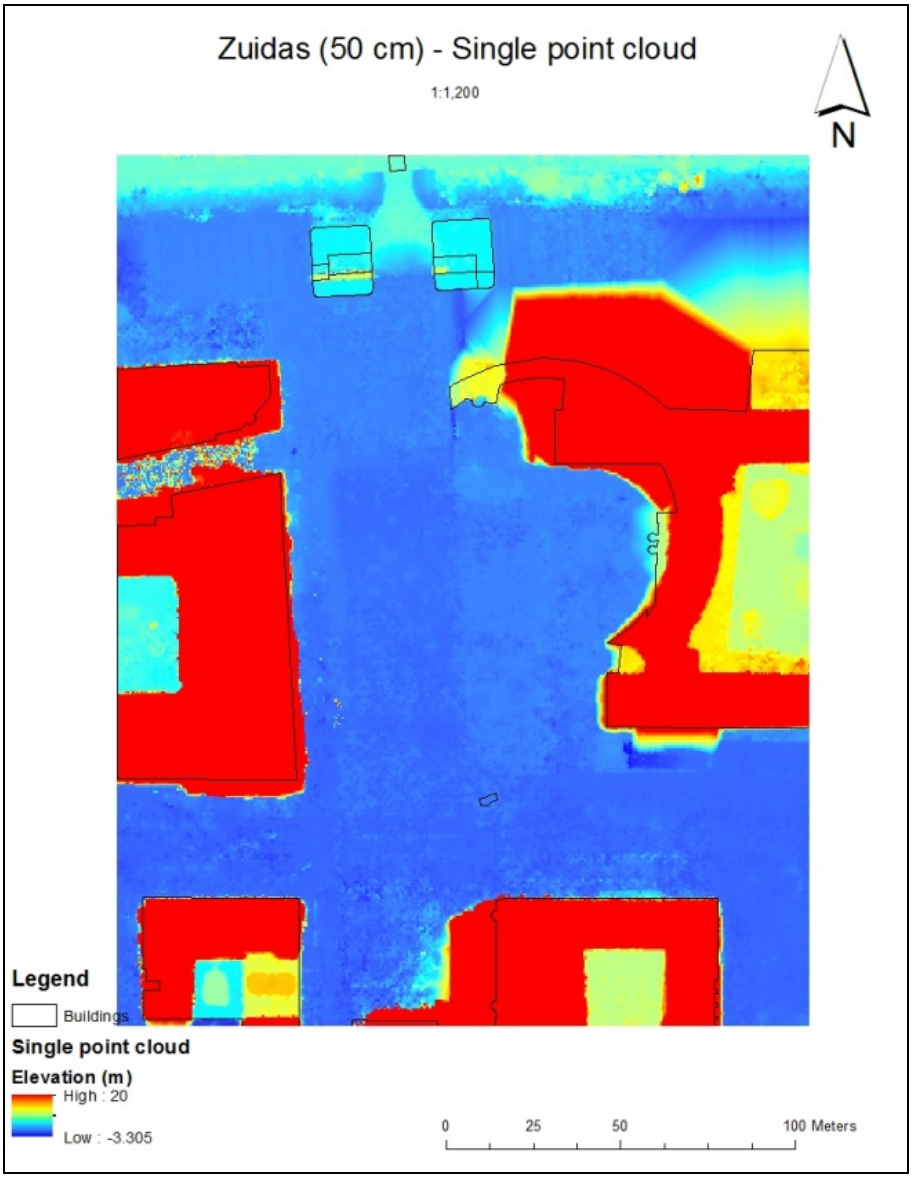

Figure 11a: DEM created from a single point cloud

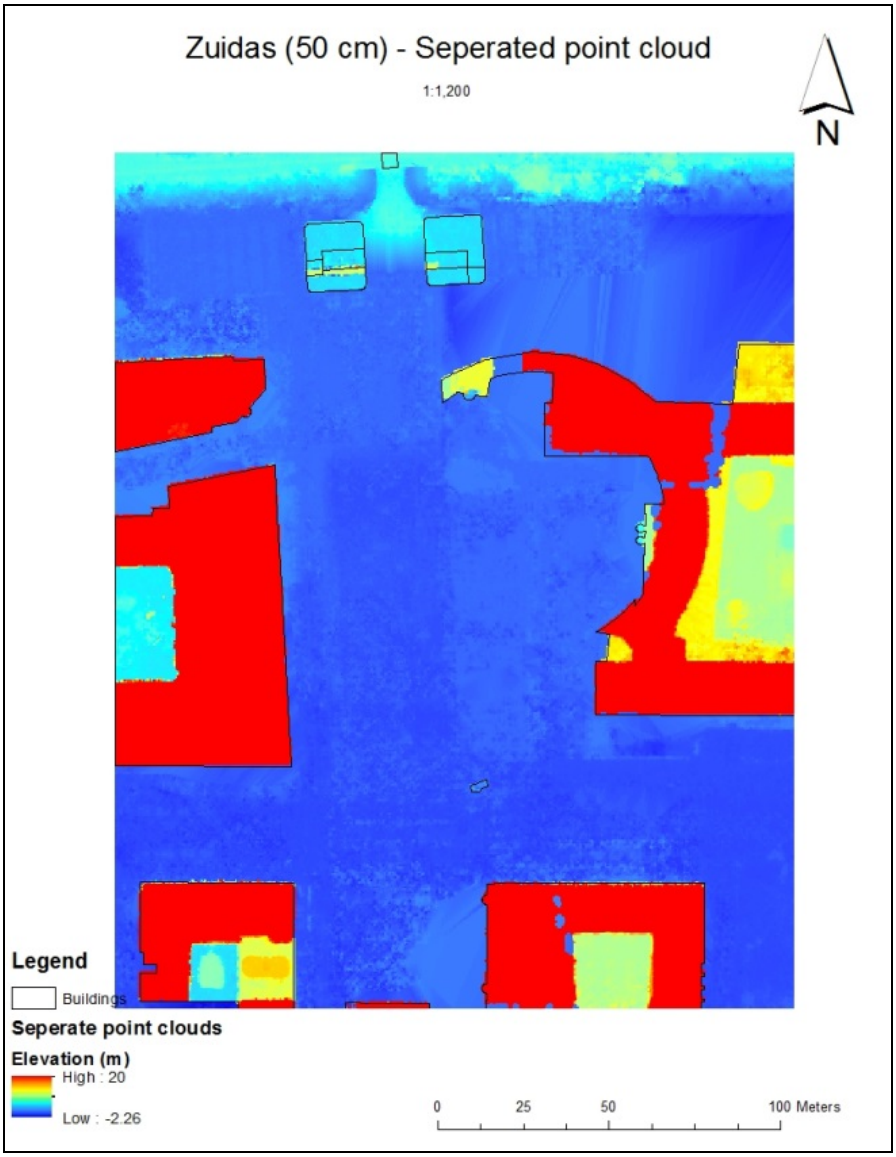

Figure11b: DEM created from a separated point cloud

To understand the influence of point cloud filtering and DEM construction on the final DEMs several DEMs were compared (fig. 12). Four SGM point cloud data sets were used as the basis for the DEMs (10 and 80 points per m^2, both filtered and unfiltered). The DEMs differ in resolution (25 cm, 50 cm, 1 m, 2 m) and construction (IDW, averaged). With unfiltered only simple 'soft' filtering took place to delete water bodies. With filtered, 'extreme' filtering took place, including deleting water bodies, all vegetation, all outliers and unknown points. In extreme filtering only the spatial objects like buildings and the ground level data is kept. The constructed DEMs are as follows (of the AHN2 only the 50 cm raster was used for the accuracy test) (fig. 12):

1. SGM 10 points IDW DEMs unfiltered (25cm, 50cm, 1m, 2m)
2. SGM 10 points averaged DEMs unfiltered (25cm, 50cm, 1m, 2m)
3. SGM 10 points IDW DEMs filtered (25cm, 50cm, 1m, 2m)
4. SGM 10 points averaged DEMs filtered (25cm, 50cm, 1m, 2m)
5. SGM 80 points IDW DEMs unfiltered (25cm, 50cm, 1m, 2m)
6. SGM 80 points averaged DEMs unfiltered (25cm, 50cm, 1m, 2m)

7. SGM 80 points IDW DEMs filtered (25cm, 50cm, 1m, 2m)
8. SGM 80 points averaged DEMs filtered (25cm, 50cm, 1m, 2m)
9. AHN DEM constructed from Lidar point cloud (25cm, 50cm, 1m, 2m)

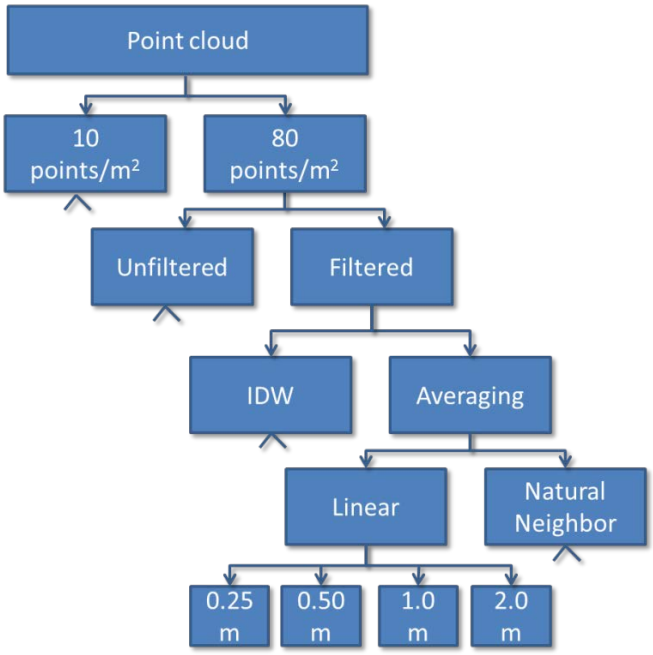

Figure 12: Overview of all constructed DEMs from the SGM point cloud. Not shown are the scenarios for 10 points/m², these are identical to the 80 points/m².

The AHN2 Lidar DEMs available does not hold grid data for the buildings and it contains gaps in the data points (fig. 13). These DEMs could not be used within the hydrological model. For the model a closed grid was needed. To construct a closed grid the original AHN2 Lidar point cloud was used. Here the 'bare earth' Lidar point cloud data is used to create the ground DEMs. The data for the spatial objects, buildings, was taken from the SGM point cloud. Merging the building and ground raster formed the AHN2 DEM (fig. 10 + 13). The DEM construction method used to make closed AHN2 grid was the averaging method and linear void fill.

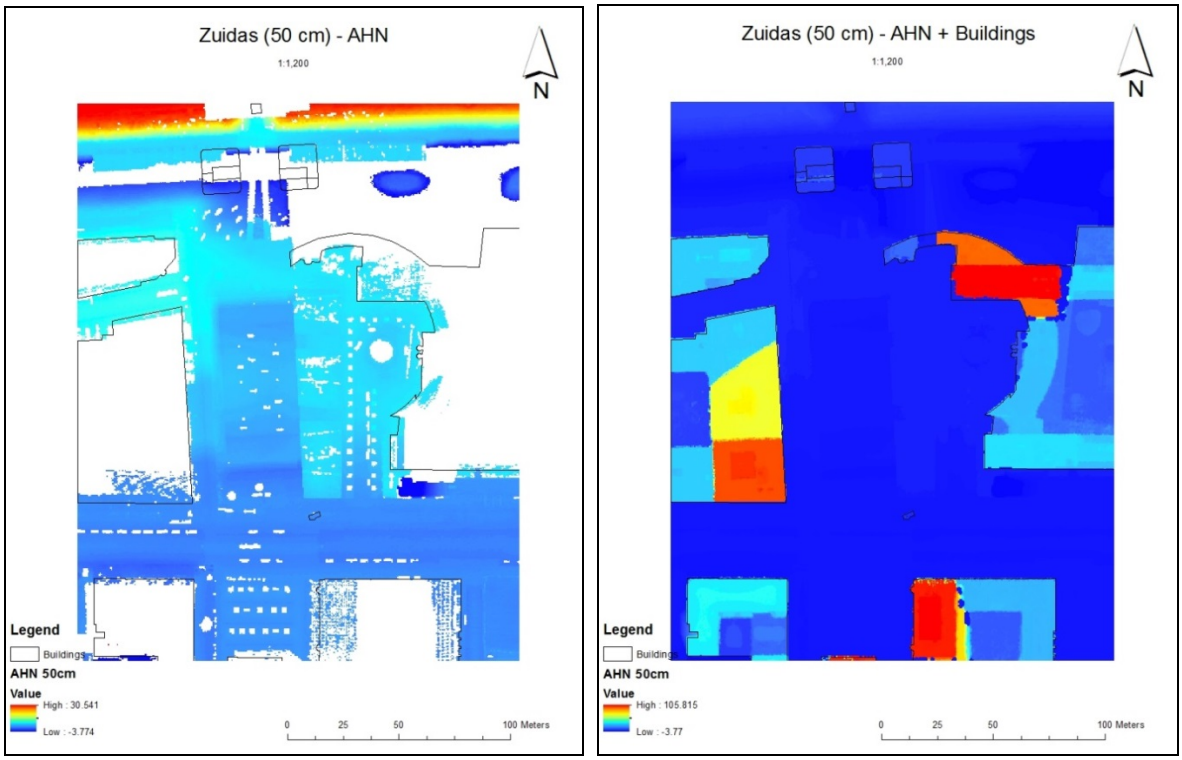

Figure 13: The AHN data only contains ground level data (left) for use within the model a closed grid is required. Merging the AHN ground data and the SGM spatial objects data form a closed grid (right).

3.1.2 DEM accuracy testing

After the DEM construction the accuracy of all the DEMs (each of the SGM resolutions and AHN2) was tested (fig. 11). This answered the first sub-question (chapter 1.3). The DEMs were tested by comparing them with the datasets of manually measured elevation data. In the municipality of Amsterdam the engineering bureau has gathered land data with exact heights. For the research area these were gathered in a map with elevation data of the ground and spatial objects. There are over 2500 known data points. All the 2500 measurements were compared with the constructed DEMs.

The bias adjusted RMSE (root mean square error) was one of the outcomes of the DEM accuracy test. First the mean bias error (MBE) (eq. 1) was calculated to remove the bias in the RMSE (eq. 2). The MBE is calculated in meters. The bias was removed as there can be a systematic error between the two datasets.

Eq. 1: $$MBE = \frac{\sum_{i=1}^{n}(O_i - H_i)}{n}$$

n = number of observations
i = location of the height measurement
O = height from land survey measurements (m)
H = height from SGM or AHN2 (m)

The bias-adjusted RMSE was used to show the standard deviation between the sample (constructed DEMs) and the observed data (land survey measurements) (eq. 2). To obtain a bias adjusted RMSE the height from SGM of AHN2 (H) was adjusted with the MBE.

Eq. 2:
$$RMSE = \sqrt{\frac{\sum_{i=1}^{n}(O_i - (H_i - MBE))^2}{n}}$$

n = number of observations
i = location of the height measurement
O = height from land survey measurements
H = height from SGM or AHN2

Equation 3 is the mean absolute error (MAE) which is another measure to observe how close the land survey measurements (O) are to the elevation values from SGM or AHN2 (H). It is the average of the absolute errors.

Eq. 3:
$$MAE = \frac{\sum_{i=1}^{n}|O_i - H_i|}{n}$$

n = number of observations
i = location of the height measurement
O = height from land survey measurements
H = height from SGM or AHN2

The coefficient of determination (R^2) was also included to compare the observed data (land survey measurements) with the elevation values from the SGM and AHN2. The R^2 can range from 0 to 1, the higher the R^2 the closer the observed data fits the simulated data (SGM or AHN2 elevation values).

Special attention was paid to the AHN2 due to the age of the digital elevation model. The land measurements are from 2013, while the AHN2 data was from 2008 (Van der Zon, 2013). It was possible that certain areas have changed in the Zuidas. Thus close attention was paid to large differences between the datasets. Some of these outliers were removed, after inspection of aerial photographs and construction plans. Further profiles are constructed from the land survey measurements and the constructed DEMs to visually compare the elevation values. Over the width of a street two profiles were constructed to compare the DEM construction methods and the DEM grid cell size to the land survey measurements.

3.1.3 DEM derivatives

Next to the RMSE of the elevation values also the catchment area and flow patterns of the different DEM resolutions were compared. This gave insight into the possible importance of resolution for the study site. Usually a decrease in resolution (larger grid sizes) results in a loss of information (Kuo et al., 1999). For a DEM this can mean that its derivatives, slope and aspect, can change when peaks or valleys are not adequately represented due to the larger grid size. A change of slope and aspect can result in different flow patterns (Bruneau et al., 1995). This made it important to know if the resolution influences the flow pattern and thus the catchment area in urban system. Kienzle (2004)

already stated that raster resolution has a profound effect on DEM derivatives, only in his research the highest resolution was 5 m.

Catchments areas were determined within the PCRaster program. The program determines the catchment area with help from the constructed DEMs. First the local drain direction (ldd) was determined. The ldd is explained later in the hydrological model section (3.3). The ldd was used to help determine the catchment area. In the research it was presumed precipitation that falls within the catchment area will stay within the area. This was off course only a modeling assumption as in reality other effects (e.g. wind, or man-made drainage systems) could change the flow of water.

The catchment area of the several DEMs was also visually compared to see differences in size, change in number, and the interaction with the objects on the topographic map (GBKA). Histograms were created for slope, to show the changes when increasing grid cell size or using different DEM sources. A histogram is a graphic representation of the frequency of certain data. It gives an overview of the distribution of the data, making it possible to compare to compare the data. In the case of slope, classes are created for every 5 percent interval. For each class a count was made of the number of cells that fall within that class. As the four grid sizes do not contain the same number of cells they were adjusted to the number of cells in the 100 centimeter grid (i.e. 25 cm grid was divided by 16, 50 cm grid was divided by 4, 2 meter grid was divided by 0,25). Catchments areas smaller than 100 m^2 were not included to mitigate the border effect. During catchment area determination the border of a grid acts an artificial boundary for the water. This results in very small catchment areas which in reality does not exist.

3.1.4 DEM choice

Taking the outcome of the DEM accuracy test and looking at the differences in DEM derivatives a choice was made which DEMs were used for the simulations in the hydrological model (fig. 12). Using all the available DEMs would result in too many simulations in the time available for the research. The choice was determined firstly on filtering, secondly on the DEM construction methods, thirdly on the thinning process. If the unfiltered DEMs gave the same result in the accuracy test as the filtered DEMs they would also be used for the hydrological simulations. Secondly one of the four DEM construction methods was chosen for use in the model. This depended partly on the coefficient of determination (R^2) and lowest bias-adjusted RMSE with the land survey measurements. Thirdly the choice was made if the available DEM sources should be reduced. Three sources were available: Lidar AHN, SGM 80 points/m^2, and SGM 10 points/m^2. Lidar AHN and SGM 80 were already decided beforehand to be used. The SGM 10 was dependent on the difference in results with the SGM 80 in the accuracy test. Otherwise it would give no added value to the study. All of the four different resolutions were used in the hydrological model to test grid size.

3.2 Rainfall-runoff model

The rainfall-runoff model used the constructed digital elevation models to predict water problems in urban areas (fig. 14). The urban hydrological model was constructed in PCRaster. PCRaster is a software program for environmental spatial temporal modeling. For this research it was used in conjunction with Python. Python is a scripting language which helps automate the modeling process. The model input include a DEM, a map containing the Manning's n for surface roughness, a map for the runoff infiltration rate, and a precipitation time series. The model was raster based and required an initial map (called a clone map in PCRaster). This initial map determines the extent of the model

area. The constructed DEMs was used as initial map, for each of the study areas and each of the resolution an initial map was needed.

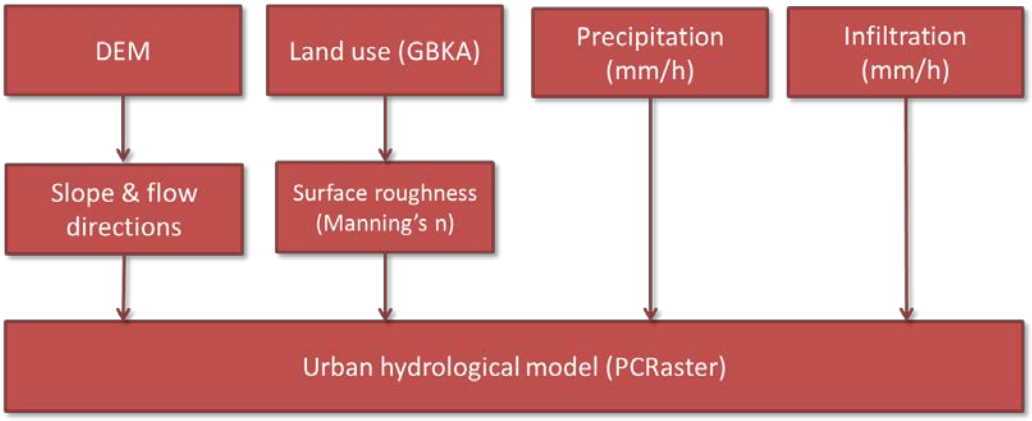

Figure 14: Overview of PCRaster model

The DEMs constructed in section 3.1 were tested in the PCRaster model (fig. 15). It was assumed that all precipitation that falls on rooftops would gather there before it flows directly in the sewage system, thus it will not be used in the runoff-ponding simulation. Furthermore rainfall and discharge on open water was not included. Flow in the model was simulated with Manning's equation for flow (eq. 5). The sewage system (storm drains) were not simulated in the model. This is due to the complexity of including this and the theory that even if included it will never work as effectively as expected (Dottori et al., 2013). Water was able to infiltrate with a fixed rate in the model depending on the type of land cover (table 2). Time step of the model was in seconds.

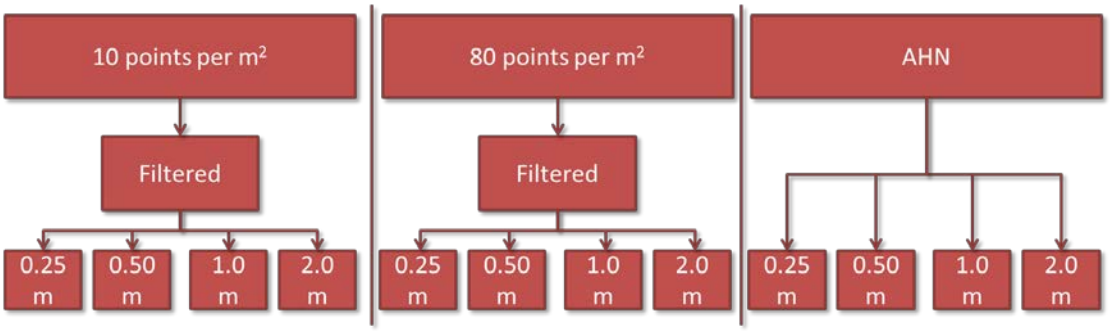

Figure 15: The chosen DEMs after the accuracy testing

Table 2: Overview of infiltration rate and Manning's n per land cover

Land cover	Infiltration (m/h)	Manning's n
Building	-	0.99
Paved	0.001	0.01
Unpaved (grass)	0.050	0.30

To use the constructed DEM grids within PCRaster they were converted to the PCRaster map format. The constructed DEMs are in Tiff (Tagged Image File Format), which is not readable within PCRaster. The Tiff was converted to an ASCII file with xyz data, which basically is a text file with space-separated columns containing coordinates and elevation values. Multiple GIS software programs are

capable of this (i.e. Q-GIS, ESRI ArcGIS). Important in the ASCII is the information that is needed about the extent of the Tiff file. This includes the number of rows and columns, the upper left x and y coordinates of the grid, and the length of the cells. The ASCII file could then be imported within the hydrological model script, where it was converted to the PCRaster Map format.

The Manning's equation for flow was used to simulate the surface flow (eq. 4) (Chow et al., 1988). It is a simplified flow equation that only includes the slope between cells (including the water level) and the roughness factor flow by Manning (n). The discharge (Q) depends on the surface area where the water flows. The water surface (A) and the cross-section (R), together with the water slope (between the cells) are used to determine the discharge. The simplified shallow water equation used assumes that all terms except friction (Manning's n) and slope are not important.

Eq. 4: $$Q = \left(A * \sqrt{S} * R^{\frac{2}{3}}\right)/n$$

Q = discharge per cell (m3/s)
A = wetted surface (m^2)
S = water slope surface (-)
R = wetted perimeter (m^2)
n = Manning coefficient

For use within the model equation 4 was adapted into a PCRaster function (fun. 1). The wetted surface (A) is dependent on Alpha, which is a variable for surface roughness and discharge which is limited by the flow width. Alpha is based on slope (S), Manning's n, the wetted perimeter (R) and the width of the water flow (beta). The slope in the model includes the water level and the DEM at each time step.

The kinematic wave formula from de Roo (1998) was adapted for use within the hydrological model. PCRaster includes the kinematic wave equation as a function call in its modeling environment, also providing the direction of flow with the ldd. The side flow (q) is not used in this model. The beta coefficient is constant (0.6), this value is used for broad sheet flow like overland flow (de Roo, 1998).

Fun. 1: Q = kinematic (ldd, Qold, q, Alpha, Beta, NrTimeSlices, ΔT, ΔX)

ldd = local drain direction
Qold = discharge at previous time step (m^3/s)
q = side-flow
Alpha = alpha coefficient (-)
Beta = beta coefficient (-)
NrTimeSlices = number of iterations
dT = time step (s)
dX = cell length

The flow direction was determined with the function ldd (local drain direction) within PCRaster. Figure 16 shows an example grid with elevation values. For each cell the slope to its neighboring cells was determined, the steepest slope determines the eventual flow direction. Only one direction is possible, if two cells have the same steepest slope, the last compared cell is chosen. Figure 16 also shows the 8 possible flow directions in the right image. The numbers show the order in which the

cells are compared. If no neighboring cell is lower, the cell is defined as a pit or sink, shown in figure 16 as blue rectangle cell. Only when the water level in the pit rises above the water level in a neighboring cell flow direction will change. For every time step a new local drain direction map was generated from a map which combines the DEM and the water level (delta h) at the time step.

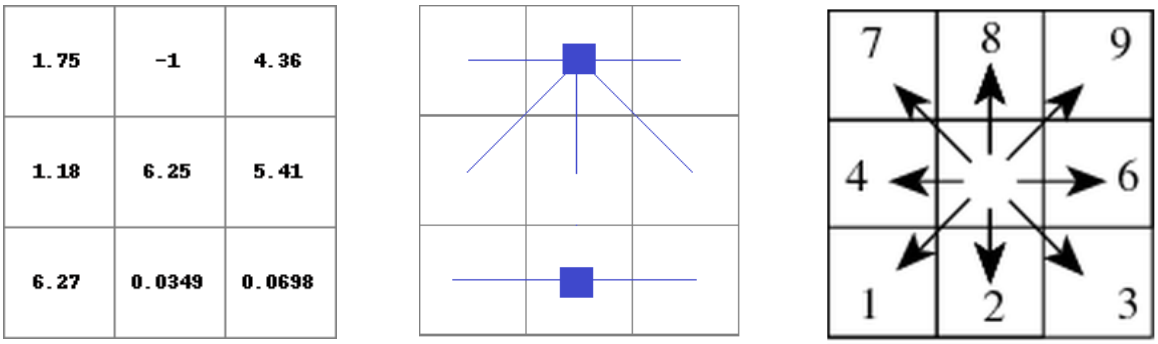

Figure 16: Example of determining flow direction within PCRaster. Image 1 shows the elevation values, image 2 the direction of flow towards a pit, and image 3 the possible flow directions (source: pcraster.geo.uu.nl).

3.3 Model simulations

The last research question deals with the analysis of the models output (chapter 1.3). Figure 17 shows a detailed overview of the third stage of the research. As there was no known gauged data for discharge and water depth available, the conducted research became a benchmark test for the constructed DEMs within the urban hydrological model.

3.3.1 Comparison tests

An analysis was performed by using the outcome of the highest resolution DEM available (25 cm) as a reference. In theory the highest resolution will have the most similarity with reality. In the city of Amsterdam there are known areas where water gathers on the streets during storm events. This information was used to assess the model output.

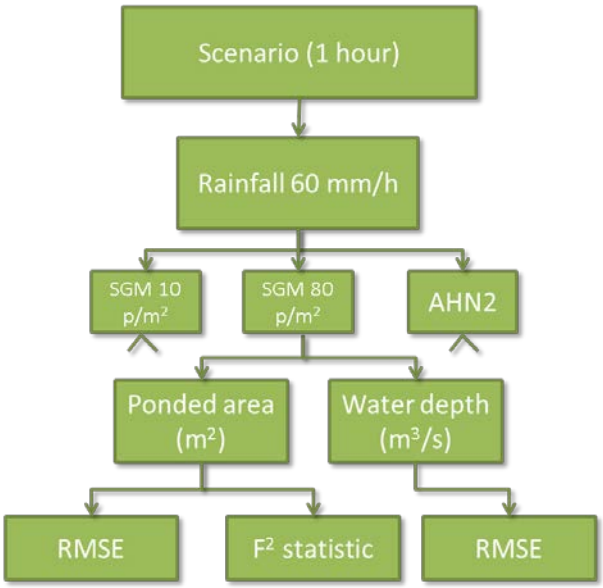

Figure 17: Workflow of the model run and the testing of the output

The methodology used in the research of Fewtrell et al. (2011), who also had no access to gauged data, was used as a blueprint. RMSE was used to show the difference between the reference grid

(the highest resolution) and the other grid sizes (eq. 2). This was done by testing both the average water level and the ponded area. One scenario was performed to test the model and the constructed DEMs. The scenario is the once in a 100 years rainfall event, which is a storm event of 60 mm/h. The model was limited to a stationary input of precipitation. A model run lasted 1 hour, after which the average water level per minute was determined. The time step in the model was 1 second.

The models output (the number of ponded cells) was compared with the F^2 statistic to understand how the DEM sources and the four grid scales were related to each other (Aronica et al., 2002; Werner et al., 2005). The F^2 statistic looked at the flooded or ponded area that is considered wet and the spatial similarities (eq. 6 + 7). A value of 1 is given to the parameter if it fits the observation (table 3). In the F^2 statistic a value of 1 means that predicted and observed values perfectly overlap. While a value of -1 means no correlation at all between the predicted and observed values. The F^2 statistic was chosen as it takes the spatial distribution into account by comparing the cells of two grids at the same location.

Eq. 6: $$F^2 = \frac{A^{ref} \cap A^{mod}}{A^{ref} \cup A^{mod}}$$

In equation 8 A^{ref} is the ponded area of the reference grids size, and A^{mod} the ponded area in the other modeled grids. The F^2 statistic determined the ratio between the number of cells that have the same outcome in both the reference as the other grids resolutions. Thus understanding the similarities between the different resolutions. Equation 6 was reformulated as the following:

Eq. 7: $$F^2 = \frac{\sum_{i=1}^{n} P_i^{D1M1} - \sum_{i=1}^{n} P_i^{D0M1}}{\sum_{i=1}^{n} P_i^{D1M1} + \sum_{i=1}^{n} P_i^{D1M0} + \sum_{i=1}^{n} P_i^{D0M1}}$$

The formula in equation 7 explains in detail how the grids were compared. P is the accumulated value of the number of cells that are given a value of 1 for either both wet (D_1, M_1), or differ in both models (D_0M_1, D_1M_0) (table 3). The time step is given with i, making it is possible to show over time how the F^2 statistic changes. In this research only the situation at the end of the model run was used. The number of pixels is given in n. If none of the cells in both the reference and model were ponded (D_0M_0) the (simplified) F^2 equation could not be used (eq. 7). In this study ponding always took place. The overlapping dry cells are excluded from the equation, as there is only interest how the ponded cells overlap.

Table 3: Matrix of available combinations in the F^2 statistic

	Dry in model (M0)	Wet in model (M1)
Dry in reference model (D_0)	not applicable	D_0, M_1
Wet in reference model (D_1)	D_1, M_0	D_1, M_1

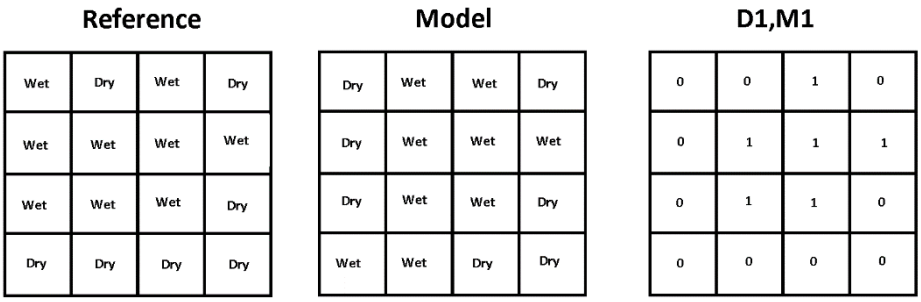

Figure 18: Example of the F^2 statistic

The example in figure 18 shows two grids (reference and model) with the observation of D_1M_1. The values to fill in the equation (8) are: $D_1M_1 = 6$, $D_0M_1 = 3$, $D_1M_0 = 3$. This results in a F^2-statistic of 0.75.

A problem that occurs when using different resolutions and the F^2 static is the lack of same sized grid cells. Thus to adequately use the method the observed grids model output were downscaled to the grid size of the reference DEM, because of the downscaling no essential information was lost (fig. 19).

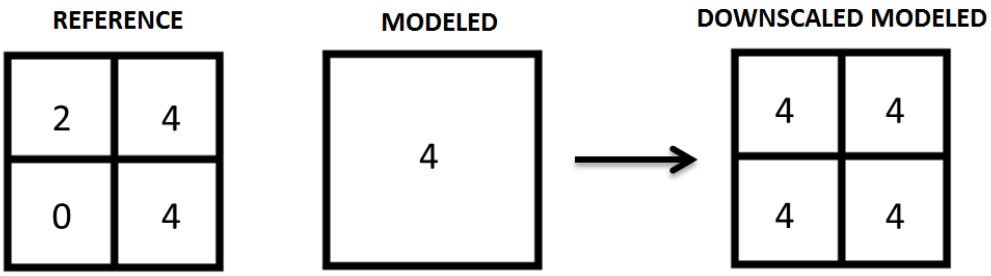

Figure 19: Example of grid resampling for comparison statistic

3.3.2 Effect of resolution on the hydrological model

To understand the influence of the DEM sources (AHN, SGM 80 p/m^2, or SGM 10 p/m^2) the DEMs were resampled and aggregated. Resampling was shown in figure 19 of the previous section. Aggregation is the other way around, i.e. upscaling the grid (fig. 20).

When resampling to a higher resolution the output of model (water and ponded area) was compared to understand the influence of grid size. If aggregating to a lower resolution the hydrological model should give the same output (water level and ponded area). If not the hydrological model does not function correctly or the influence of resolution is greater than expected.

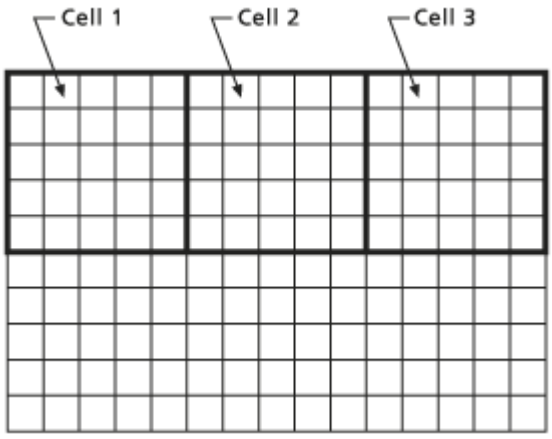

Figure 20: Upscaling the grid, the starting grid from 10 by 15 is aggregated to 2 by 3.

3.4 Study site

To understand the influence of the DEMs topographical complexity on the results two different urban areas were selected. The areas are the business area Zuidas and the residential area Rivierenbuurt (fig. 21). Both sites are situated in the city of Amsterdam.

The Zuidas is an area in development. The current estimates are that the plans are completed by 2035. The Zuidas holds high-rises (e.g. WTC Tower, ABN AMRO building), 10 football fields, and many other office buildings. Furthermore there are several parks and open (construction) areas. Although it is mostly a business area, there are some residential buildings. Much of the existing situation will change in the coming years, making the (outdated) AHN2 irrelevant for this site.

The second area is the Rivierenbuurt, which was built in the 1920's and 30's. This area is a more typical residential area with some wide streets (with tramlines), densely placed buildings, some surface water and many trees. During the storm event of July 28th 2014 this area dealt with extreme rainfall runoff and ponding problems.

For both areas a study area of ± 1 km^2 was chosen to model the effects of rainfall in the area (fig. 21). The exact study area in the study site was determined in PCRaster depending on the upstream catchment area. This is the hydrological defined area which contributes to the water flow.

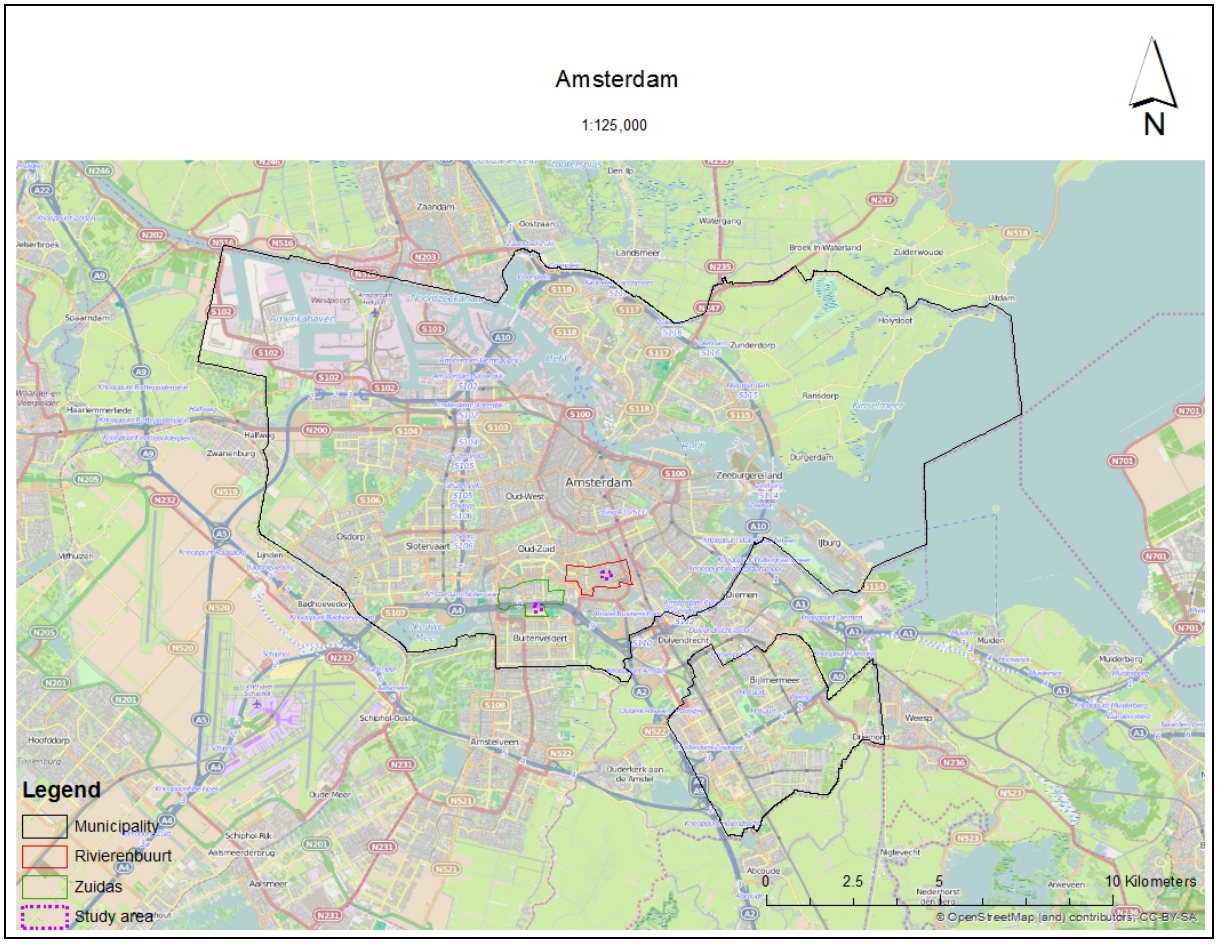

Figure 21: Municipality of Amsterdam with the neighborhoods Rivierenbuurt (red) and Zuidas (green), and the two study areas (purple) highlighted.

3.5 Software

- ERDAS IMAGINE 2014 for point cloud construction, classification and filtering.
- A GIS program capable of raster construction from point clouds (e.g. ERDAS IMAGINE, ArcGIS, Neuron GIS, Qgis, FME). Most of the maps were made with ArcGIS 10.2.2.
- PCRaster and Python. The rainfall-runoff model was constructed in this program. Idle was used as a Python shell. The flow direction and catchment area was also determined with the PCRaster functions.
- Microsoft Excel and PCRaster were used for the comparison analyses (F^2 statistic and RMSE).

3.6 Data

- The topographic map used for the land use is the GBKA (Grootschalige Basiskaart Amsterdam). From this map, the Manning's n and the infiltration rate was determined. The GBKA is updated frequently from the aerial photographs and from buildings plans. It is also used to help in the classification process of the point clouds. Topographic maps in the Netherlands are highly detailed and under lot of scrutiny as they are used for official purposes by institutions like the cadaster to maintain property rights.
- The SGM point cloud were constructed from digital aerial photographs available at the municipality of Amsterdam. The photographs were taken in March and April 2014. The resolution of the photographs is 10.7 cm. The average flying height when the photographs

were taken was 4350 m. The flying height was limited due to the proximity of the airport Schiphol. The municipality lies within the Control Zone (CTR) where it is not allowed to fly lower due to the landing zone of the other aircrafts (fig. 22). The flying height limits the resolution to 10.7 cm. The general flying height in other parts of the Netherlands is 1200 m making resolutions possible up to 3 cm.

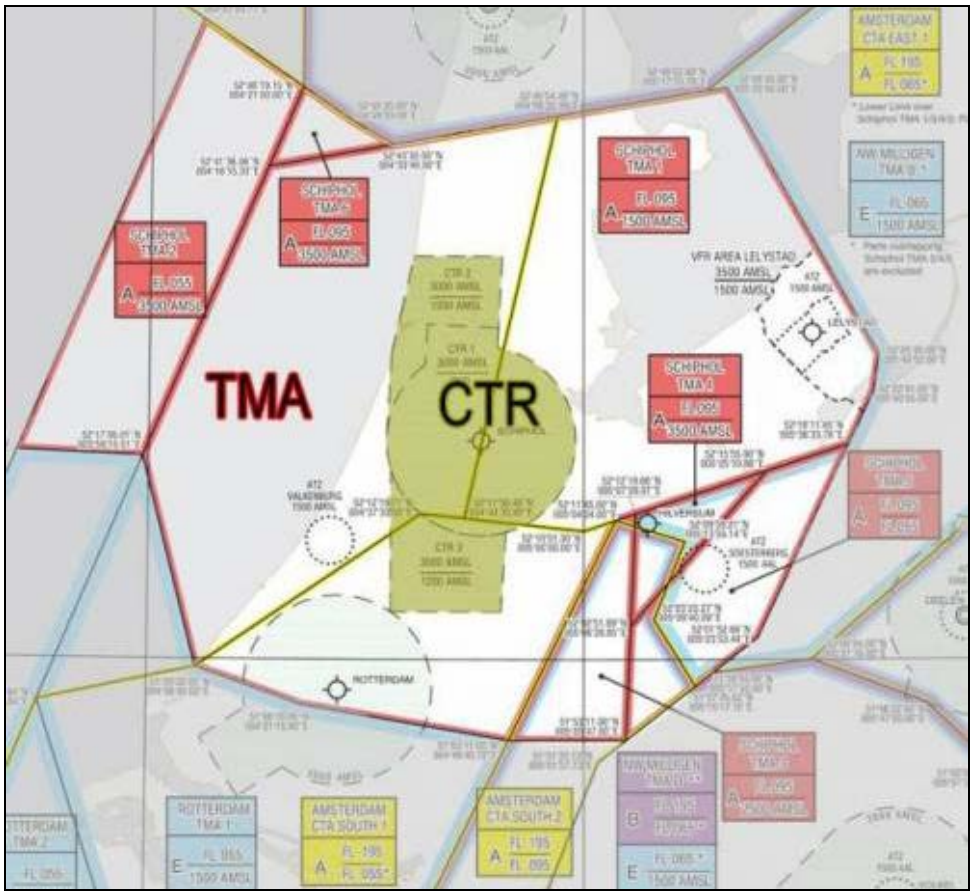

Figure 22: The Control Zone (CTR) limits flying height for the aerial photographs to 14.000 feet (4250 meter) (source: Dienst Basis Informatie, Amsterdam)

- The accuracy of the DEM was tested with known elevation data (available at the municipality). This land survey data was gathered in a file with X and Y coordinates. Figure 23 shows a map with the location in the Zuidas area.

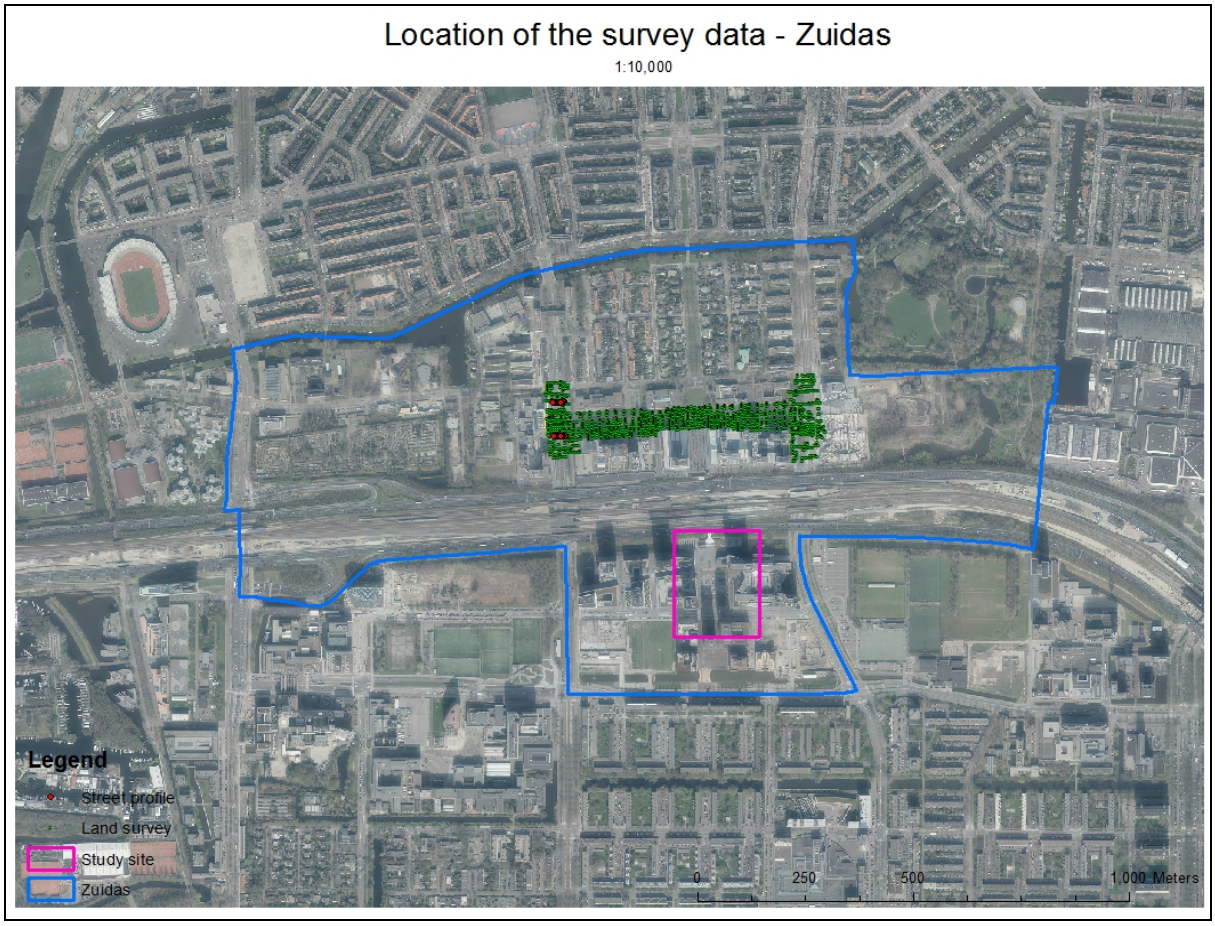

Figure 23: Location of the survey data in the Zuidas neighborhood (green and red dots). Red dots are the survey data used for the street profiles.

4 RESULTS

4.1 DEM construction and accuracy

4.1.1 Point clouds to DEM

The digital elevation models were derived from the aerial photographs. Elevation maps of the Rivierenbuurt and the Zuidas are shown in figures 24 and 25. Both of these were constructed from the unthinned SGM (80 p/m^2) point cloud. The DEM construction method used was the averaging method and linear void fill. In both of the maps the elevation values are limited to show the fluctuation of the surface. A thin outline represents the location of buildings taken from the topographic map (GBKA). Outside of the line small red patches can be determined, these patches are either vegetation or parked cars. Only 'soft' filtering was performed on these DEMs. To the east, the Amstel river is located. This is represented by the blue patches. The SGM method, like Lidar, is not able to measure water correctly. It results in a noise ridden dataset, making it impossible to detect the real elevation height. A small road can be seen in this noise, which is the bridge over the Amstel.

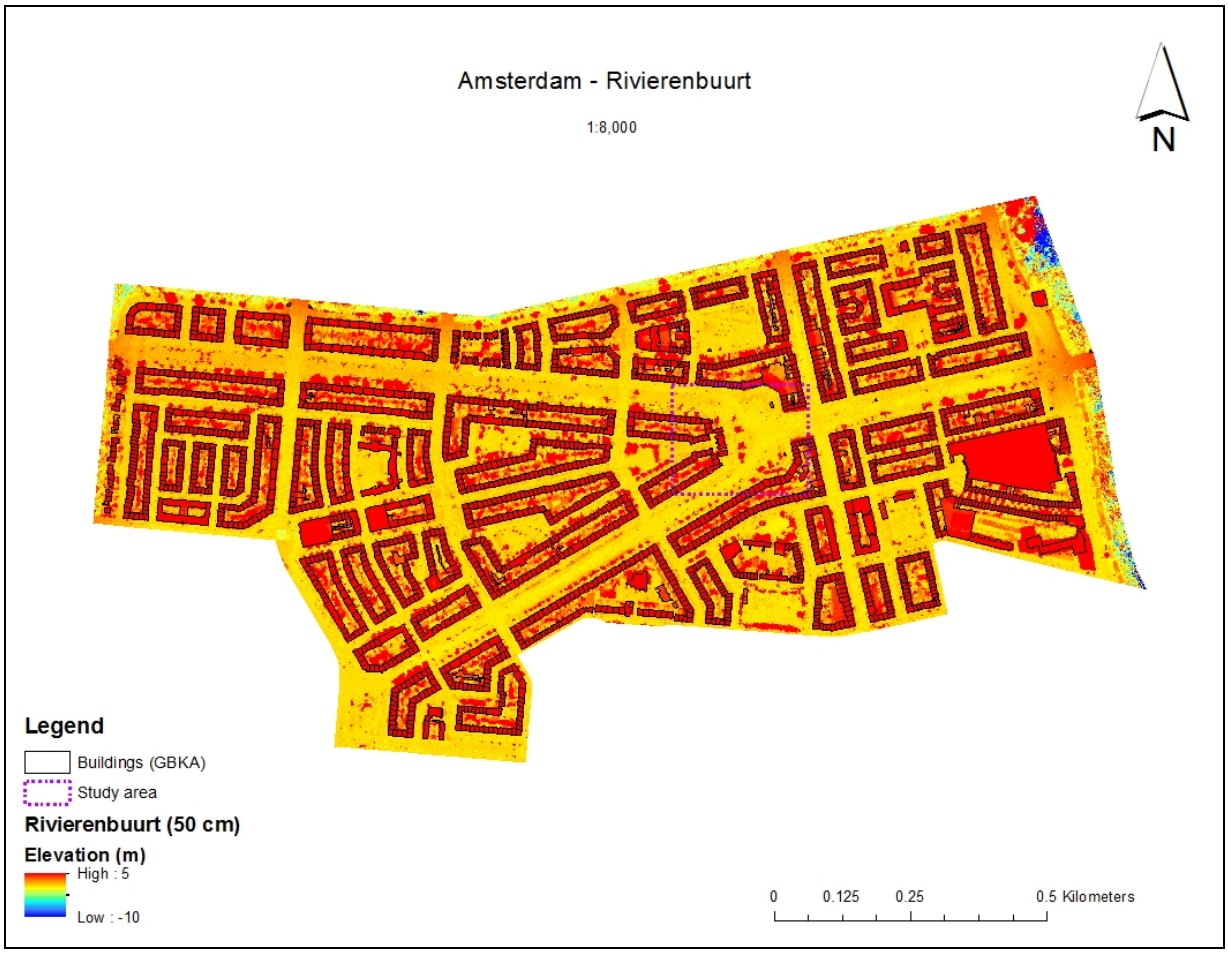

Figure 24: Elevation map of the Rivierenbuurt (SGM 80 DEM 50 cm unfiltered)

The Zuidas area looks different than the Rivierenbuurt. This area lacks vegetation around buildings. Almost no dark red patches of outliers (i.e. trees) can be seen around the buildings in the south of the map. The blue areas in the Zuidas map are not waterbodies. They lack the noise usually associated with water. The two areas here are construction sites, which both are in early development and lie lower than the other parts in area.

Figure 25: Elevation map of the Zuidas (SGM 80 DEM 50cm unfiltered)

The exact study sites in the Rivierenbuurt and the Zuidas used are shown in figures 26 to 29. These images provide more detail and a closer view of the surface in the DEM. Here the SGM DEM is compared with the AHN2 DEMs. The elevation values of the buildings in all four of the DEMs was taken from the SGM point cloud as the AHN2 dataset lacks this data. In all four DEMs the elevation was maximized at 2.5 meters to show the fluctuation in the ground level. All four DEMs were constructed with the same technique (averaging and linear void fill).

The two SGM DEMs have noticeable patches in the map. The dark blue area in figure 26 represents the road. With some effort the verge of a road can be determined. Looking at figure 27, the verge is much more pronounced. The road, and all of the surface area, looks much smoother in the AHN2 DEM. The patchiness in the SGM DEM partly comes from the vegetation in the verges and the backyards, these were manually filtered out of the point cloud. The AHN2 Lidar point cloud was already filtered during the remote sensing to easily represent a 'bare earth' dataset.

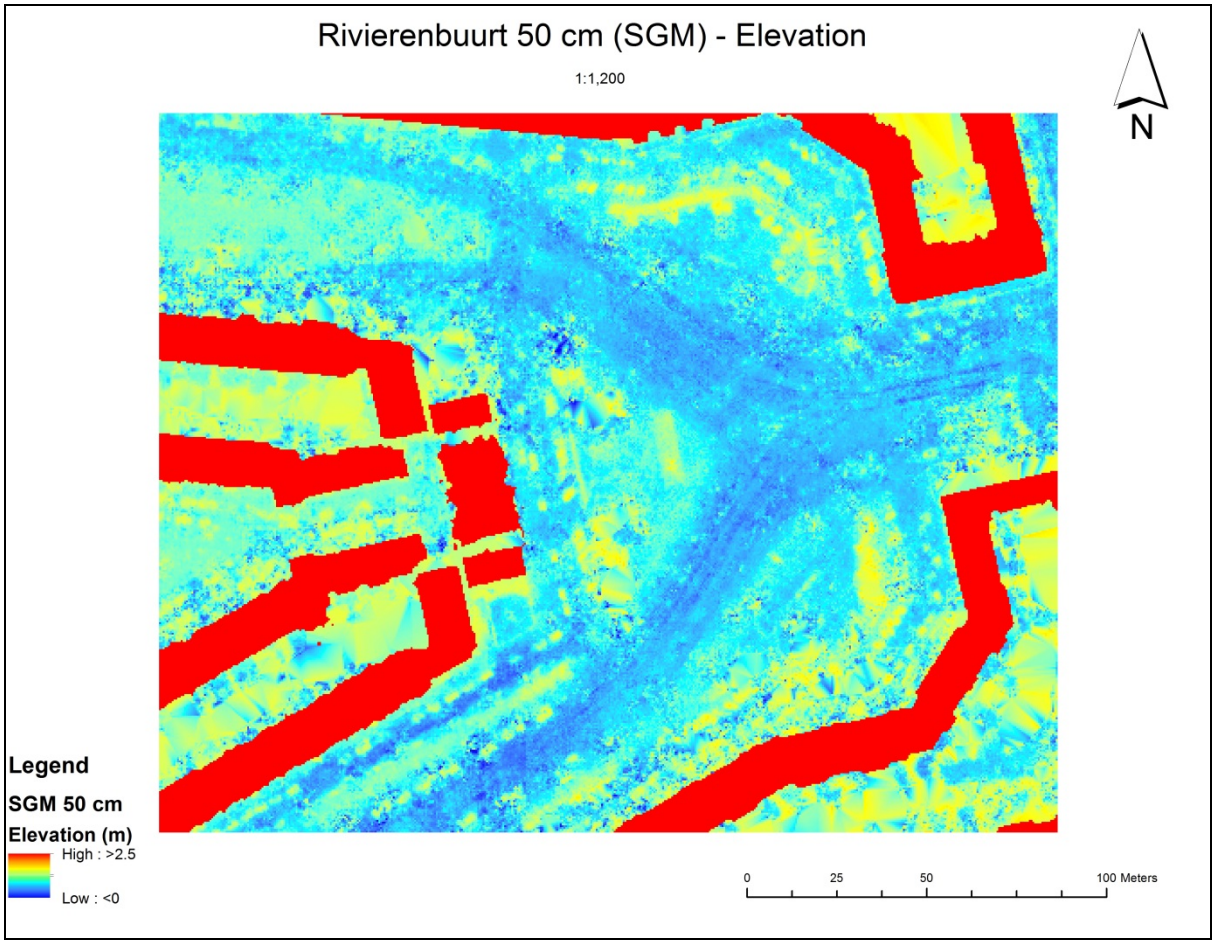

Figure 26: Elevation map of the Rivierenbuurt study site (SGM 80 DEM 50 cm)

In the AHN DEM of the Rivierenbuurt the courtyards of the house can neatly be distinguished from each other (fig. 27). As Lidar can see through vegetation it gave a clearer view of how the surface looks behind the houses.

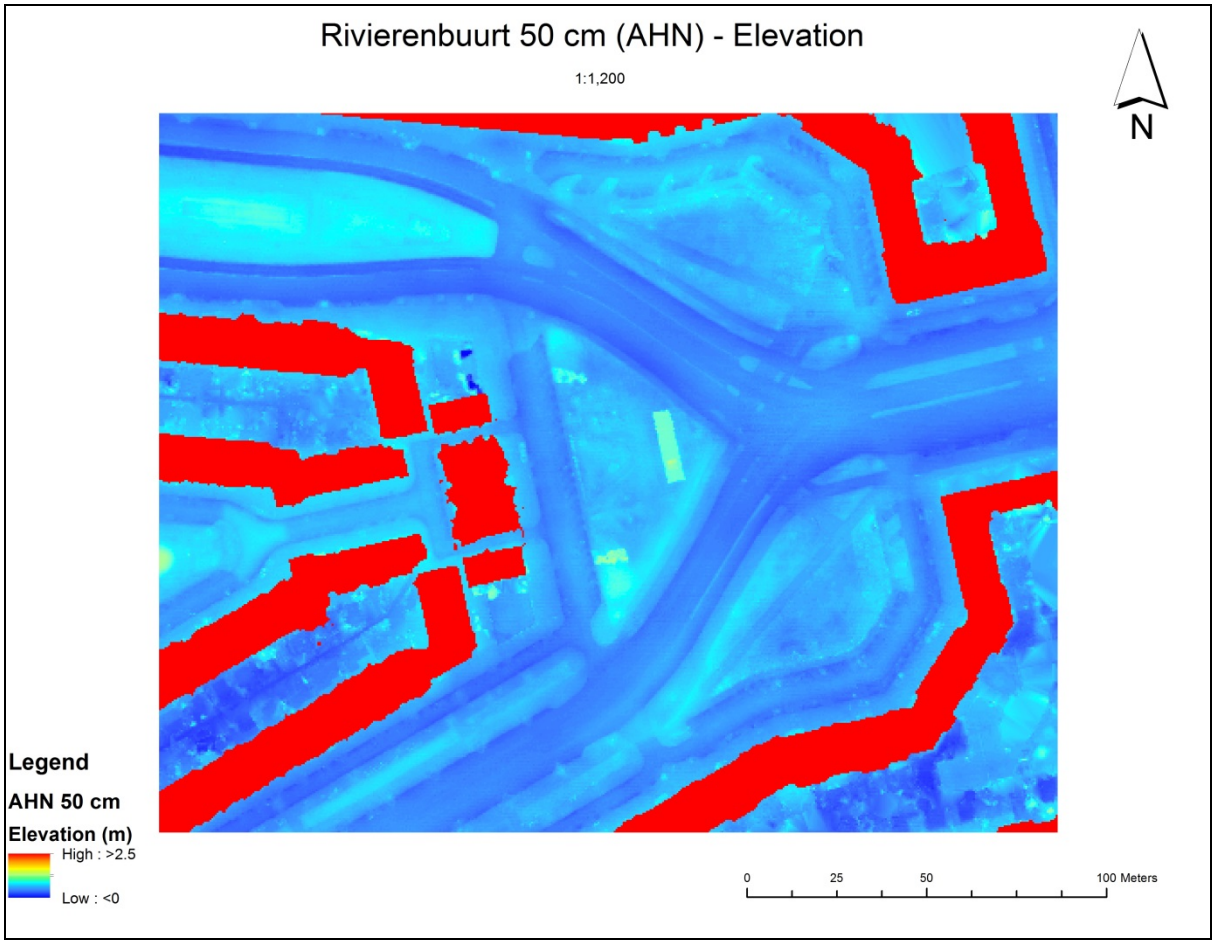

Figure 27: Elevation map of the Rivierenbuurt study site (AHN 50 cm). Buildings in AHN are taken from the SGM point cloud.

The Zuidas SGM DEM shows the same unstructured patches as the Rivierenbuurt. Only in this area the patches came from a different source. In the Rivierenbuurt vegetation in the verges of the road resulted in noise, here shadows from the high rises made it difficult to create a smooth dataset. On the north side of the buildings small patches of dark orange can be detected. In these areas shadow is cast by the buildings on the surface. In the AHN2 DEM (fig. 29) only a smooth surface is seen as Lidar is not bothered with shadow. Lidar does have trouble when no laser signal is received back. High rises can obstruct the view of the surface, but this problem also occurs in aerial photographs with tall buildings.

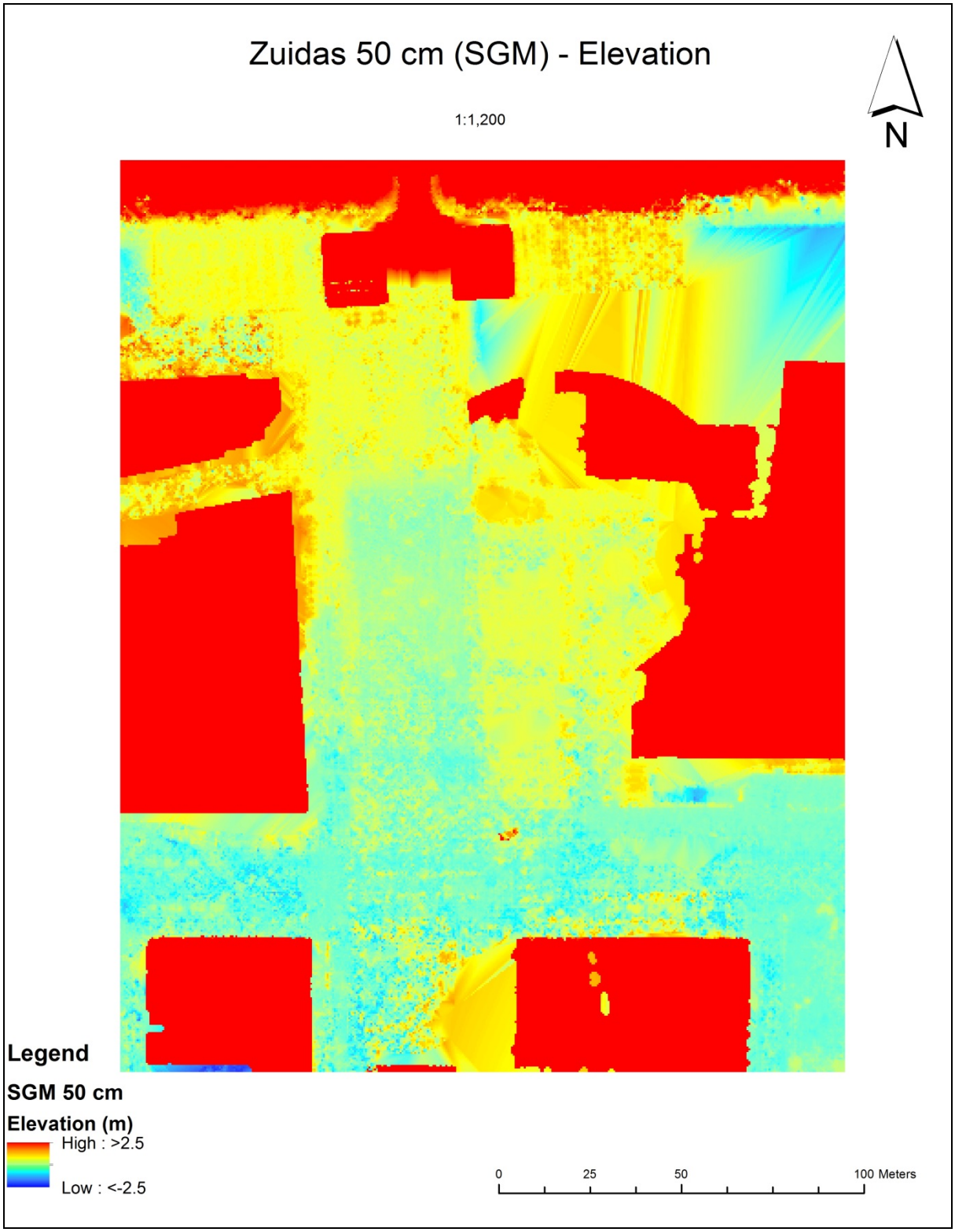

Figure 28: Elevation map of the Zuidas study site (SGM 80 DEM 50 cm)

The dark blue patches in the north of the AHN2 DEM are water bodies and the entrance to the train station (fig. 29). The Lidar dataset was better in dealing with the slope around the water bodies. The shore around these waterbodies also suffered from noise in the SGM point cloud. Making it quite possible that too many points in the SGM point cloud were filtered and the slope between

waterbody and surface was removed. Thus making the existence of a waterbody unnoticeable in the SGM DEM.

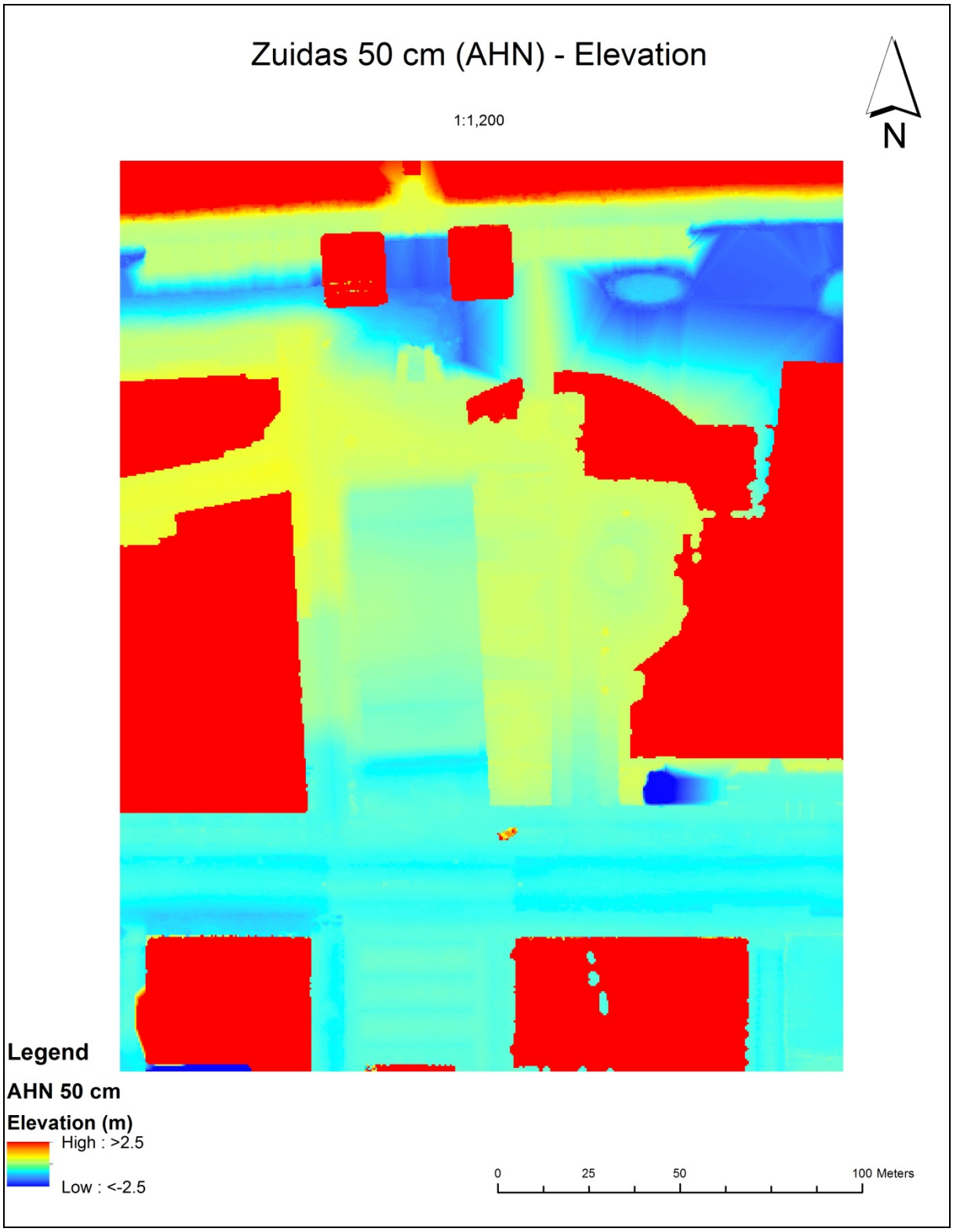

Figure 29: Elevation map of the Zuidas study site (AHN 50 cm). Buildings in AHN are taken from the SGM point cloud.

4.1.2 DEM accuracy test

2500 Land survey measurements were used to test the accuracy of the constructed SGM DEMs (thinned and unthinned) and the AHN2 (50cm) (fig. 22). Table A-1 in Appendix A shows all of the accuracy test outcomes. The highest R^2, smallest bias, lowest mean absolute error, and lowest root mean square error (RMSE) was noticed for the AHN (fig. 30 + 31). For the constructed DEMs the largest difference was between the filtered and unfiltered DEMs. The filtered DEMs showed greater similarity with the land survey measurements. This was not surprising as the filtered data lacks vegetation and other non-ground objects except for buildings. Knowing that the unfiltered data does not resemble the land survey data it means that it can be excluded for the remainder of the research. The bias-adjusted RMSE is higher than the filtered data (1.7-1.8 to 0.8-0.9), and the R^2 is lower (0.30-0.33 to 0.65-0.70).

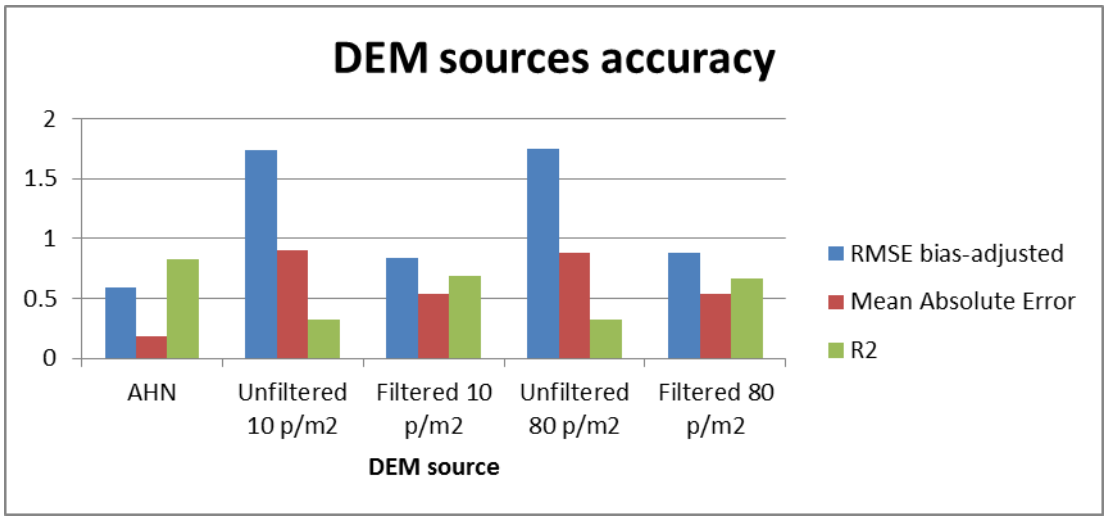

Figure 30: Accuracy of all the available DEM sources, all the resolutions are summed and then averaged. RMSE and MAE, closer to 0 is better. R2 is the coefficient of determination, closer to 1 is better.

The four different methods for DEM construction (IDW, averaging, linear void fill, and natural neighbor void fill) did not differ much (fig. 31 and 32). The change of the bias-adjusted RMSE ranged 0.08 between the DEM construction methods. Between resolution sizes the difference was also small only 0.12 for the bias-adjusted RMSE. The bias and MAE largely show the same difference between the land survey data and the constructed DEMs, a difference between 0.49 and 0.55. The number of points per s22quare meters shows a slight preference for the non-thinned point cloud (80 p/m^2). Overall the bias-adjusted RMSE is better for the non-thinned point cloud (maximum difference 0.08), but slightly worse when considering the R^2 (maximum difference 0.03).

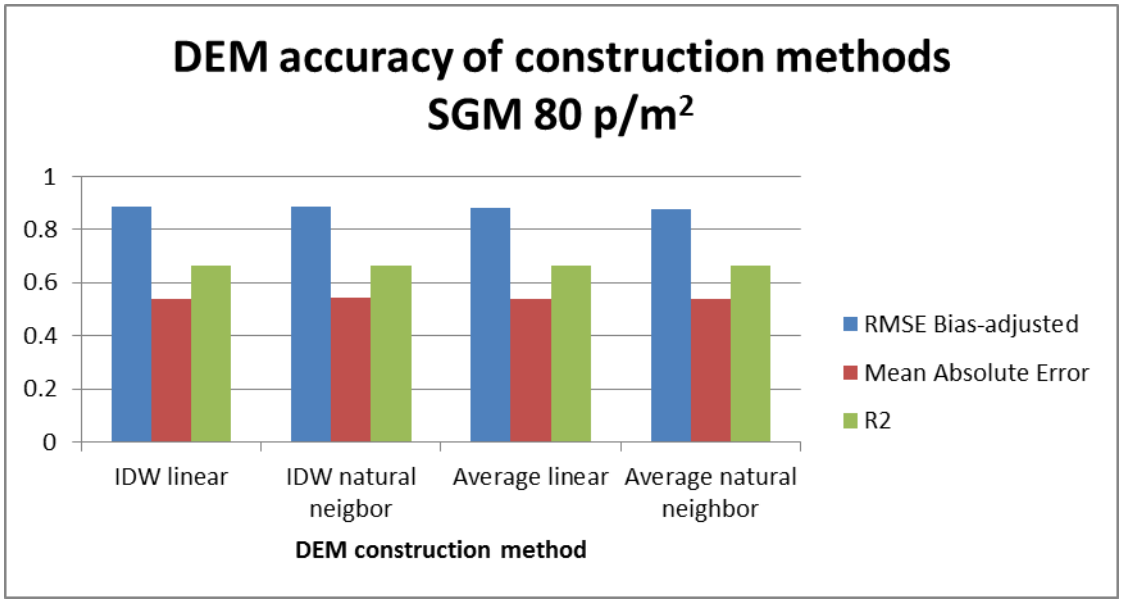

Figure 31: Accuracy of all the available construction methods for SGM 80 p/m^2. RMSE and MAE, closer to 0 is better. R^2 is coefficient of determination, closer to 1 is better.

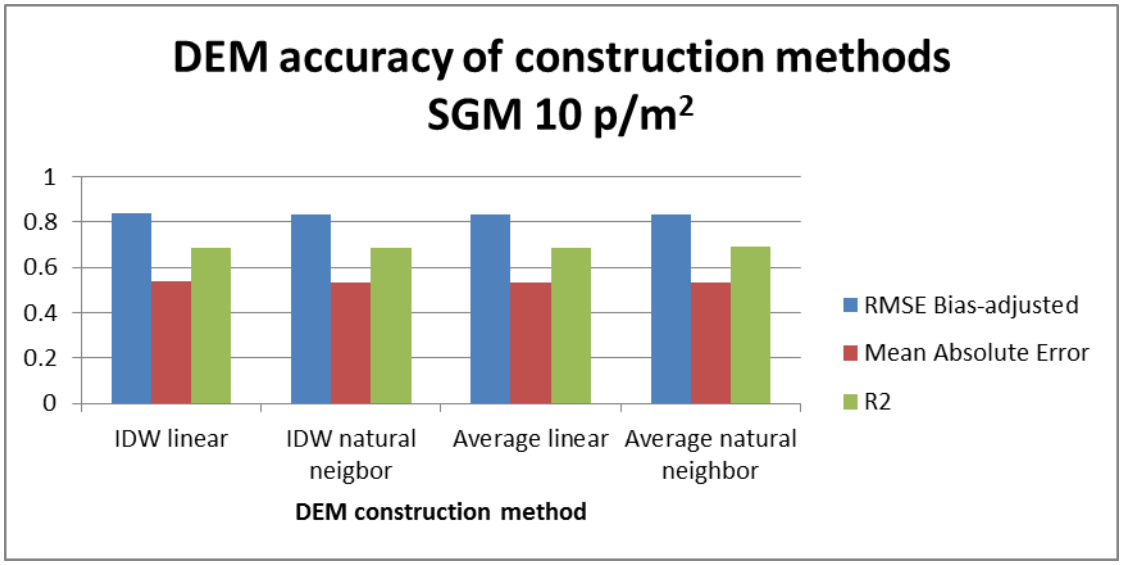

Figure 32: Accuracy of all the available construction methods for SGM 10 p/m^2. RMSE and MAE, closer to 0 is better. R^2 is coefficient of determination, closer to 1 is better.

Resolution was not important when comparing DEM accuracy. There was no clear change when scale was increased (fig. 33). Only the SGM DEMs were used for this comparison test as only the 50 cm AHN2 was available for this test. Most of the 2500 land survey measurements fall outside of the hydrological models study area.

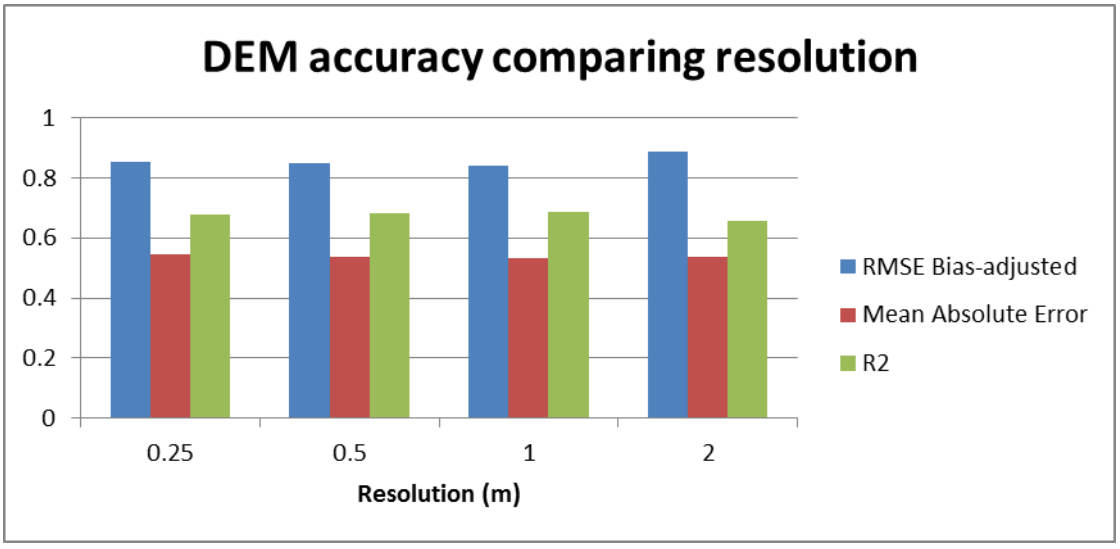

Figure 33: Accuracy of the available grid sizes compared. RMSE and MAE, closer to 0 is better. R^2 is coefficient of determination, closer to 1 is better.

To show the differences on a small scale two street profiles were made of the Parnassusweg in the Zuidas neighborhood. These show in detail the differences between the land survey data, the AHN2 and the several SGM DEMs (fig. 34)

Figure 34: Location of street profiles (Parnassusweg) in the Zuidas area.

The first profile showed great similarity between the DEM sources until the far right side of the street (fig. 35). At that location the AHN2 DEM shows a dip while the land survey measurement gives a peak. The peak can be traced back to a small area of grass. This peak was also shown in most of the SGM DEMs, only the 2 meter grid cells do not give this peak.

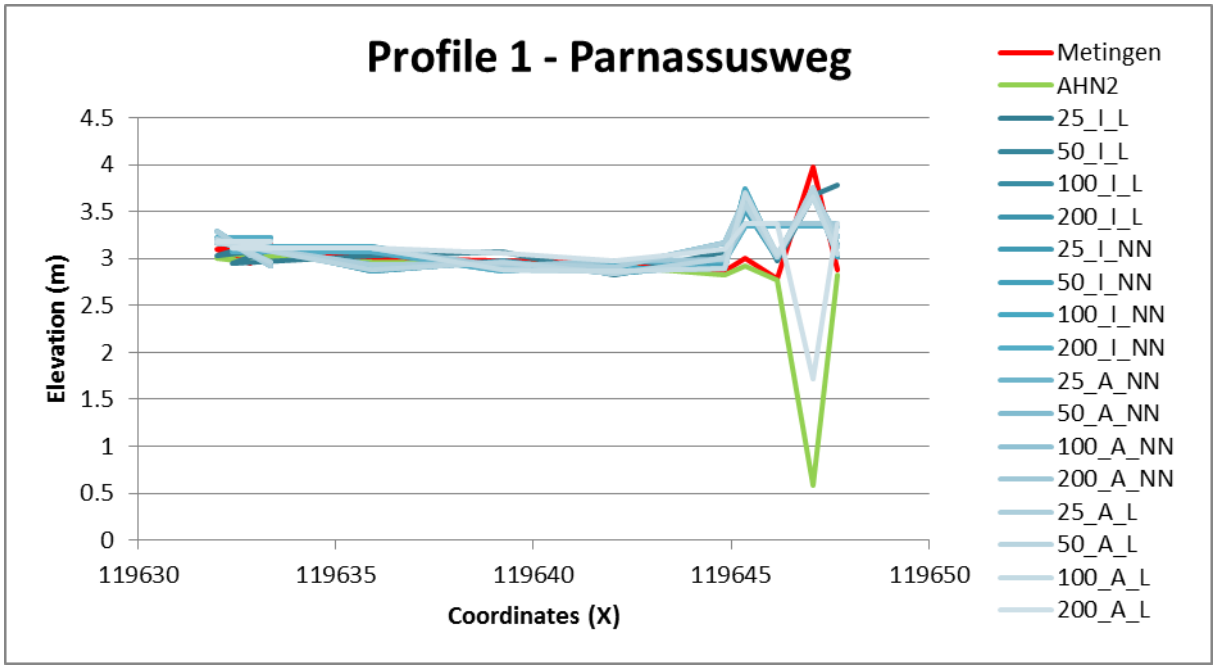

Figure 35: Comparison between 4 different methods of DEM construction, 4 different resolutions, AHN, and land surveys. I = IDW, A = Averaging, L = Linear, NN = Natural Neighbor.

Figures 36 and 37 show a close up of profile 2, here the difference in resolution is more noticeable. The SGM elevation values fluctuate more than the other lines (fig. 36). Only the AHN2 (green line) resembles the land survey measurements (red line).

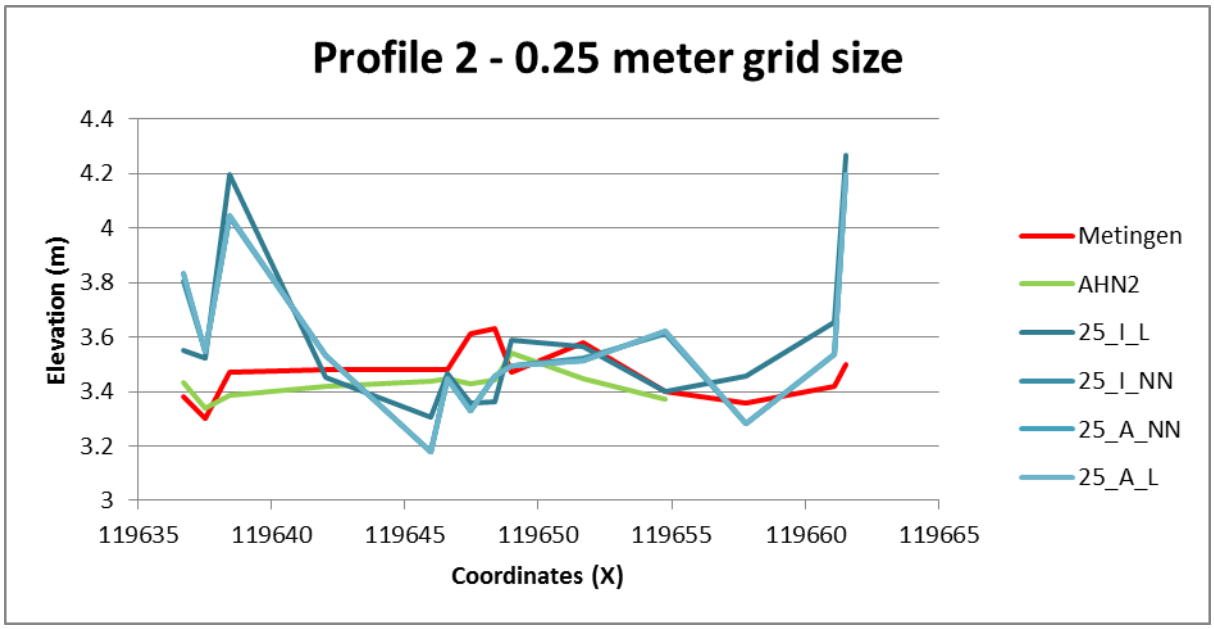

Figure 36: Comparison between 4 different methods of DEM construction (25 cm), AHN, and land surveys. I = IDW, A = Averaging, L = Linear, NN = Natural Neighbor.

The 2 meter grid cells show more resemblance with the land survey data (red line) then the smaller grid cells, because of the large size the 2 meter cells are more averaged or smoother along the profile line (fig. 37).

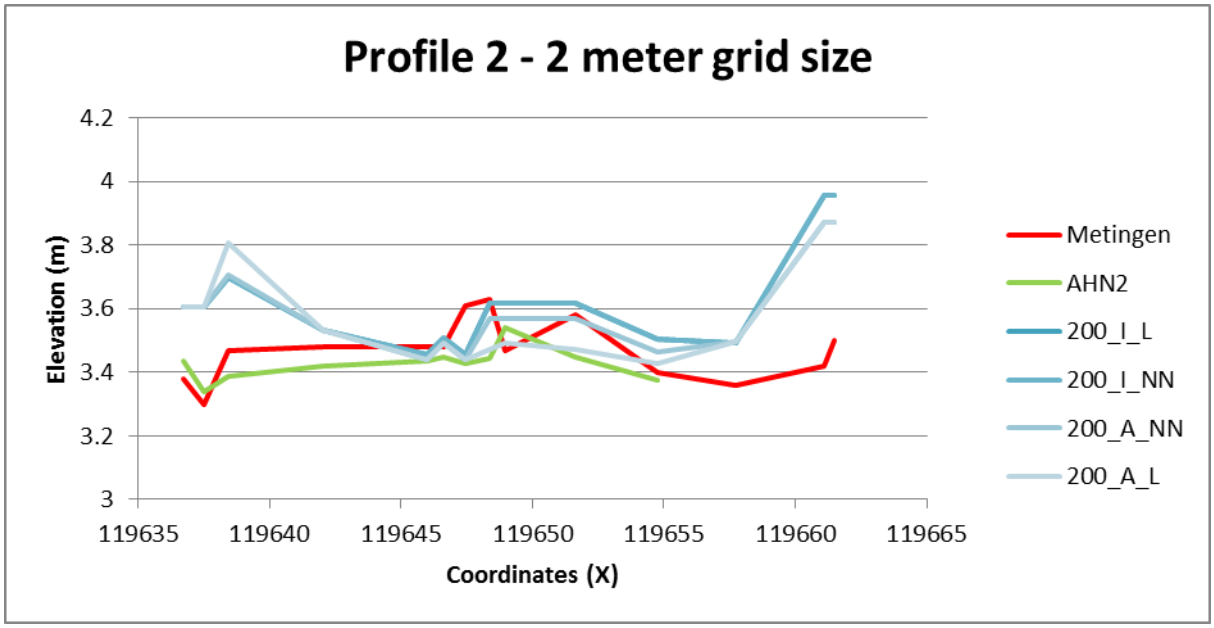

Figure 37: Comparison between 4 different methods of DEM construction (2 m), AHN, and land surveys. I = IDW, A = Averaging, L = Linear, NN = Natural Neighbor.

4.1.3 Static test of DEM and DEM derivatives

The difference in elevation values in the study areas was compared between the SGM 80 DEM and the AHN DEM (fig. 38 + 39). The 50 cm grid resolution was used for this comparison. Figure 38 shows that the blue patches are located on the side of the road and in the backyards of the buildings. These patches can be traced back to the lack of SGM to represent the 'bare earth' surface. Even with help of the topographic map (GBKA) to determine the land cover, and the use of the RGB colors it was not possible to remove all of the vegetation in the point cloud. This results in an unevenness in the SGM DEM.

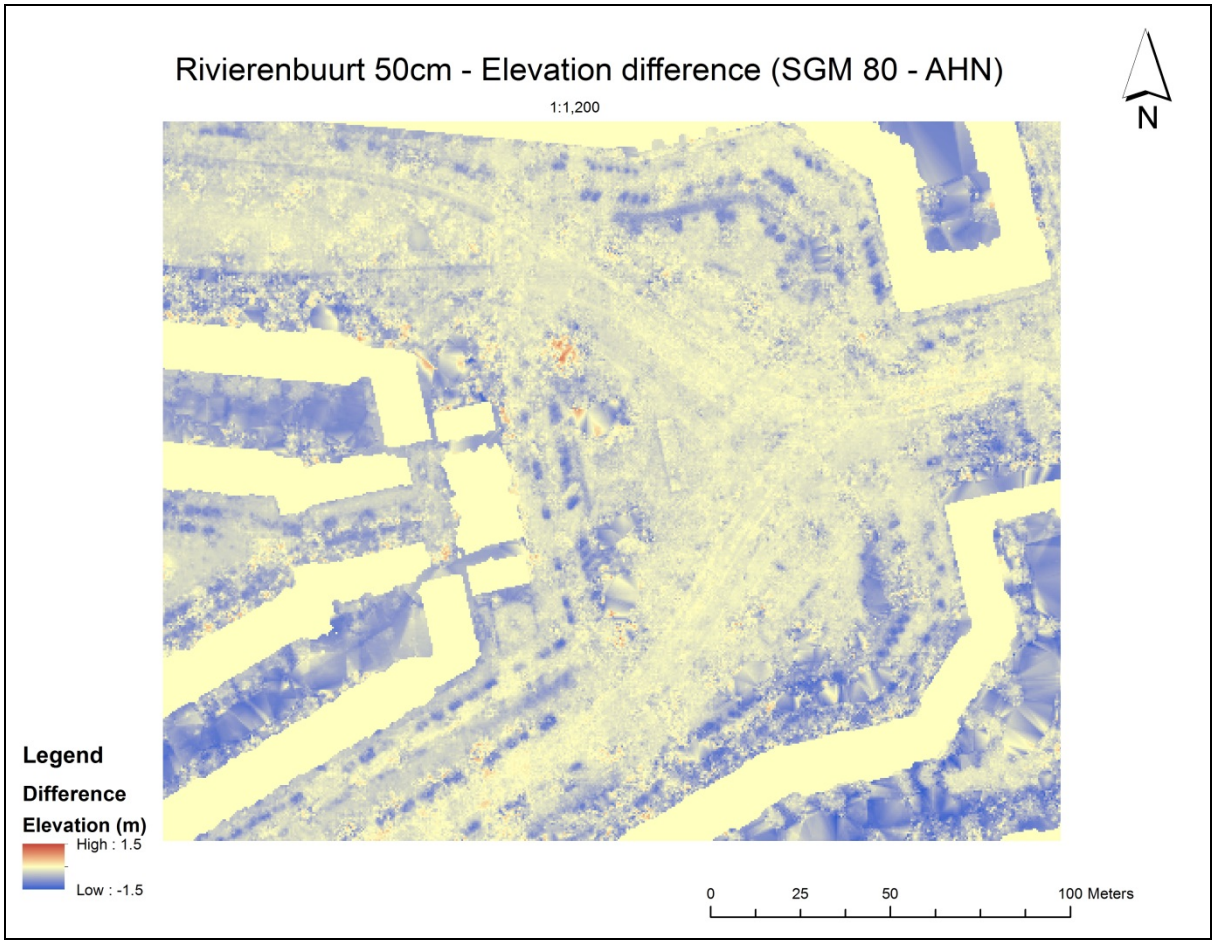

Figure 38: Difference between SGM 80 and AHN DEM for the Rivierenbuurt

Figure 39 gives a larger range of elevation values. This was done because of the larger differences in the study area. The tunnel in the north of the area was not represented well in the SGM DEM. This was likely due to the moment when the two datasets were created. The entrance to the train station Amsterdam-Zuid was changed between the time that the AHN2 was created and the aerial photograph was taken. The dark red patch in the southwest corner can be traced back to a difference between the buildings in the SGM and AHN2 DEMs. In the AHN2 DEMs the building is a whole block. While in the SGM DEM there was a small gap on the left side, it is possible that during the filtering process too much of the point cloud was removed. Quite possible due to obscureness of the points in the cloud by vegetation cover.

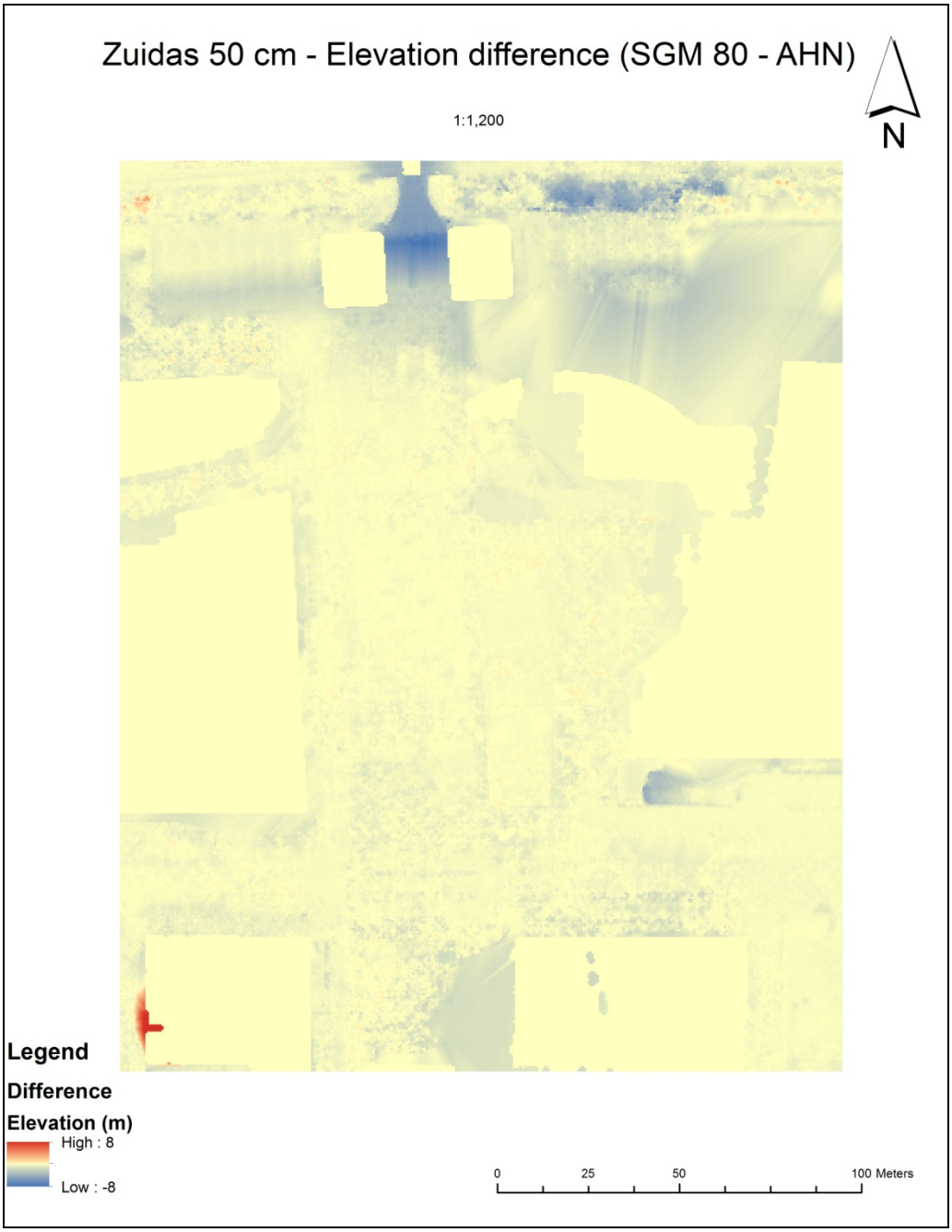

Figure 39: Difference between SGM 80 and AHN DEM for the Zuidas

Changing the resolution has an effect on the information stored within the cells. Histograms were created to show the differences between DEM sources, and between the grid resolutions. Appendix A-2 shows the all of the outcome for slope and catchment areas.

Figures 40a and b show the histograms of slope classes in the Rivierenbuurt. The frequency numbers are adjusted as the number of cells are not equal in each of the used grids. The AHN2 shows a more uniform distribution for each of the slope classes than the SGM 80 DEM. In the SGM histogram the numbers differ a lot between grid sizes.

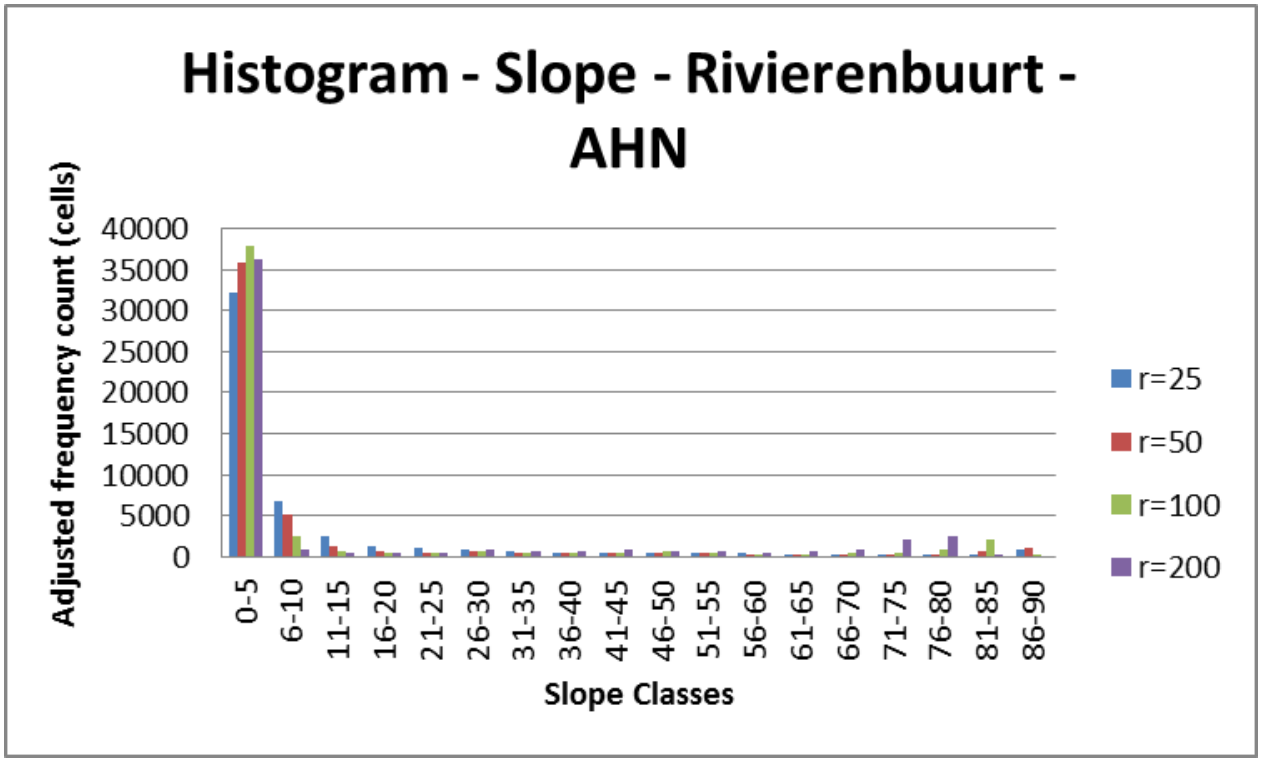

Figure 40a: Frequency count of slope classes of the AHN Rivierenbuurt DEM (r = resolution in cm)

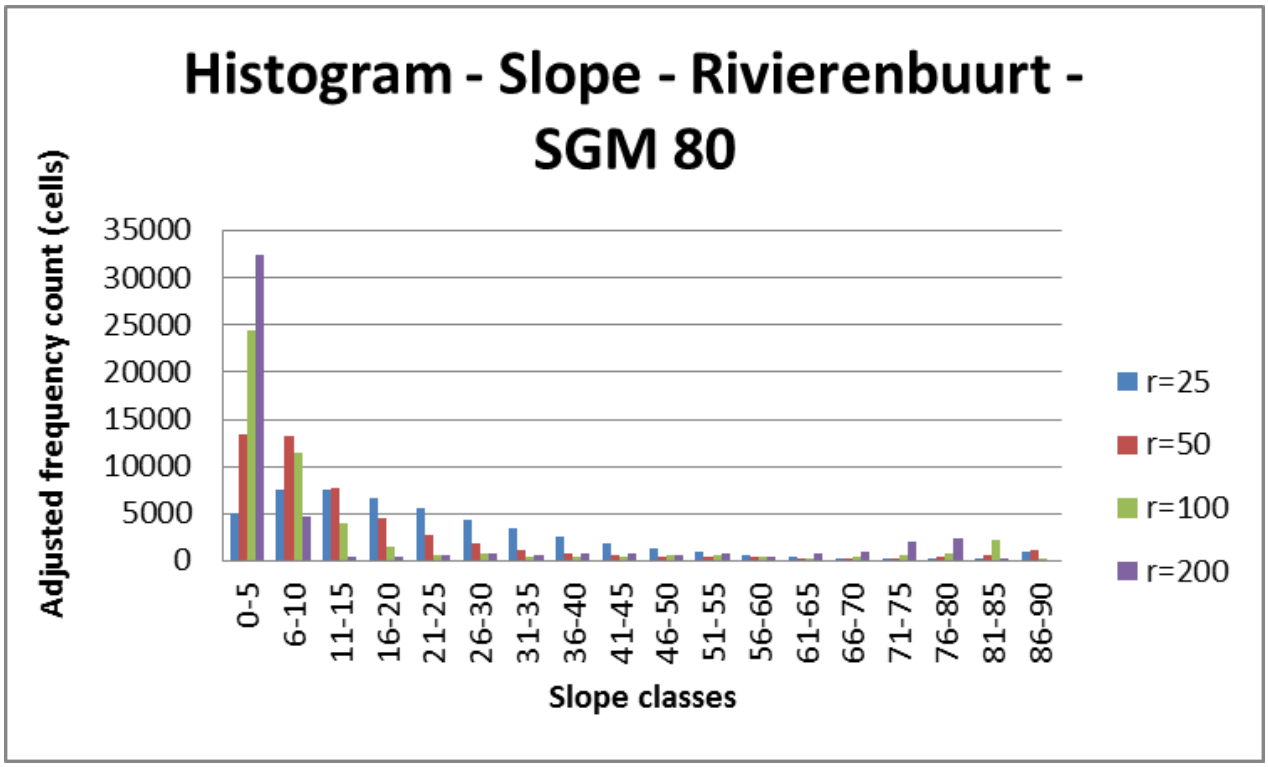

Figure 40b: Frequency count of slope classes of the AHN Rivierenbuurt DEM (r = resolution in cm)

The below figure shows the outcome of the number of catchments per DEM source and grid size in the Rivierenbuurt (fig. 41). The SGM 80 and SGM 10 DEMs show no similarity in the number of catchments in the study site, as the number of catchments is larger in the thinned SGM DEM. All of

the grid sizes show a small decrease for the larger grid cells (1 and 2 m) compared to the smaller grid cells (25 and 50 cm).

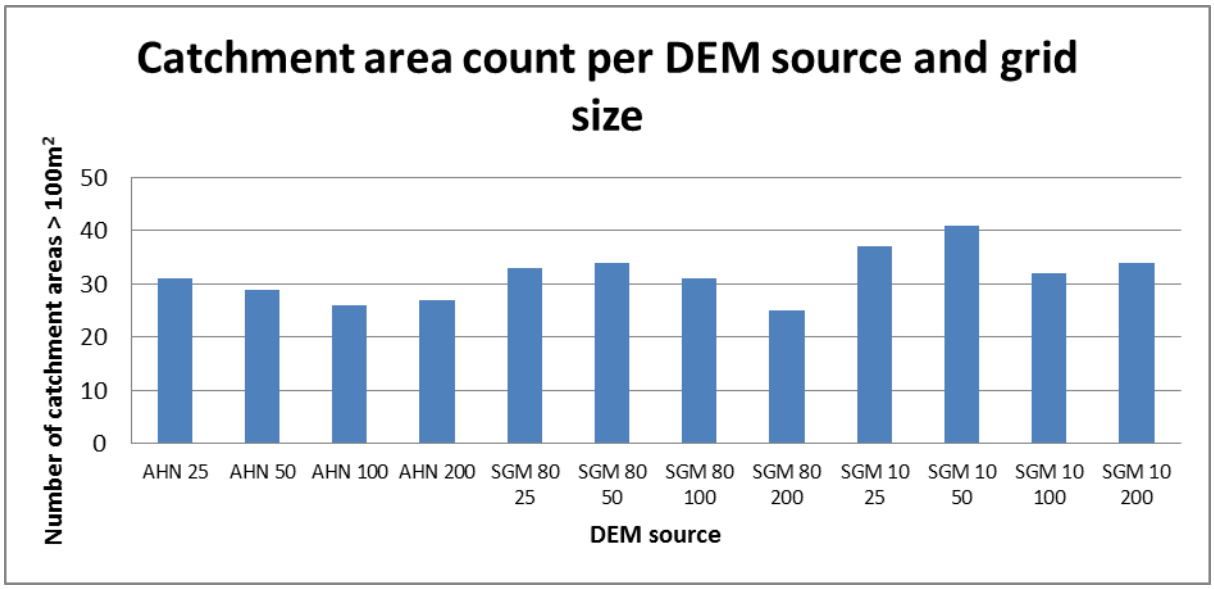

Figure 41: Number of catchment areas per DEM source and grid cell size in the Rivierenbuurt

4.1.4 DEM choice

Not all of the constructed DEMs were used in the hydrological model (fig. 11). This was due to available time for the research and because the DEM accuracy test showed that many of the DEMs were largely equal to each other. The first choice made was the exclusion of the unfiltered point cloud DEMs. These unfiltered DEMS did not perform as well as the filtered DEMs (fig. 30).

The second choice made was which DEM construction method should be used. The four different methods do not differ much, (fig. 31 + 32). Thus including all of them in the dynamic model is redundant. A choice was made to use the averaging and linear void fill method. These are also the default options in the GIS software used.

The last choice was the inclusion of the thinned DEMs of 10 points/m^2. This was done as the DEM accuracy test did not give an absolute answer to if the thinned point cloud DEMs were equal to the unthinned DEMs (fig. 31 + 32). The bias-adjusted RMSE was lower for the thinned point cloud, while the R^2 was better for the unthinned DEMs. Table 4 shows an overview of the chosen DEMs for use in the hydrological model.

Table 4: Choice of DEMs for use in hydrological model

DEM sources	DEM construction method	Resolution (m)
SGM 80 p/m^2	Average, linear void fill	0.25, 0.5, 1, 2
SGM 10 p/m^2	Average, linear void fill	0.25, 0.5, 1, 2
AHN2	Average, linear void fill	0.25, 0.5, 1, 2

4.2 Distributed Hydrological Model

4.2.1 Water level

The average water level was taken from each of the study sites. The average water level was only calculated were there are no buildings and no water bodies, thus giving a representative value for the map and making it comparable with the two study sites. Each source of DEM is compared with each other. The model simulation contains a one hour scenario, at the end of the model the average water level in the site was calculated.

The Rivierenbuurt shows a bigger change in water level per DEM source (fig. 42). None of the DEM sources gave the same output, only the SGM 10 and SGM 80 showed some similarity. The SGM 10 point cloud gave a lower average water level than the SGM 80 point cloud. The water level increases with the grid size. This was not the case for the AHN2, here the water level at 1 and 2 m resolution was lower.

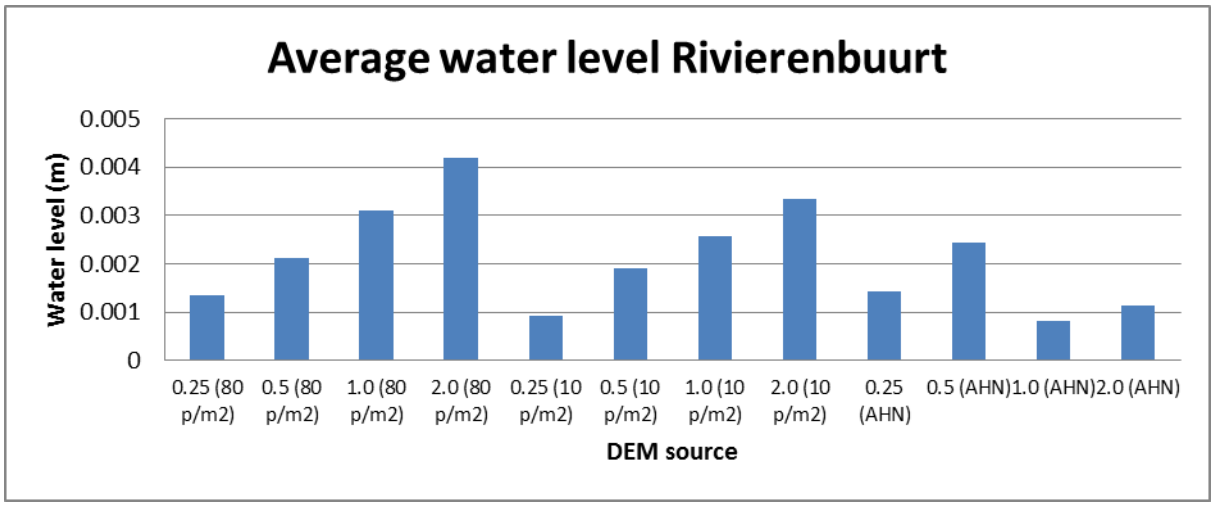

Figure 42: Average water level per minute for the Rivierenbuurt study site

The Zuidas study showed a different pattern for the average water level (fig. 43). Here all of the DEM sources showed the same distribution per grid size. Also when comparing the DEM sources with each other, lots of similarity can be seen. All of the DEM sources peak at 1 m, and drop a little at 2 m.

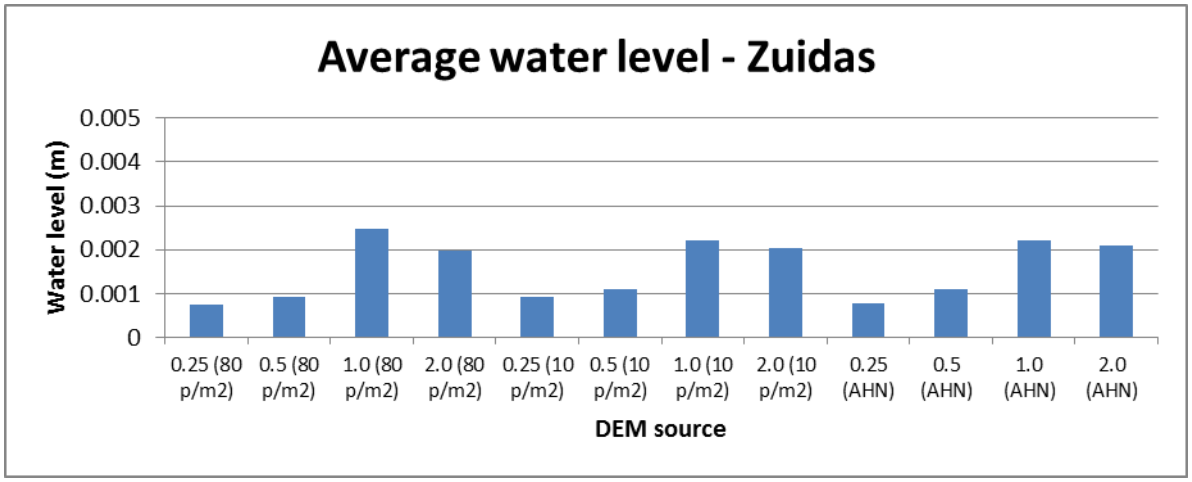

Figure 43: Average water level per minute for the Zuidas study site

The influence of resolution was tested by aggregating the 25 cm DEMs to a smaller resolution. Here 25 cm, became 50, 100 and 200 cm. The aggregated DEMs for the Rivierenbuurt show more or less the same average water levels (fig. 44). Only for the AHN there is a dip at the larger grid cells (1 and 2 m). This is the same kind of dip as in the standard scenario (fig. 42). Only here the average water level was lower than in the standard scenario.

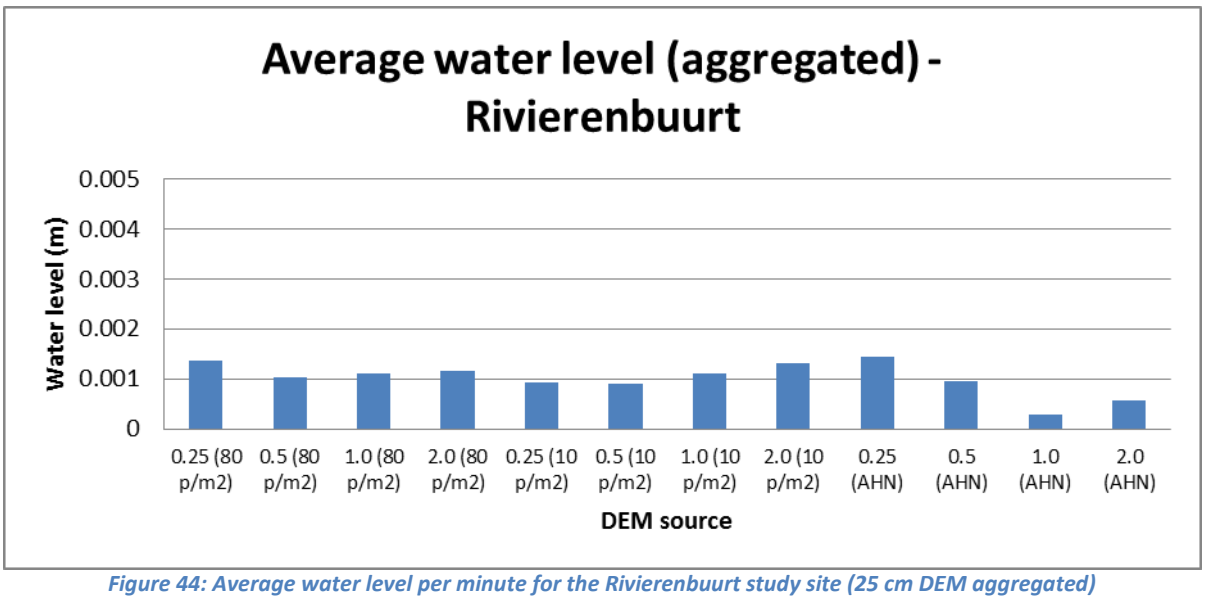

Figure 44: Average water level per minute for the Rivierenbuurt study site (25 cm DEM aggregated)

As in the standard scenario the aggregated DEMs in the Zuidas show a different pattern than in the Rivierenbuurt (fig. 45). The Zuidas aggregated DEMs do not show the same average water level at each resolution, but gave the same pattern as with the standard DEMs (fig. 43). Again the 1 m DEMs gave the highest average water level.

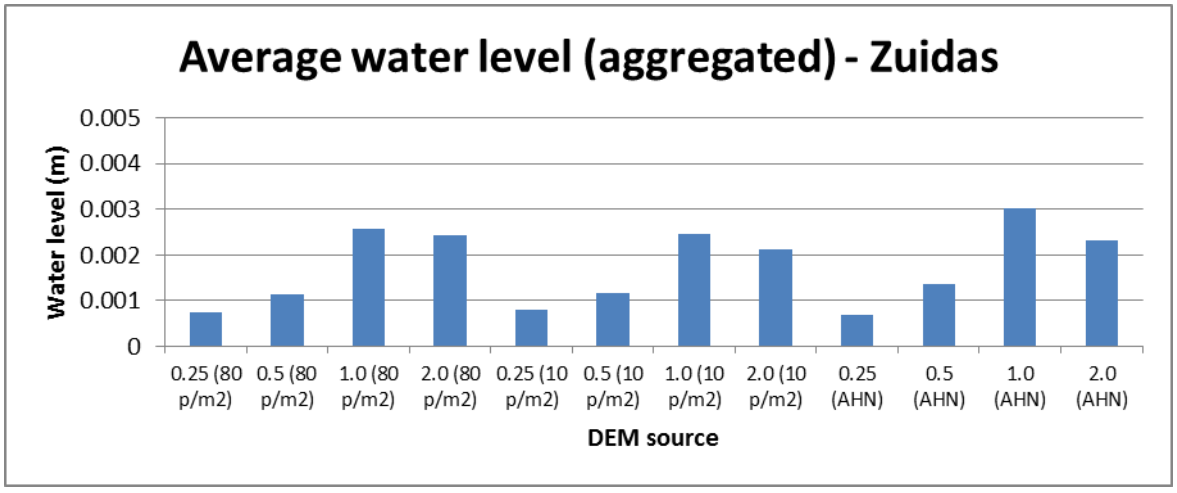

Figure 45: Average water level per minute for the Zuidas study site (25 cm DEM aggregated)

4.2.2 Ponded areas

An area was seen as ponded when the water level was higher than 0.5 cm. Lower water levels are also visualized, but there are just seen as wetted cells. The ponded area in the Rivierenbuurt is shown in figures 46 and 47. The SGM DEM shows a very scattered pattern in the ponded area (fig. 46). In the 50 cm DEM shown the water gathers in the verges by the road. Only the streams here are not straight as expected on the sides of road, but are very erratic. This can be attributed in the lack of smoothness in the SGM DEM (fig. 26).

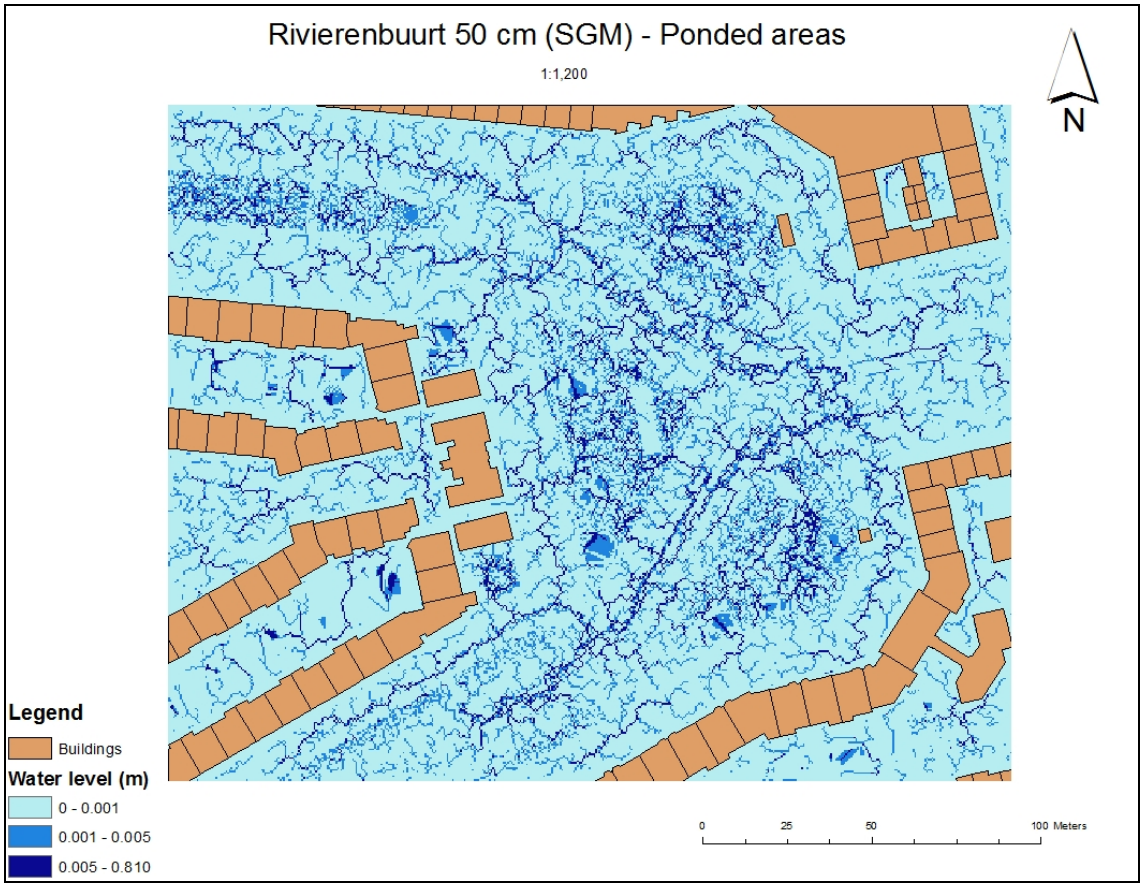

Figure 46: Ponded area (at least 0.005 m) and shallow inundated areas (between 0.001-0.005 m) in the Rivierenbuurt area for the SGM 80 p/m^2 DEM

The AHN shows a pattern that was expected of the study site. Water flows along the sides of the roads or pavement and accumulates on the grassy areas on the verge of the road (the triangle shaped area in the middle) (fig. 47). Here the straight streams along the side of the roads can likely be attributed to the smoothness of the DEMs surface (fig. 27).

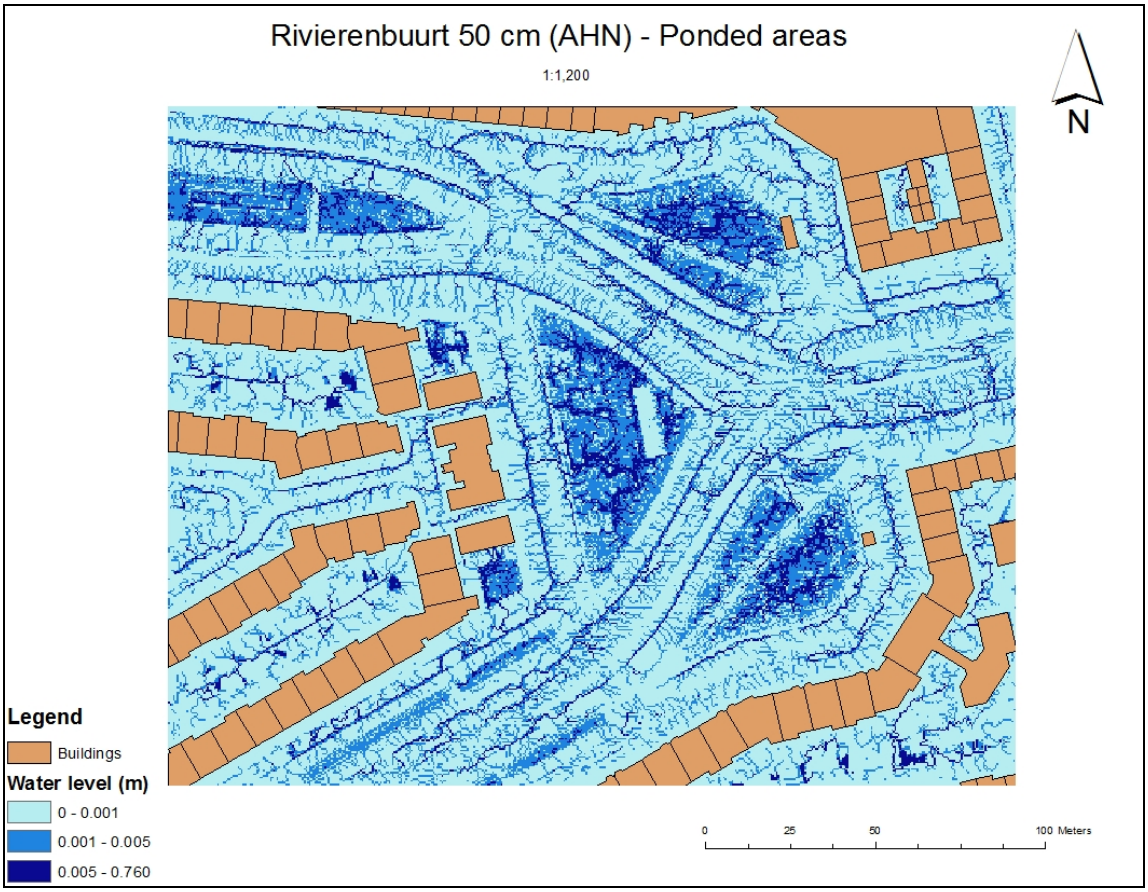

Figure 47: Ponded area (at least 0.005 m) (between 0.001-0.005 m) in the Rivierenbuurt area for the AHN DEM

For the Zuidas the pattern was almost identical as the Rivierenbuurt (fig. 48 + 49). The AHN gives straight lines along the road or pavement (fig. 49), while the SGM gives a more scattered view (fig. 48). Not only the shown figures this can be seen, but also in the other grids sizes with all used methods (Appendix C). In the parts of the Zuidas site where shadow disrupted the SGM process, as could be seen in the earlier elevation map (fig. 28), the water does not gather as is expected. In between the two buildings on the west side of the area no ponding takes place, while this is one of the areas which has problems during rain events.

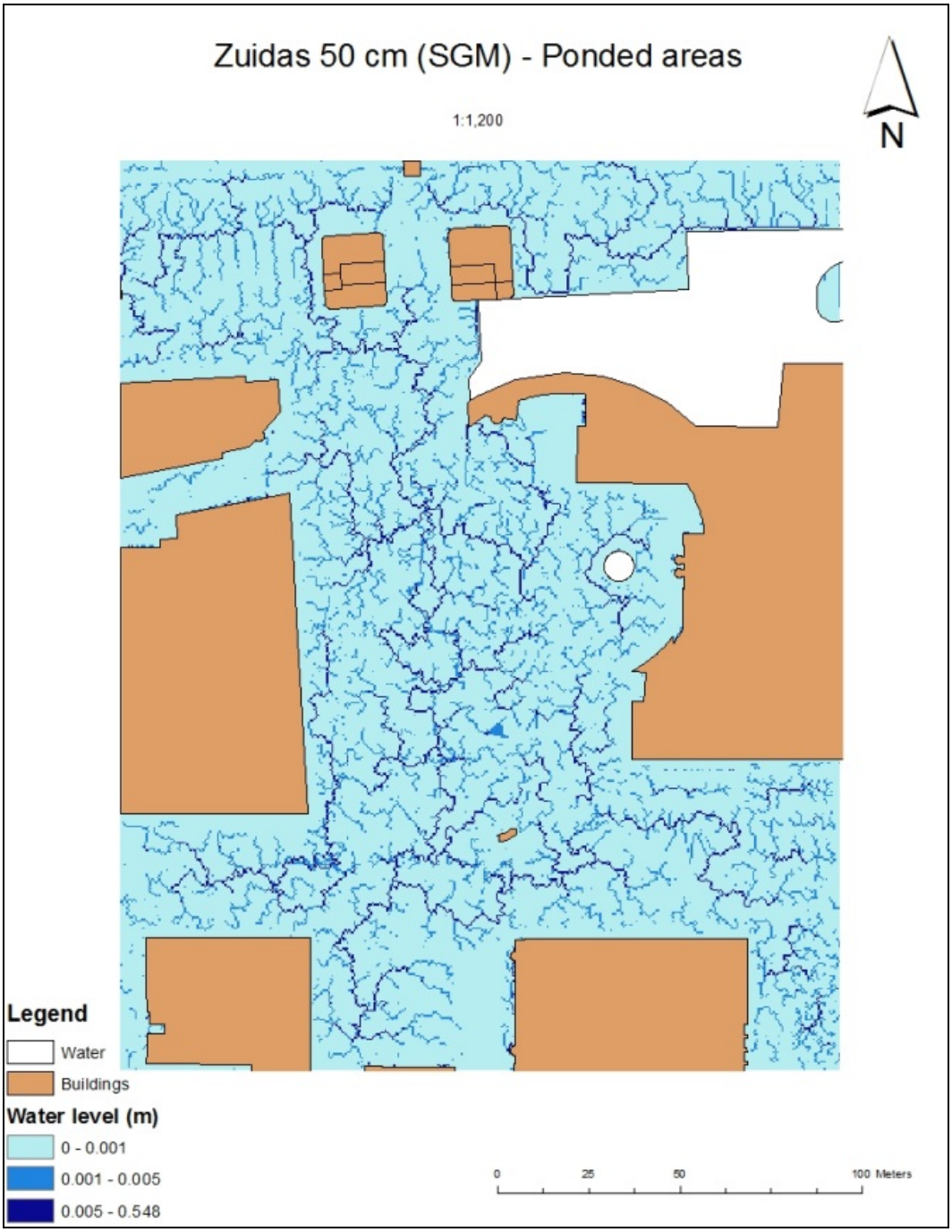

Figure 48: Example ponded area (at least 0.005 m) (between 0.001-0.005 m) in the Zuidas area for the SGM 80 p/m^2 DEM

The pattern of the water ponding in the AHN DEM was as expected (fig. 49). Water flows and ponds neatly at the side of the road, gathers in the lower areas, and even flows in the direction of the train station entrance (the tunnel in the north). This tunnel was flooded during the rain event of July 28th 2014.

Figure 49: Example ponded area (at least 0.005 m) (between 0.001-0.005 m) in the Zuidas area for the AHN DEM

The ponded area in the study site can differ between grid sizes (fig. 50). In figure 50 two AHN DEMS were compared in the Zuidas study site. These were the 50 cm and 100 cm grid. In the map the buildings were drawn with a small black line, as per the location in the GBKA. The ponded area in the 100 cm grid was much larger than in the 50 cm grid. Here it seems that a large area is under water, while in the other only a small section experiences ponding. Close to building, in the left image, ponding takes place at two locations. Something that did not occur in the right image. This reinforces the notion that choosing the correct grid size is very important otherwise problems can either be exaggerated or become unnoticed.

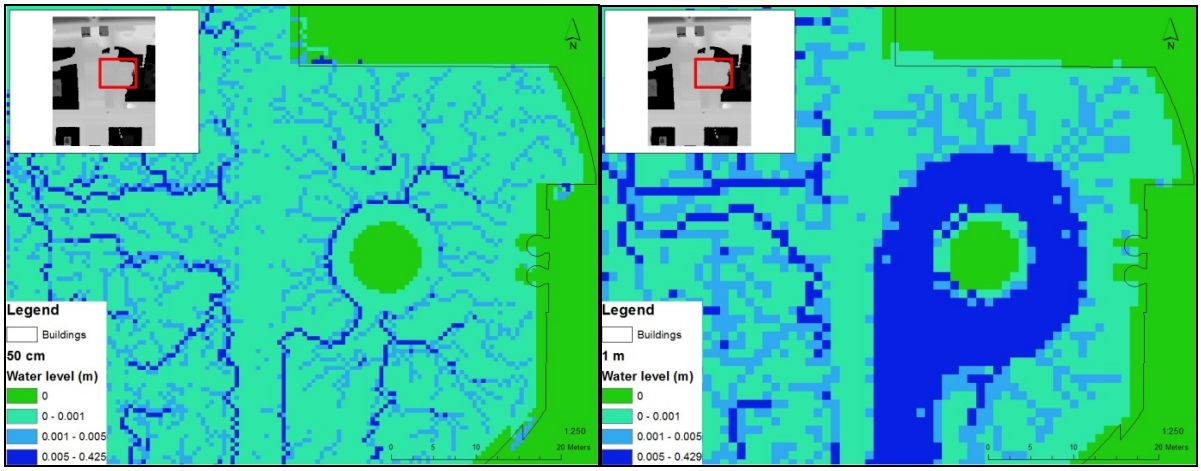

Figure 50: A close-up to the study site Zuidas, here the 50 and 100 cm AHN resolutions are compared.

The three DEM sources and study sites were also compared with the F2-statistic to see if there is similarity in the location of ponded area. A F2-statistic value of 1 means perfect similarity, while -1 means no similarity. None of the DEM sources showed any similarity with each other (fig. 51 + 52). This was also the case for the Zuidas study site (Appendix C). No similarity was found in the spatial distribution of ponded cells.

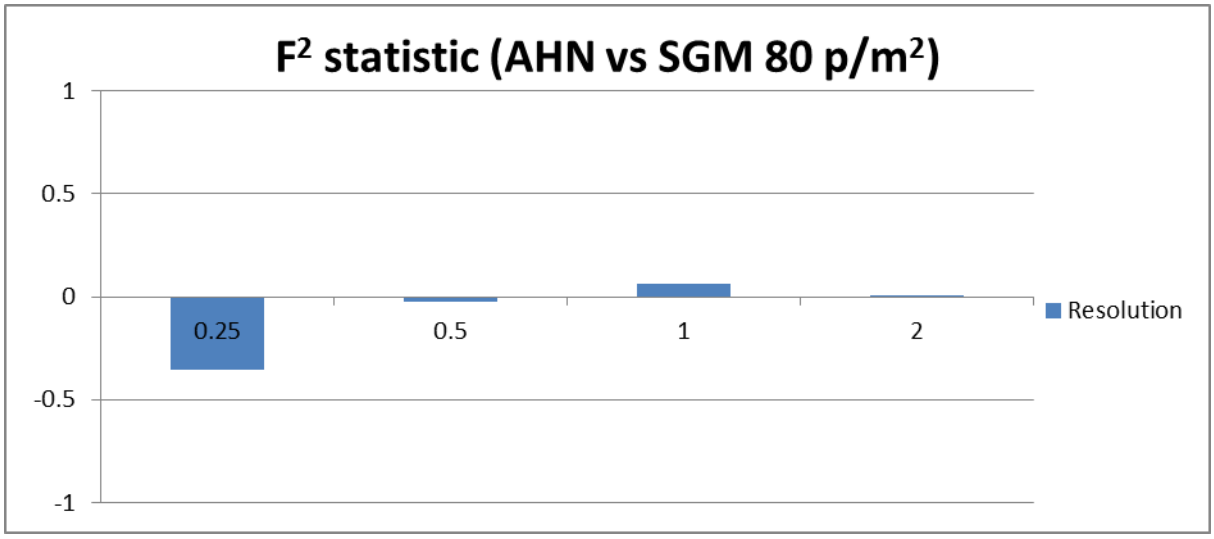

Figure 51: F^2 statistic SGM 80 p/m^2 compared with the AHN in the Rivierenbuurt. 1 is perfect similarity between the DEM sources and -1 is no similarity.

The thinned SGM 10 DEMs also showed no similarity with the unthinned SGM 80 DEMs (fig. 52), meaning that more changed than showed in the earlier DEM accuracy test (fig. 31 + 32).

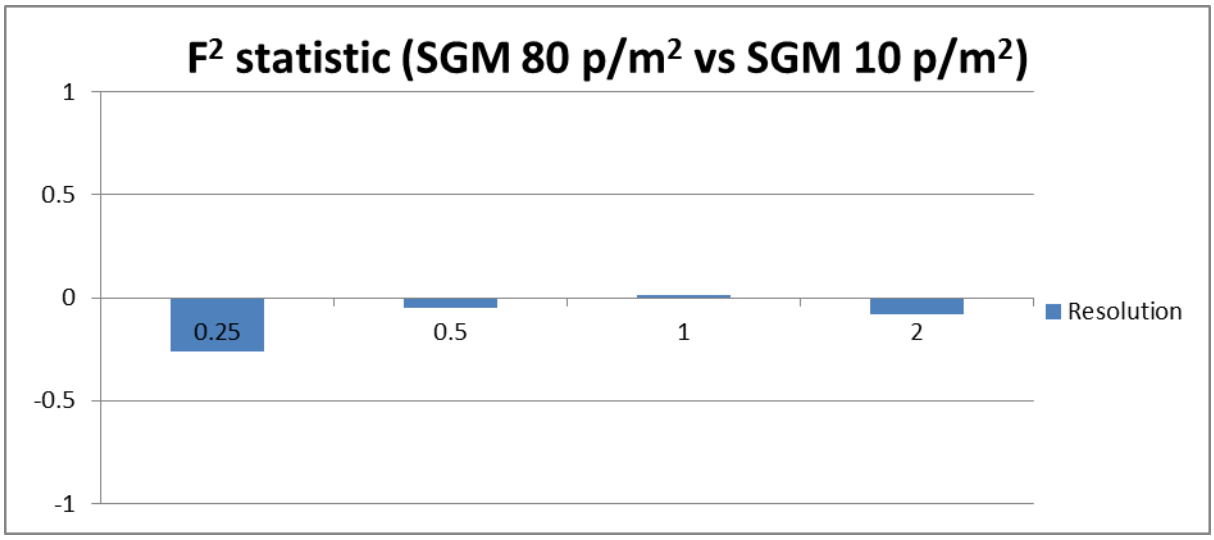

Figure 52: F^2 statistic SGM 10 p/m^2 compared with the SGM 80 p/m^2 in the Rivierenbuurt. 1 is perfect similarity between the DEM sources and -1 is no similarity.

Aggregating the 25 cm AHN DEM to understand the influence of resolution did not increase the ponded area in the Rivierenbuurt (fig 53). It lessened the number of streams and the changed the location of some of the ponded areas. In the Rivierenbuurt study site the 1 m DEM has almost no more ponding in the verge of the road. While this part contains grass in which water was expected to gather.

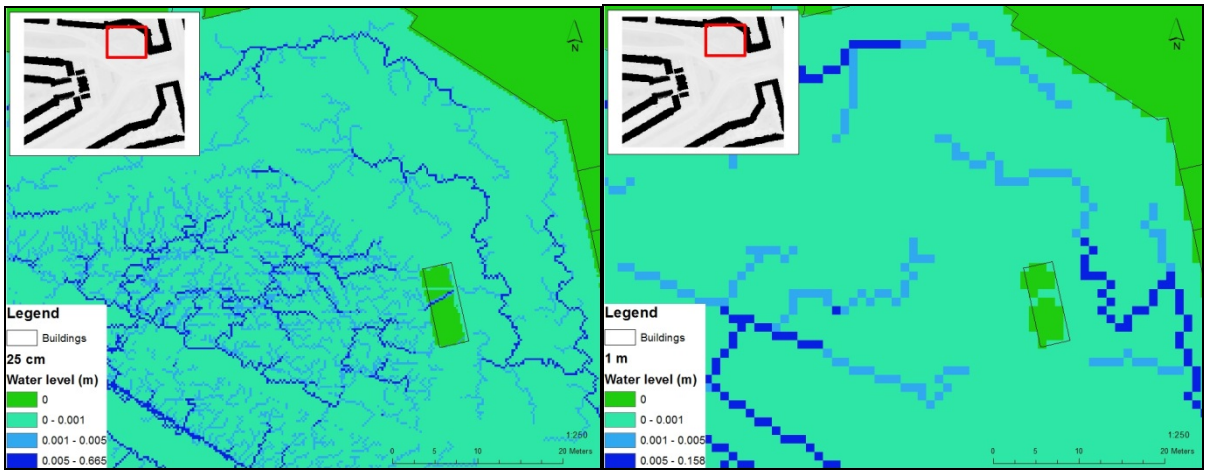

Figure 53: Close up of the aggregated DEMS (25 and 100 cm) of the Rivierenbuurt study site.

The Zuidas study site gave a different outcome when aggregating the 25 cm DEM (fig. 54). The 25 shows very little ponding, but in the 1 m grid there was a different outcome. A bigger area was ponded and ponding at a small inlet by the building (north in the image) did not occur. The same effect as in the standard scenario (fig. 50). Again it was shown that choosing the correct grid size is very important.

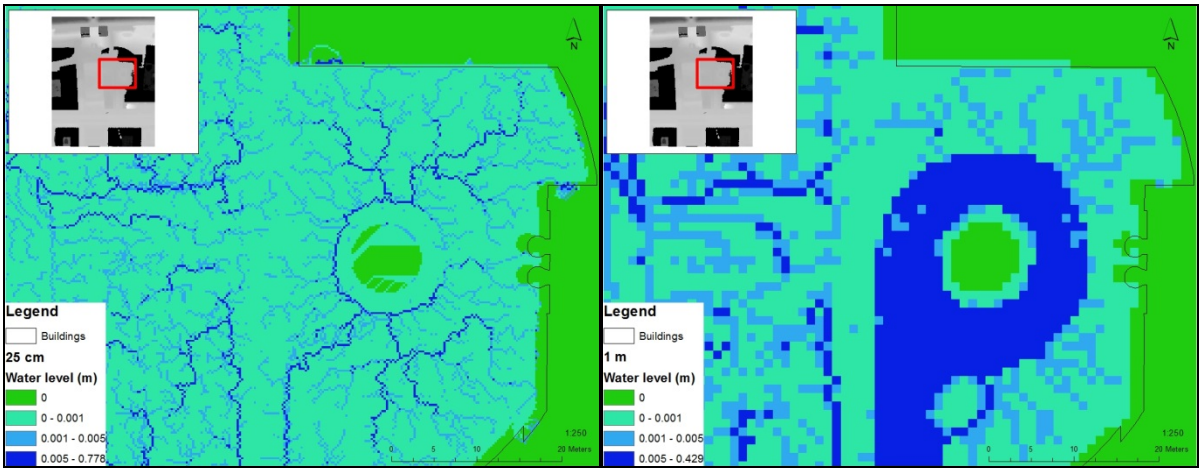

Figure 54: Close up of the aggregated DEMS (25 and 100 cm) of the Zuidas study site.

5 DISCUSSION

This research tried to combine two objectives. One was constructing digital elevation models from digital aerial photographs which could match the quality of a Lidar DEM. The other was constructing a hydrological model to test the constructed DEMs and look at the effect of resolution on the models output. Both objectives were partly met, although the successfulness can be debated. The SGM DEMs were constructed but cannot hold themselves against the quality of the AHN2 DEM. A hydrological model was constructed and showed the areas at risk with ponding. Some of these areas (i.e. the entrance to the train station in the Zuidas) showed similar problem areas as in the real world. The optimum resolution was not found in the output of the model. The differences in grid sizes were however noticeable, only defining which one is best is troublesome when no gauged data is available to test the data against.

5.1 Accuracy test

Three comparison tests were applied to compare the accuracy of five DEM sources to land survey measurements. Every test (i.e. bias adjusted RMSE, MAE, and R^2) showed that the Lidar derived DEM has the highest accuracy (fig. 30). The accuracy test showed no change when comparing a thinned (10 p/m^2) and unthinned (80 p/m^2) SGM DEM.

It is further shown that filtering was a necessity in the SGM process, without filtering the accuracy was much less reliable. Next to filtering, DEM source was the only other factor which showed significant change in the accuracy test. None of the other factors (construction method and resolution) showed a difference.

Thinning the point cloud did not reduce the results for the SGM DEM when compared to the land survey measurements (fig. 30). Although the thinned point cloud has only 10% of the original point cloud this did not result in worsened results, not in this case. It even outperforms the SGM 80 DEM with the R^2 result (0.70 vs 0.66). The accuracy tests showed no significant differences between SGM 80 and SGM 10, making them in this case equal in quality.

The research of Gehrke et al. (2010) showed that a SGM point cloud can achieve an horizontal accuracy of 5 cm or better compared to land survey measurements and a Lidar DEM. This was not achieved in this research. This can be attributed to the quality of the aerial photographs, which were taken at a higher altitude than the standard flying height due to the proximity of Amsterdam to the Schiphol airport.

5.2 Static test and DEM choice

5.2.1 Static test of DEM and DEM derivatives

The difference in elevation values between the SGM and Lidar DEMs was one of the things which was compared in the static test. One of first things that could be seen in the visual comparison was the noise in the SGM derived DEM. This was particularly noticeable in the areas with vegetation and the roads with (parked) cars present. These areas (vegetation and cars) are not present in the Lidar DEM as they are already filtered in the AHN2 DEM.

For the Rivierenbuurt the courtyards behind the houses showed a large difference between the SGM and Lidar DEM (fig. 38). This can be attributed to the amount of vegetation. These differences can also be seen next to roads. These verges next to road have areas that contain patches of vegetation and have not been adequately removed in the filtering process. The Zuidas area does not have much vegetation and the differences here can mostly be attributed to other factors (fig. 39). A difference over time, due to the age of the AHN dataset. The only patches of vegetation are in the north of the study site, which results in some fuzziness in the elevation differences. The other differences come from the high-rises in the area, which cast shadows on the surface or even overlap some part of the road in the photograph. The darker color resulted in more noise than in areas where there was no shadow in the SGM point cloud. The blocks in both maps where there was no difference in elevation were the buildings. These values were taken from the SGM point cloud and as such show no difference in elevation. Here SGM proved its value, buildings experienced much less noise in the point cloud than the surface. Making it more easily usable.

Catchment areas change when using different grid scales for the same study area. It was expected that a high resolution DEM would show more catchment areas as there is more fluctuation in such a high detailed map. In the end the number of catchments did not differ much between the grid sizes. It was difficult to compare the number of catchment areas of each resolution as there is a border effect in each of the maps. Also it is unknown if the size of the study site determines the size of the catchment area as no test was undertaken to show this effect. The DEM sources showed no similarity in the number, location, or size of the catchment areas (fig. 41).

The other DEM derivatives failed to give insight in the optimum resolution. The histograms could not provide more insight into this. The lack of significant change in elevation and the relative high detail of the DEMs could have attributed to this. As Dottori et al. (2013), Blanc et al. (2012), Chen et al. (2012), Fewtrell et al. (2011) already state everything smaller than 2 m was already considered high resolution. Thus the statement by Kienzle (2004) that change in resolution has a profound effect on the DEM derivatives could not be underlined.

5.2.2 DEM choice

The choice in DEMs which were used in the hydrological model was done in coherence with the research questions. As such both AHN and SGM 80 p/m^2 must be chosen and the four grid sizes as well. Otherwise the basis of the research was eliminated. As the research of Chen et al. (2012) states that higher resolution data could lead to better models it was needed to use the thinned SGM DEMs (10 p/m^2) for comparison. Even though no difference was detected between SGM 10 and SGM 80 DEMs in the accuracy test the static test showed differences when it came to the number of catchment areas.

The unfiltered SGM DEMs were deemed uninteresting as the accuracy test already showed large differences with the filtered SGM DEMs. The DEM construction methods were all equal to each other, this probably has to do with the (high) resolution of the data. The sheer number of points in the point cloud make the methods indistinguishable of each other. If the number of points per square meter would be further reduced (or in other words thinned) there would more likely be more differentiation between the construction methods.

Earlier in the research it was decided that DEM construction from point cloud should not be performed in the standard method. The standard being directly converting from point cloud to raster. Although this standard method is adequate for rural areas, this was not the case for urban areas. Most urban areas consist of buildings with strict 90 degrees angles between buildings and the surface level. By first separating the point cloud by type (surface or spatial object) and constructing a raster per type it was possible to create these angles. The separated grids are then combined again to achieve a strict separation of height in the raster. Foregoing this method will result in slope between buildings and slope in the DEM which does not exist in reality (fig. 10).

Topographic maps of the Amsterdam municipality were used to classify the point cloud. This data is highly detailed and in this research were used to classify the point cloud as they originate from the same source: aerial photographs. In the Netherlands this data is kept up to data by several governmental institutions like the municipality, province, or state. This is not always the case in other countries and as such this method is not universally applicable.

5.3 Hydrological model

The hydrological model has a number of shortcomings. One is that no gauged data was available to calibrate the model. The outcome of model was discussed with hydrology specialists of the municipality who know the location of areas which experiences ponding in the Amsterdam area. This showed that some of the model outcomes showed resemblance with reality. Another shortcoming is that allocation for Manning's n is based on the topographic map from Amsterdam. It is possible that in the case of the AHN2, which is several years old, some points have changed. This can lead to small discrepancies. The storm drains were not included in the model, as Dottori et al. (2013) states that in modeling storm drains are not that important as they will never work according to what is expected. Further, precipitation that falls on buildings is excluded in the model. It is assumed that all rainfall water is gathered on the roof and flows into a drainage or sewage system. In reality it is possible that it flows onto the streets, but the locations were this happens are unknown. Thus the model which was made is a bit simplified but it fulfilled its purpose.

The average water level in both study sites and all of the available DEMs showed much fluctuation. The only resemblance that was seen was between the SGM 10 and SGM 80 DEMs. They show the same pattern in both study sites. The average water level is different between the study sites (fig. 42 + 43). This is partly due to the occurrence of water bodies in the Zuidas study site.

Resolution influences the average water level in the model greatly. Again there was no similarity between the grid scales with the average water level. Aggregating the 25 cm DEM to smaller resolutions had an unexpected result. Expected was that per resolution the outcome would be similar as the standard run. This was the case for the Zuidas area (fig. 45). Only the Rivierenbuurt showed the same average water level for all the grid scales (fig. 44). This effect cannot be explained.

A visual comparison of the ponded area between the SGM and AHN2 DEM shows no resemblance (fig.46-49). The AHN DEM gave a more realistic performance. Water flowed down the gutters on the side of the street. While in the SGM DEM it was more randomly spread, there were no straight streams along the streets which was expected.

The F^2-statistic fails to give any resemblance between any of the chosen comparisons (Appendix C). Even the SGM 10 and SGM 80 DEMs showed no resemblance although the average water level did

show some similarity. There was even no resemblance in the F^2 statistic when aggregating the 25 cm raster (Appendix C, table 7). This cannot be seen in the close up figures. Here some of the same patterns are seen between the 25 cm and 50 cm grid (Appendix C, figure C-2). Thus it is possible that the streams have shifted a bit which results in no resemblance in the F^2 statistic. This is a shortcoming of the F^2-statistic, as it only looks at a cell-by-cell comparison.

Evaluating the hydrological model on Chen et al. (2012) two major indicators, accuracy and efficiency, was difficult because of the lack of gauged data to measure its accuracy. Less detail in the resolution (2 m) led to faster model runtimes. Computing time of the model was only a problematic with the 25 cm grid, which took considerably longer than the other three (10 minutes compared to 2 minutes) for both study sites. For this research 50 cm is a very useful grid scale to predict ponding. More detail is shown and it was less likely to lose information where ponding takes place. As the 1 meter resolution showed that some ponding locations did not show up. An optimum resolution cannot be found in the accuracy test or in the histograms. From the hydrological model only the visual interpretation was useful as no similarity could be found between the grid scales (F2 statistic). As Dottori et al. (2013) states it is mainly dependent on the research objective. What does the researcher want to know?

5.4 Concluding comments

A direct visual comparison of the SGM and Lidar DEMs showed a difference in smoothness in the surface (fig. 25-28). Lidar has it, SGM lacks it. This can be attributed to two points. One is the differentiation Lidar can make between 'bare Earth' and vegetation. This means that Lidar does not need filtering to achieve a 'bare Earth' model. A SGM point cloud undergoes manual filtering of vegetation points as the SGM only sees the top of every pixel in the aerial photograph. It cannot see through the leaves. As filtering was manual there can be human error in the filtering process. It is difficult to see in a point cloud where the vegetation ends and the surface begins. Even with the RGB colors present, the points in cloud remained very small and very abundant.

The second point is the flying height of the aerial photographs used for the SGM DEM. The general flying height to take aerial photographs is 1200 meters, because of Amsterdam's proximity to Schiphol this was not possible as the general flying height was in the landing zone of other aircrafts approaching Schiphol (fig. 22). The flying height for the aerial photographs in Amsterdam was above 4300 meters. This reduces the detail in the stereo-images, which leads to noise in the SGM point cloud. This noise can be filtered, but the former point arises again that this is a manual process which could lead to errors.

6 CONCLUSION

The SGM derived DEMs could not hold up to the quality of the Lidar DEMs. At least in this case site, which is limited by the quality and lack of detail in the aerial photographs. In all tests the AHN outperformed the SGM. In the DEM accuracy test the SGM DEM proved to have less similarity than the AHN with the land survey measurements. And in the output of the hydrological model, the AHN DEM gave a more realistic output than the SGM DEM. The optimum raster resolution could not be established, due to the lack of gauged data to test the output of the model. The DEM accuracy test showed almost no change when grid size was compared. The hydrological model showed that choosing the correct grid size is important, because of the differences in model output. The chosen grid size must fit the researcher's objective.

6.1 DEM accuracy evaluated against land survey measurements

The accuracy test was used to show which of the DEM sources had the most similarity with the land survey measurements. Overall the Lidar AHN DEM source gave the best results (most similarity). On all three tests (bias-adjusted RMSE, mean absolute error, and R^2) the Lidar AHN DEMs performed better (fig. 30).

The other four DEMs performance only differed between the SGM 80 and 10 filtered and the SGM 80 and 10 unfiltered. Without filtering the vegetation and noise (from the SGM point cloud, the SGM DEM mean absolute error was triple the value of the AHN2 Lidar DEM. After filtering it was only twice the mean absolute error of the AHN2.

The influence of the several DEM constructions methods and grid resolution was also compared. The DEM construction method was not important when comparing them with the land survey measurements. No change was detected between the four used raster construction methods (fig. 31 and 32). Resolution also had no influence on the DEMs performance in the accuracy test (fig. 33).

What was important in DEM construction was the addition of attribute type to points in the point cloud. In the urban system the occurrence of strict 90 degrees angles is the norm, this occurs between a building and the surface. The point cloud was separated on attribute type (ground level or spatial object) and then each separate point cloud was transformed to a raster before adding them together. With this construction the spatial objects no longer have a slope at the building edge which enhances its use for hydrological models.

6.2 DEM derivatives compared by DEM source and raster resolution

The constructed DEMs were also visually compared to see the differences in elevation. A visual comparison of the AHN2 and SGM DEMs already gave an indication of the performance of the AHN2 DEM (fig. 26 - 29). The AHN2 grid consists of a smoothness that the SGM grid lacks. Patterns like the road and the verges can clearly be distinguished, something which was more difficult in the SGM DEM. There are large differences between the elevation values of SGM and AHN Lidar (fig. 38 -39). This was due to the occurrence of vegetation and noise in the SGM point cloud. Inadequate filtering to obtain a 'bare earth' model resulted in a less than smooth surface level. In the Zuidas area noise in the point cloud was created by the shadow of the high rises.

Another important fact in the difference in quality between the AHN Lidar DEM and the SGM DEM was the quality of the aerial photographs. These were taken at a higher height than the standard flying height used to take aerial photographs.

The DEM derivatives (slope and catchment area) were also compared for each of the DEM sources and grid scales. From the static test no grid size preference can be determined. The histograms did not gave an optimum resolution for slope (fig. 40). Resolution does seem important when determining catchment area. Although no optimum grid size can be determined, catchment size and location do change when the resolution changes (Appendix A2, figure A-10 + 11). Also the number of catchments differ a little according to graph (fig. 41).

6.3 Influence of DEM sources and raster resolution on the hydrological model

The quality of the constructed DEMs was tested in the hydrological model. It was found that the source of the DEM matters for the average water level in the study area. Each of the DEM sources results in a different outcome. Although without gauged data to compare the output it was impossible to say which level was correct. Especially in the Rivierenbuurt the average water level fluctuates depending on grid size and DEM source (fig. 42). Here the AHN2 Lidar, SGM 80 unthinned and SGM 10 thinned DEMs each show a different average water level. In the Zuidas study area the average water level was quite similar per DEM source (fig. 43), but like the Rivierenbuurt the raster resolution influences the average water level. An increase of the cell size increases the average water level here.

The areas were ponding takes place were also tested for each of the constructed DEMS. Ponding in the AHN2 DEM performs as expected. Water gathers in the gutters, alongside the streets and in the lower areas (fig. 47 + 49). The output was thus realistic, it also showed ponded areas which caused problems during the rain event of July 28th 2014. The SGM DEM showed more fluctuation in its pattern of ponded area (fig. 46 + 48). The water paths are less straight, which can be attributed to the DEM lacking smoothness. Resolution influences the location where water accumulates. The F^2-statistic showed that there was no similarity between grid sizes or DEM source. The SGM DEMs also showed no similarity in ponded area with the AHN2 DEMs. Optimum grid resolution was not found in the hydrological model. What was shown is that resolution changes the outcome of the model a lot.

6.4 Main conclusion

Overall the performance of the SGM DEM cannot be compared with the AHN2 Lidar DEM. The study shows that the Lidar AHN outperforms the SGM DEMs. The accuracy test and the differences with the outcomes of the hydrological model showed that the Lidar DEM was superior. The problem of the SGM DEM can be traced back to the quality of the aerial photographs. In the study area of Amsterdam the flying height of camera planes was higher than the standard flying height. This results in a SGM point cloud that has a large range of elevation points on the surface level, or in other term a surface that was surrounded by noise. The subsequent filtering and DEM construction results in a grid that lacks smoothness, which was expected from man-made urban structures (i.e. roads or sidewalks).

The height and location of buildings can be taken from the SGM point cloud, this data was used to add to the Lidar point cloud to construct a completer DEM of the study area. The noise surrounding

rooftops was far less than on the ground level. As the AHN2 was limited in obtaining building heights, it was useful to combine the buildings of the SGM point cloud to the Lidar point cloud. This was necessary for the hydrological model as the buildings obstructs the flow of the water.

7 RECOMMENDATIONS

7.1 Noise reduction in aerial photographs and point clouds

This study was limited by the quality of the SGM point cloud compared to the AHN Lidar point cloud. The flying height was seen by this research as the main limiting factor, it would be preferred to fly lower to take the photographs. Unfortunately this is not possible due to air traffic regulations. To increase the accuracy of the point cloud it is possible to use more than two stereo-images. More photographs increase the number of pixels that can be used and could increase precision. A greater overlap between stereo-images is another possibility. Currently the overlap is 60%, an 80% overlap could give an increase in the quality of the point cloud.

Another possibility is the combination of terrestrial point clouds and airborne point clouds. Terrestrial point clouds are taken from the ground level, usually from cars. This eliminates the flying height problem, but the problem of parked cars which obstruct the view will still exist.

7.2 Lack of hydrological data

No gauged data was available for the Amsterdam area. Also the locations of storm drains are not known within the two study sites. For a future study it would be interesting to measure the discharge at storm drains. It would be preferred to calibrate a model with known outlets as storm drains and to have an idea of what the water level can be during a storm event.

7.3 Optimum grid scale

One of the goals of the research was to compare grid scales of the high resolution DEMs and find the optimum for use in a hydrological model. Dottori et al. (2013), Blanc et al. (2012), Chen et al. (2012), Fewtrell et al. (2011) state everything smaller than 2 m is already considered high resolution. The lowest resolution used in this research is 2 m. The histograms were not able to find an optimum grid scale within the four used scales (25, 50, 100 and 200 cm). It is possible that the resolution was already at such a high or optimum scale, that no difference can be found. It would be informative to this research to look at grid scales of larger than 2 m to compare them with the results of this report.

REFERENCES

Aronica, G., Bates, P. D., & Horritt, M. S. (2002). Assessing the uncertainty in distributed model predictions using observed binary pattern information within GLUE. *Hydrological Processes, 16*(10), 2001-2016.

Beven, K. (2000). Uniqueness of place and process representations in hydrological modelling. *Hydrological Earth Systems Science, 4*(2), 203-213.

Blanc, J., Hall, J. W., Roche, N., Dawson, R. J., Cesses, Y., Burton, A., & Kilsby C.G. (2012). Enhanced efficiency of pluvial flood risk estimation in urban areas using spatial temporal rainfall simulations. *Journal of Flood Risk Management, 5*(2), 143-152.

Blok, M. (2010). WOLK brengt extreme wateroverlast in beeld. *Riolering*, March 2010. Retrieved from http://www.tauwweetwaterspeelt.nl/downloads/WOLK-wateroverlast.pdf (August 12 2014).

Chen, A. S., Evans, B., Djordjevic, S., & Savic, D. A. (2012). A coarse-grid approach to representing building blockage effects in 2D urban flood modelling. *Journal of Hydrology, 426-427*, 1-16.

Chocat, B. (2012). Urban Hydrology Models. *Mathematical Models, Volume 2,* , 155-212.

Chow, V. T., Maidment D. R., & Mays L. W. (1998). Applied Hydrology. McGraw-Hillbook Co., New York.

Climate Scenarios (2014), KNMI `14: Climate Change scenarios for the 21st Century. Scientific Report WR2014-01, KNMI, De Bilt, The Netherlands. Accessed on 1 October 2014. <http://www.climatescenarios.nl/>

Dottori, F., Di Baldassarre, G., & Todini, E. (2013). Detailed data is welcome, but with a pinch of salt: Accuracy, precision, and uncertainty in flood inundation modeling. *Water Resources Research, 49*(9), 6079-6085.

DUIC (2014). Noodweer in Utrecht. Accessed on 1 October 2014. <http://www.duic.nl/nieuws/noodweer-in-utrecht-hoog-catharijne-gedeeltelijk-afgesloten-operatiekamers-antonius-ontruimd/>

ESRI (2014). Working with LAS classification in ArcGIS. Accessed on 1 February 2015 <http://resources.arcgis.com/en/help/main/10.2/index.html#//015w00000047000000>

Fewtrell, T. J., Bates, P. D., Horritt, M., & Hunter, N. (2008). Evaluating the effect of scale in flood inundation modelling in urban environments. *Hydrological Processes, 22*(26), 5107-5118.

Fewtrell, T. J., Duncan, A., Sampson, C. C., Neal, J. C., & Bates, P. D. (2011). Benchmarking urban flood models of varying complexity and scale using high resolution terrestrial LiDAR data. *Physics and Chemistry of the Earth, Parts A/B/C, 36*(7–8), 281-291.

Gallegos, H. A., Schubert, J. E., & Sanders, B. F. (2009). Two-dimensional, high-resolution modeling of urban dam-break flooding: A case study of Baldwin Hills, California. *Advances in Water Resources, 32*(8), 1323-1335.

Gehrke, S., Morin, K., Downey, M., Boehrer, N., & Fuchs, T. (2010). Semi-global matching: An alternative to LIDAR for DSM generation. *International Archives of the Photogrammetry, Remote Sensing and Spatial Information Sciences, Calgary, AB, 38 (B1).*

Grontmij (n.d.). WODAN123: een nieuwe aanpak van wateroverlast in de stad. Retrieved from http://www.grontmij.nl/Productinnovaties/documents/WODAN123%20een%20nieuwe%20aanpak%20van%20wateroverlast%20in%20de%20stad.pdf (August 12 2014).

Haala, N., & Rothermel, M. (2012). Dense multi-stereo matching for high quality digital elevation models. *Photogrammetrie, Fernerkundung, Geoinformation, 2012*(4), 331-343.

Heywood, D.I., Cornelius, S.C. & Carver, S.J., (2011). An Introduction to Geographical Information Systems, 4th edition. Harlow: Pearson Education

Hexagon Geospatial (2013). Creating Customized Spatial Models With Point Clouds: Using Spatial Modeler Operators To Process Point Clouds in Imagine 2014. White paper. Accessed on 1 February 2015. <http://www.hexagon-solutions.com.cn/Libraries/White_Papers/Creating_Customized_Spatial_Models_with_Point_Clouds_WhitePaper.sflb.pdf>

Hirschmüller, H. (2005). Accurate and efficient stereo processing by semi-global matching and mutual information. Paper presented at the *Computer Vision and Pattern Recognition, 2005. CVPR 2005. IEEE Computer Society Conference on, 2*. pp. 807-814.
Hirschmüller, H. (2008). Stereo processing by semiglobal matching and mutual information. *IEEE Transactions on Pattern Analysis and Machine Intelligence, 30*(2), 328-341.

Höhle, J., & Höhle, M. (2009). Accuracy assessment of digital elevation models by means of robust statistical methods. *ISPRS Journal of Photogrammetry and Remote Sensing, 64*(4), 398-406.

Johnson, D. (2013). Santa Barbara watershed delineation using ArcHydro. Accessed on 15 October 2014. <https://www.behance.net/gallery/3179252/Santa-Barbara-Watershed-Delineation-Using-ArcHydro>

Kenward, T., Lettenmaier, D. P., Wood, E. F., & Fielding, E. (2000). Effects of digital elevation model accuracy on hydrologic predictions. *Remote Sensing of Environment, 74*(3), 432-444.

Kienzle, S. (2004). The effect of DEM raster resolution on first order, second order and compound terrain derivatives. *Transactions in GIS, 8*(1), 83-111.

KNMI (2014). Neerslagstatistiek. Accessed on 1 October 2014. <http://www.knmi.nl/klimatologie/achtergrondinformatie/neerslagstatistiek.pdf>

Krebs, G., Kokkonen, T., Valtanen, M., Setälä, H., & Koivusalo, H. (2014). Spatial resolution considerations for urban hydrological modelling. *Journal of Hydrology, 512*(0), 482-497.

Kuo, W., Steenhuis, T. S., McCulloch, C. E., Mohler, C. L., Weinstein, D. A., DeGloria, S. D., et al. (1999). Effect of grid size on runoff and soil moisture for a variable-source-area hydrology model. *Water Resources Research*, 35(11), 3419-3428.

Leberl, F., Irschara, A., Pock, T., Meixner, P., Gruber, M., Scholz, S., & Wiechert, A. (2010). Point clouds: Lidar versus 3D vision. *Photogrammetric Engineering and Remote Sensing, 76*(10), 1123-1134.

Li, J., & Wong, D. W. (2010). Effects of DEM sources on hydrologic applications. *Computers, Environment and Urban Systems, 34*(3), 251-261.

Liu, X. (2008). Airborne LiDAR for DEM generation: some critical issues. *Progress in Physical Geography, 32*(1), 31-49.

Ludwig, R., & Schneider, P. (2006). Validation of digital elevation models from SRTM X-SAR for applications in hydrologic modeling. *ISPRS Journal of Photogrammetry and Remote Sensing, 60*(5), 339-358.

Maksimović, Č., Prodanović, D., Boonya-Aroonnet, S., Leitao, J. P., Djordjević, S., & Allitt, R. (2009). Overland flow and pathway analysis for modelling of urban pluvial flooding. *Journal of Hydraulic Research, 47*(4), 512-523.

Mark, O., Weesakul, S., Apirumanekul, C., Aroonnet, S. B., & Djordjević, S. (2004). Potential and limitations of 1D modelling of urban flooding. *Journal of Hydrology, 299*(3–4), 284-299.

Mason, D. C., Horritt, M. S., Hunter, N. M., & Bates, P. D. (2007). Use of fused airborne scanning laser altimetry and digital map data for urban flood modelling. *Hydrological Processes, 21*(11), 1436-1447.

Mitasova, H., & Mitas, L. (2001). Multiscale soil erosion simulations for land use management. *Landscape Erosion and Evolution Modeling* (pp. 321-347) Springer.

Oksanen, J., & Sarjakoski, T. (2005). Error propagation of DEM-based surface derivatives. *Computers & Geosciences, 31*(8), 1015-1027.

Van Oldenborgh, G.J., Lenderink, G., (2014). KNMI. Hoe vaak komt extreme neerslag zoals op 28 juli tegenwoordig voor, en is dat anders dan vroeger? Accessed on 1 October 2014. <http://www.knmi.nl/cms/content/120817/hoe_vaak_komt_extreme_neerslag_zoals_op_28_juli_tegenwoordig_voor_en_is_dat_anders_dan_vroeger>

Ozdemir, H., Sampson, C. C., De Almeida, G. A. M., & Bates, P. D. (2013). Evaluating scale and roughness effects in urban flood modelling using terrestrial LIDAR data. *Hydrology and Earth System Sciences, 17*(10), 4015-4030.

Parool, 2015. Veel wateroverlast door wolkbreuk boven Amsterdam. August 24, 2015. Accessed on 10 October 2015. http://www.parool.nl/parool/nl/4/AMSTERDAM/article/detail/4128343/2015/08/24/Veel-wateroverlast-door-wolkbreuk-boven-Amsterdam.dhtml

Rayburg, S., Thoms, M., & Neave, M. (2009). A comparison of digital elevation models generated from different data sources. *Geomorphology, 106*(3–4), 261-270.

Rossman, L. A. (2010). *Storm water management model user's manual, version 5.0* National Risk Management Research Laboratory, Office of Research and Development, US Environmental Protection Agency.

Rumman, N., Lin, G., & Li, J. (2005). Investigation of GIS-based surface hydrological modelling for identifying infiltration zones in an urban watershed. *Environmental Informatics Archives, 3*, 315-322.

Sampson, C. C., Bates, P. D., Neal, J. C., & Horritt, M. S. (2013). An automated routing methodology to enable direct rainfall in high resolution shallow water models. *Hydrological Processes, 27*(3), 467-476.

Skotnicki, M., & Sowinski, M. (2013). The influence of depression storage on runoff from impervious surface of urban catchment. *Urban Water Journal.*

Spijker, M., Dassen, W., & Loovers, I. (2013). Inzicht in wateroverlast en effectiviteit van maatregelen met hoogwaardig afstroom- en infiltratiemodel. Accessed on 12 August 2014. <http://www.riool.net/c/document_library/get_file?uuid=40021588-a47f-4f82-b9c6-741f4b577ba3&groupId=10180&target Extension=pdf>

Valeo, C., & Moin, S. (2000). Variable source area modelling in urbanizing watersheds. *Journal of Hydrology, 228*(1), 68-81.

Verbond van Verzekeraars (2014). Zware regenval levert forse schade op. Accessed on 8 August 2014. https://www.verzekeraars.nl/actueel/nieuwsberichten/Paginas/Zware-regenval-levert-forse-schade-op.aspx>

Walker, J. P., & Willgoose, G. R. (1999). On the effect of digital elevation model accuracy on hydrology and geomorphology. *Water Resources Research, 35*(7), 2259-2268.

Van Wayenburg, B. (2014, April 4 & 5). Overstromen op verzoek. *NRC Handelsblad*. Accessed on 8 August 2014. <http://www.nrc.nl/handelsblad/van/2014/april/05/overstromen-op-verzoek-1362338>

Wilson, J. P. (2012). Digital terrain modeling. *Geomorphology, 137*(1), 107-121.

Yu, D., & Lane, S. N. (2006). Urban fluvial flood modelling using a two-dimensional diffusion-wave treatment, part 1: mesh resolution effects. *Hydrological Processes, 2* 1541-1565.

Van der Zon, N. (2013). AHN2 Kwaliteitsdocument. Accessed on 15 July 2014. <http://www.ahn.nl/$1b6l/page/>

APPENDIX A – DEM ACCURACY & STATIC TEST

A1 DEM accuracy test

Table A-1: Outcome of the DEM accuracy test using 2500 land survey measurements (Unfiltered (U), Filtered (F), Inverse Distance Weighting (IDW), Root Mean Square Error (RMSE), Mean Absolute Error (MAE))

	(Un)-filtered	Method	Void fill	Resolution (m)	RMSE	Bias	RMSE Bias adjusted	MAE	R^2
AHN				0.50	0.6058	-0.013	0.5885	0.1837	0.8262
10 p/m²	U	IDW	Linear	0.25	1.9044	-0.824	1.7167	0.8966	0.3315
				0.50	1.9107	-0.832	1.7198	0.9034	0.3309
				1	1.9906	-0.839	1.8053	0.9250	0.3062
				2	1.9086	-0.823	1.7222	0.8997	0.3291
			Natural Neigh-bor	0.25	1.8959	-0.831	1.7042	0.9001	0.3344
				0.5	1.9114	-0.833	1.7204	0.9037	0.3309
				1	1.9906	-0.839	1.8052	0.9250	0.3062
				2	1.9086	-0.823	1.7222	0.8997	0.3291
10 p/m²	U	Average	Linear	0.25	1.9044	-0.824	1.7167	0.8967	0.3315
				0.5	1.9106	-0.832	1.7198	0.9034	0.3309
				1	1.9925	-0.840	1.8069	0.9243	0.3056
				2	1.9063	-0.830	1.7161	0.9039	0.3303
			Natural Neigh-bor	0.25	1.8959	-0.831	1.7042	0.9001	0.3344
				0.5	1.9113	-0.833	1.7203	0.9036	0.3309
				1	1.9925	-0.840	1.8609	0.9243	0.3056
				2	1.9063	-0.830	1.7161	0.9039	0.3303
10 p/m²	F	IDW	Linear	0.25	0.9492	-0.478	0.8192	0.5346	0.6960
				0.5	0.9432	-0.471	0.8160	0.5291	0.6978
				1	0.9626	-0.481	0.8327	0.5409	0.6881
				2	1.0045	-0.481	0.8809	0.5443	0.6584
			Natural Neigh-bor	0.25	0.9433	-0.479	0.8116	0.5317	0.7003
				0.5	0.9382	-0.471	0.8106	0.5280	0.7008
				1	0.9602	-0.481	0.8301	0.5400	0.6897
				2	1.0022	-0.480	0.8786	0.5431	0.6596
10 p/m²	F	Average	Linear	0.25	0.9492	-0.478	0.8192	0.5346	0.6960
				0.5	0.9430	-0.471	0.8159	0.5290	0.6978
				1	0.9604	-0.481	0.8302	0.5394	0.6896
				2	0.9971	-0.480	0.8728	0.5398	0.6629
			Natural Neigh-bor	0.25	0.9433	-0.479	0.8117	0.5317	0.7003
				0.5	0.9380	-0.471	0.8105	0.5279	0.7009
				1	0.9581	-0.481	0.8277	0.5386	0.6911
				2	0.9949	-0.479	0.8707	0.5387	0.6641
80 p/m²	U	IDW	Linear	0.25	1.9569	-0.809	1.7817	0.8897	0.3152
				0.5	1.9613	-0.812	1.7852	0.8869	0.3128
				1	1.9139	-0.813	1.7327	0.8751	0.3269

				2	1.8976	-0.827	1.7081	0.8884	0.3293
			Natural Neigh-bor	0.25	1.9580	-0.809	1.7832	0.8896	0.3150
				0.5	1.9615	-0.822	1.7853	0.8873	0.3170
				1	1.9139	-0.813	1.7327	0.8751	0.3269
				2	1.8976	-0.827	1.7082	0.8884	0.3293
80 p/m²	U	Average	Linear	0.25	1.9563	-0.810	1.7809	0.8897	0.3156
				0.5	1.9622	-0.815	1.7847	0.8853	0.3117
				1	1.9020	-0.813	1.7940	0.8769	0.3306
				2	1.8663	-0.829	1.6721	0.8899	0.3390
			Natural Neigh-bor	0.25	1.9574	-0.809	1.7823	0.8897	0.3153
				0.5	1.9624	-0.816	1.7848	0.8856	0.3116
				1	1.9020	-0.813	1.7194	0.8769	0.3306
				2	1.8663	-0.829	1.6721	0.8899	0.3390
80 p/m²	F	IDW	Linear	0.25	1.0189	-0.496	0.8899	0.5550	0.6619
				0.5	1.0064	-0.489	0.8793	0.5427	0.6681
				1	0.9843	-0.480	0.8593	0.5294	0.6788
				2	1.0349	-0.490	0.9113	0.5347	0.6478
			Natural Neigh-bor	0.25	1.0194	-0.498	0.8895	0.5563	0.6610
				0.5	1.0090	-0.492	0.8810	0.5450	0.6656
				1	0.9843	-0.481	0.8587	0.5304	0.6776
				2	1.0352	-0.491	0.9115	0.5351	0.6459
80 p/m²	F	Average	Linear	0.25	1.0302	-0.499	0.9013	0.5575	0.6539
				0.5	1.0176	-0.493	0.8901	0.5452	0.6598
				1	0.9705	-0.479	0.8443	0.5248	0.6860
				2	1.0173	-0.488	0.8924	0.5296	0.6594
			Natural Neigh-bor	0.25	1.0189	-0.498	0.8889	0.5560	0.6614
				0.5	1.0150	-0.494	0.8867	0.5458	0.6620
				1	0.9070	-0.480	0.8438	0.5259	0.6866
				2	1.0176	-0.489	0.8925	0.5299	0.6562

Table A2: Outcome of the DEM accuracy test using the AHN2 to compare with the constructed DEMs (Unfiltered (U), Filtered (F), Inverse Distance Weighting (IDW), Root Mean Square Error (RMSE), Mean Absolute Error (MAE))

	(Un)-filtered	Method	Void fill	Resolution (m)	RMSE	Bias	RMSE Bias adjusted	MAE	R^2
10 p/m²	F	IDW	Linear	0.25	1.3368	-0.664	1.1593	0.6875	0.4787
				0.5	1.3222	-0.658	1.1462	0.6786	0.4876
				1	1.3117	-0.658	1.1344	0.6853	0.4943
				2	1.2259	-0.641	1.0447	0.6622	0.5466
			Natural Neigh-bor	0.25	1.3283	-0.667	1.1483	0.6859	0.4849
				0.5	1.3119	-0.657	1.1347	0.6771	0.4930
				1	1.3047	-0.656	1.1274	0.6831	0.4980
				2	1.2240	-0.641	1.0428	0.6611	0.5478
10 p/m²	F	Average	Linear	0.25	1.3368	-0.664	1.1593	0.6875	0.4787
				0.5	1.3222	-0.658	1.1461	0.6786	0.4876
				1	1.3132	-0.658	1.1361	0.6854	0.4931

				2	1.2195	-0.641	1.0370	0.6593	0.5501
			Natural Neigh-bor	0.25	1.3283	-0.667	1.1483	0.6859	0.4849
				0.5	1.3118	-0.657	1.1347	0.6771	0.4930
				1	1.3061	-0.656	1.1289	0.6832	0.4969
				2	1.2177	-0.641	1.0353	0.6583	0.5512
80 p/m²	F	IDW	Linear	0.25	1.0162	-0.498	0.8859	0.5713	0.6619
				0.5	1.0037	-0.491	0.8753	0.5592	0.6681
				1	0.9814	-0.482	0.8551	0.5451	0.6788
				2	1.0322	-0.492	0.9075	0.5502	0.6478
			Natural Neigh-bor	0.25	1.0194	-0.498	0.8895	0.5739	0.6610
				0.5	1.0091	-0.492	0.8810	0.5628	0.6656
				1	0.9843	-0.481	0.8587	0.5475	0.6776
				2	1.0352	-0.491	0.9115	0.5521	0.6459
80 p/m²	F	Average	Linear	0.25	1.0124	-0.494	0.8836	0.5728	0.6579
				0.5	1.0039	-0.488	0.8772	0.5610	0.6603
				1	0.9500	-0.474	0.8235	0.5368	0.6915
				2	1.0033	-0.483	0.8792	0.5380	0.6569
			Natural Neigh-bor	0.25	1.0190	-0.498	0.8889	0.5735	0.6614
				0.5	1.0151	-0.494	0.8867	0.5635	0.6620
				1	0.9707	-0.480	0.8438	0.5428	0.6866
				2	1.0176	-0.489	0.8925	0.5469	0.6562

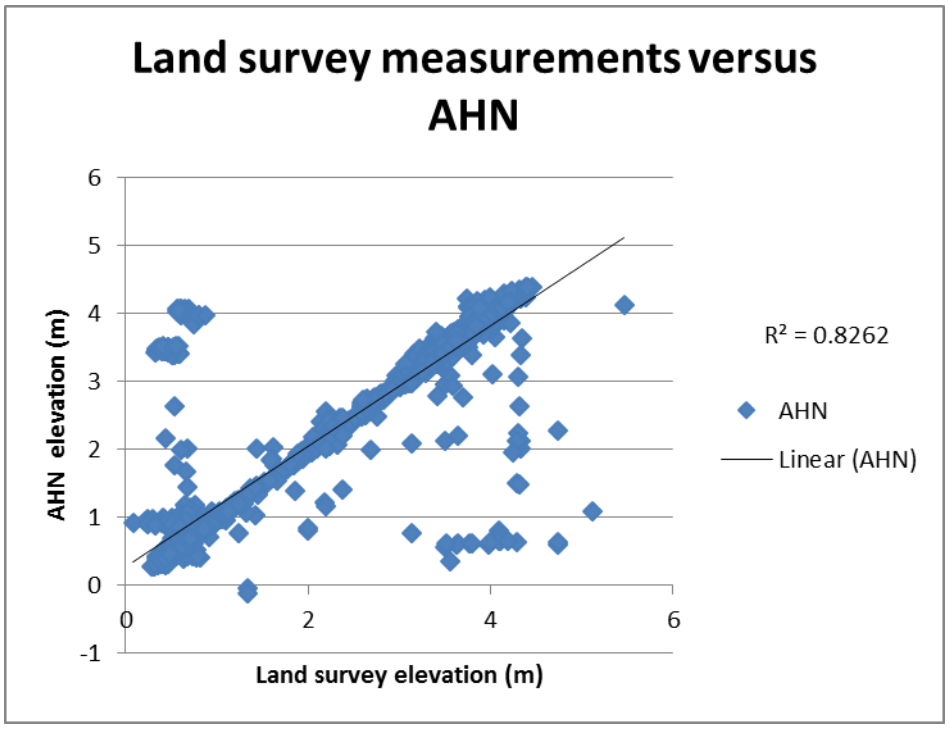

Figure A-1: Scatter plot of 2500 land survey measurements against the AHN2

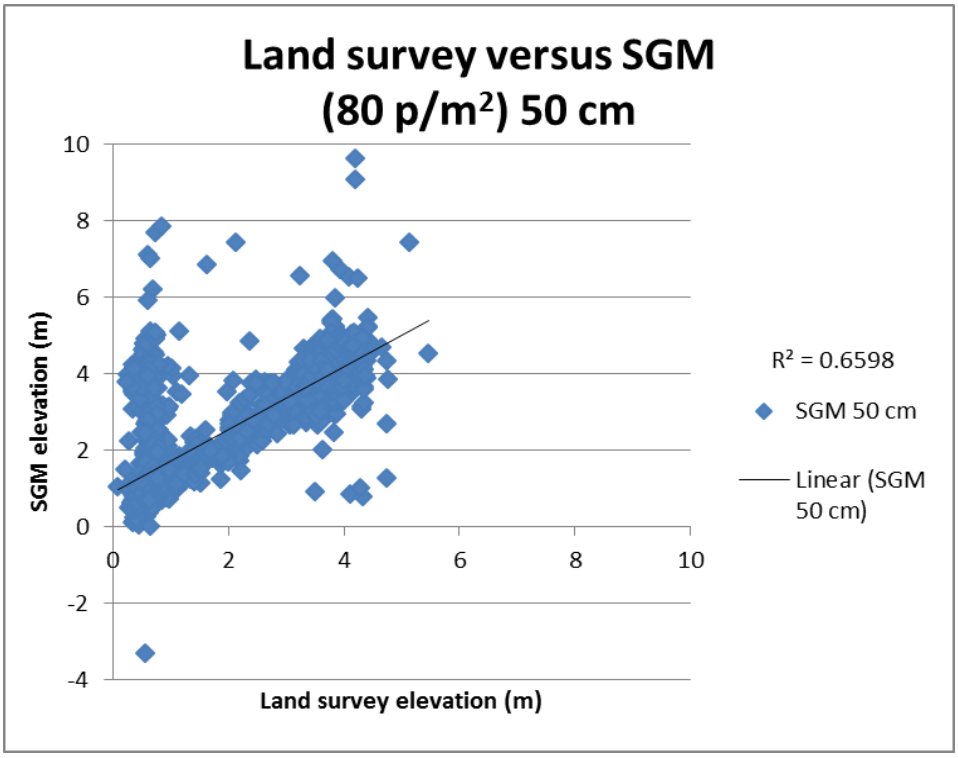

Figure A-2: Scatter plot of 2500 land survey measurements against the SGM DEM 80 p/m^2.

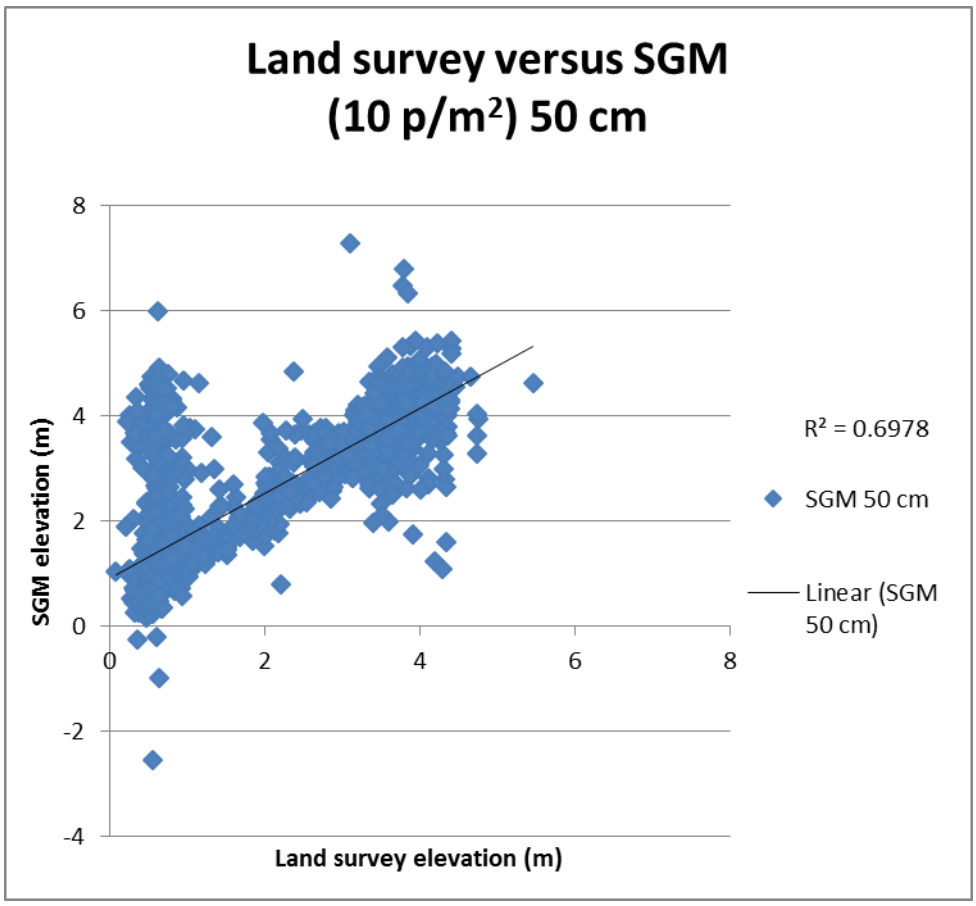

Figure A-3: Scatter plot of 2500 land survey measurements against the SGM DEM 10 p/m^2.

A2 Static test

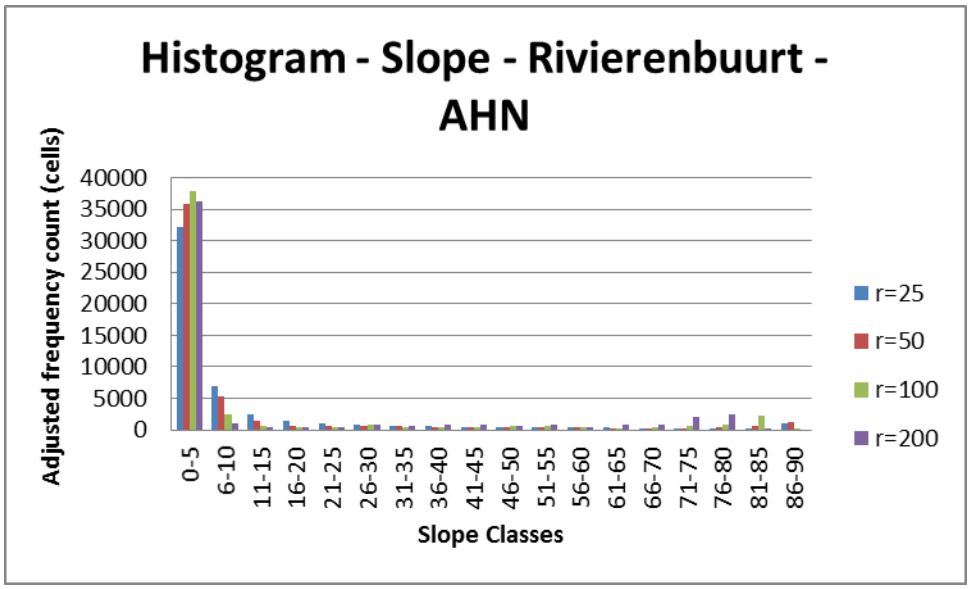

Figure A-4: Histogram slope classes in the Rivierenbuurt (AHN)

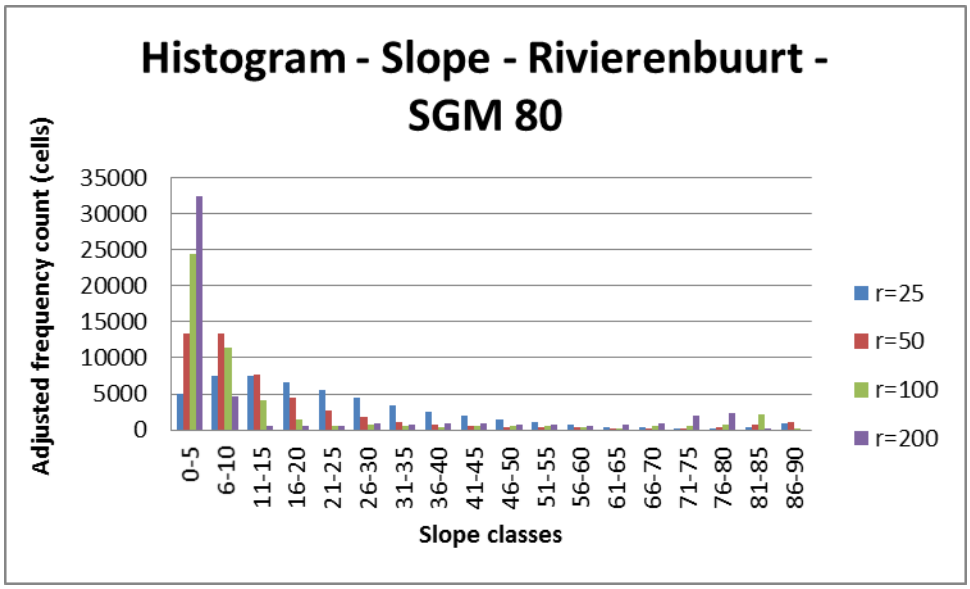

Figure A-5: Histogram slope classes in the Rivierenbuurt (SGM 80)

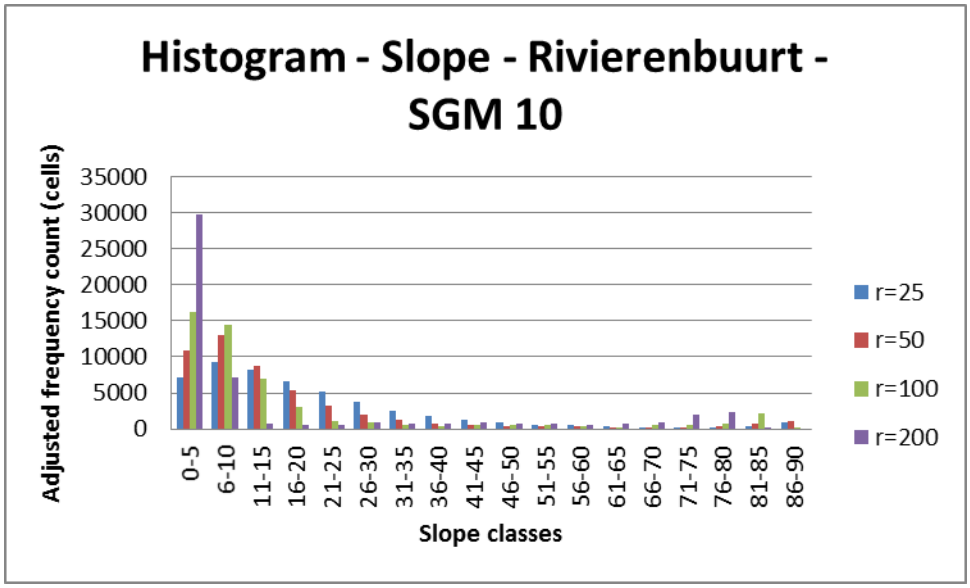

Figure A-6: Histogram slope classes in the Rivierenbuurt (SGM 10)

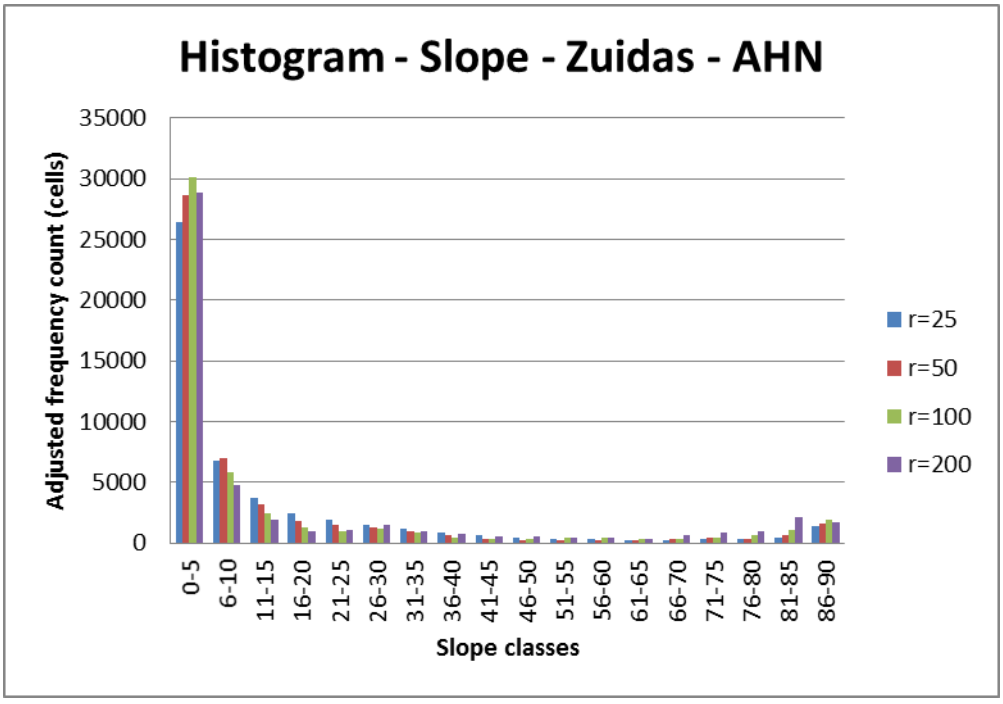

Figure A-7: Histogram slope classes in the Zuidas (AHN)

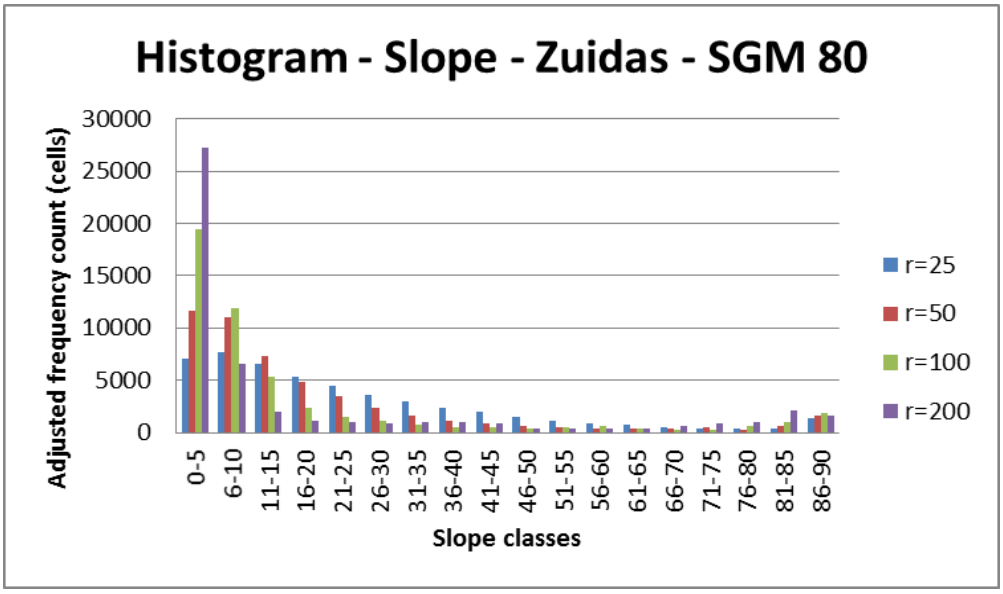

Figure A-8: Histogram slope classes in the Zuidas (SGM 80)

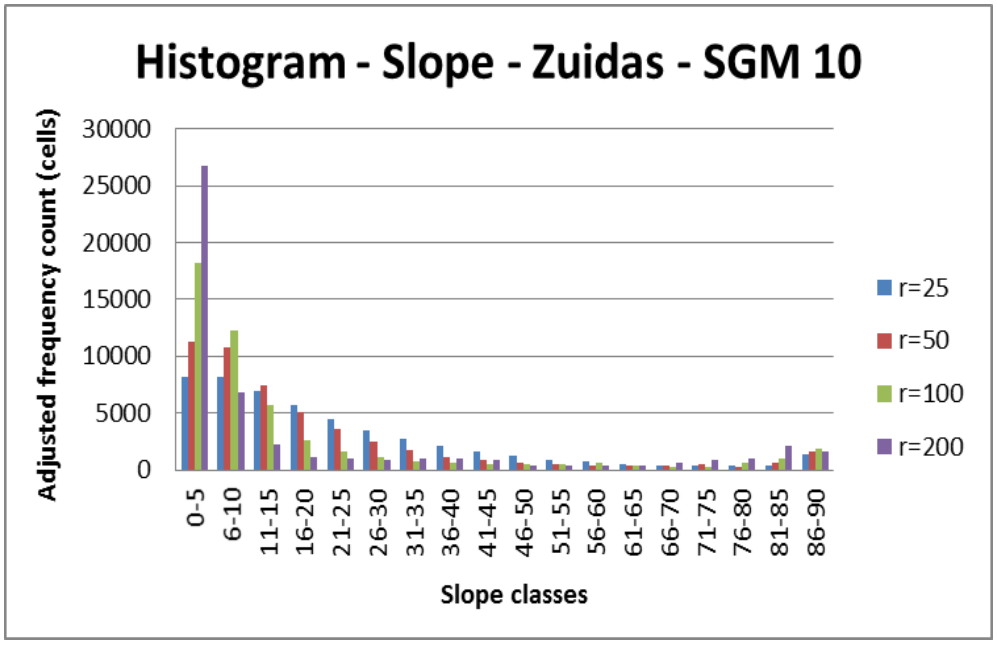

Figure A-9: Histogram slope classes in the Zuidas (SGM 10)

Table A-3: Changes in catchment area per grid size, and DEM source

Site	DEM source	Grid size (cm)	Count	Maximum area (m^2)	Mean	Standard deviation
Rivierenbuurt	AHN	25	31	9409	1535	2249
Rivierenbuurt	AHN	50	29	6836	1648	1954
Rivierenbuurt	AHN	100	26	7599	1864	2256
Rivierenbuurt	AHN	200	27	7960	1807	2165
Rivierenbuurt	SGM	25	33	14900	1390	3260
Rivierenbuurt	SGM	50	34	28277	1387	4724
Rivierenbuurt	SGM	100	31	31190	1548	5448
Rivierenbuurt	SGM	200	25	27504	1938	5335
Rivierenbuurt	thin	25	37	25371	1277	4061
Rivierenbuurt	thin	50	41	28192	1155	4309
Rivierenbuurt	thin	100	32	29930	1473	5148
Rivierenbuurt	thin	200	34	16112	1421	3348
Zuidas	AHN	25	43	9555	1097	1886
Zuidas	AHN	50	33	13817	1440	2778
Zuidas	AHN	100	31	10625	1541	2389
Zuidas	AHN	200	32	7544	1520	1970
Zuidas	SGM	25	36	26035	1291	4241
Zuidas	SGM	50	33	23481	1437	3988
Zuidas	SGM	100	29	29233	1618	5275
Zuidas	SGM	200	21	28704	2293	5975
Zuidas	thin	25	36	26723	1296	4356
Zuidas	thin	50	36	26093	1321	4260
Zuidas	thin	100	30	28136	1581	5000
Zuidas	thin	200	26	28332	1853	5382

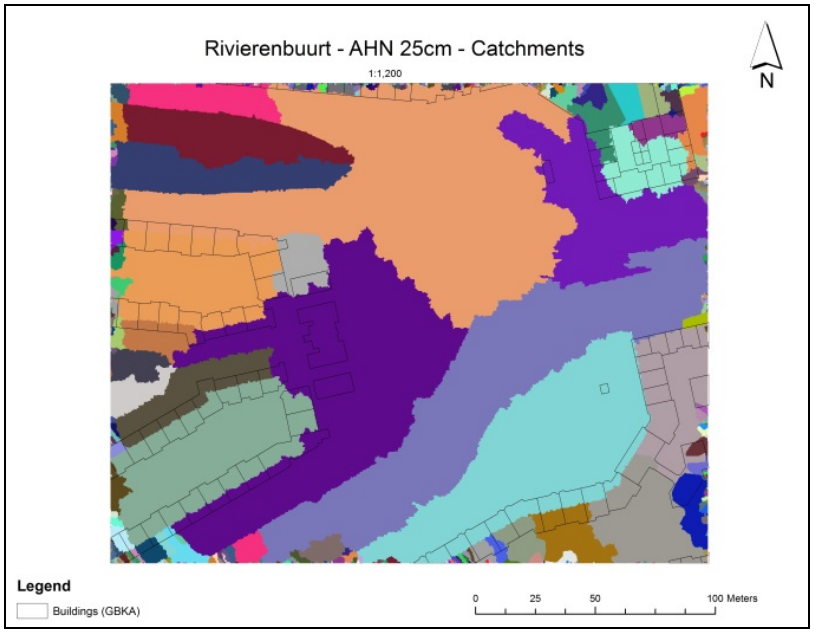

Figure A-10a: Catchments in the Rivierenbuurt study site at 25 cm for the AHN2 DEM

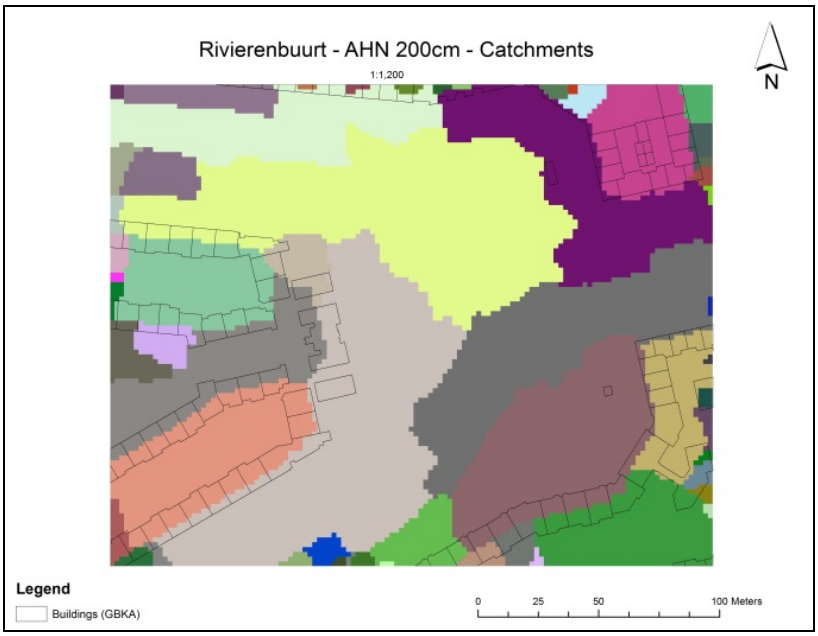

Figure A-10b: Catchments in the Rivierenbuurt study site at 200 cm for the AHN2 DEM

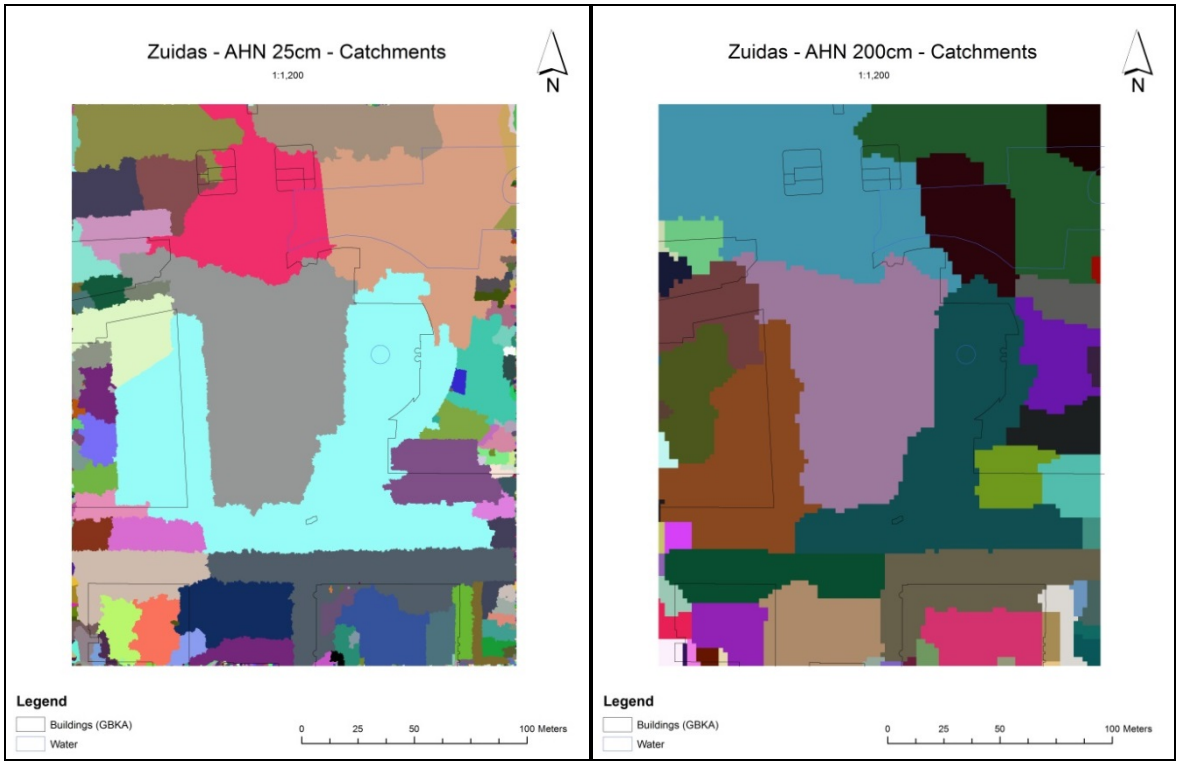

Figure A-11: Catchments in the Zuidas study site (left 25 cm, right 200 cm) for the AHN2 DEM

APPENDIX B – MODEL OUTPUT (WATER LEVEL)

Rivierenbuurt

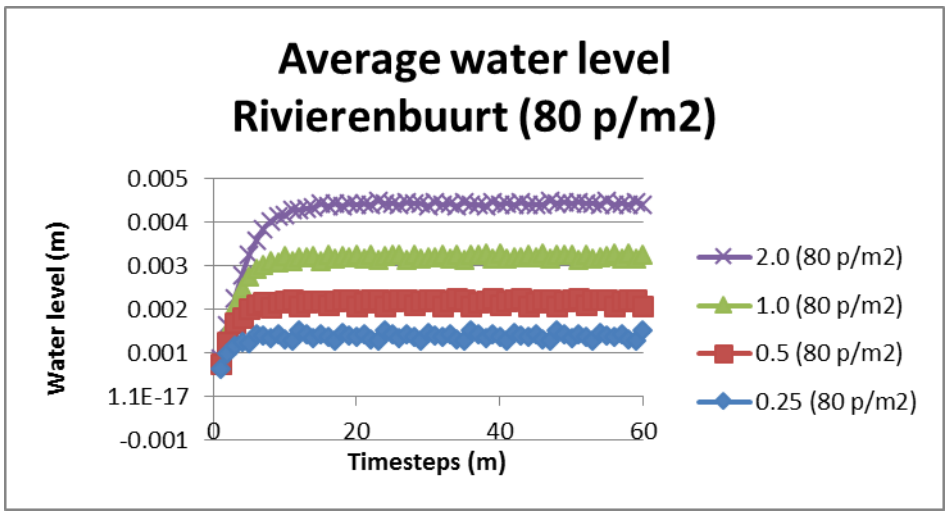

Figure B-1: Average water level in the Rivierenbuurt study site for SGM 80 p/m² DEMs

Table B-1: RMSE comparison of SGM 80 p/m² DEMs

Reference	Comparing	RMSE
0.25 (80 p/m²)	0.50 (80 p/m²)	0.00078
0.25 (80 p/m²)	1.0 (80 p/m²)	0.00176
0.25 (80 p/m²)	2.0 (80 p/m²)	0.00288
0.5 (80 p/m²)	1.0 (80 p/m²)	0.00099
0.5 (80 p/m²)	2.0 (80 p/m²)	0,00212
1.0 (80 p/m²)	2.0 (80 p/m²)	0,00113

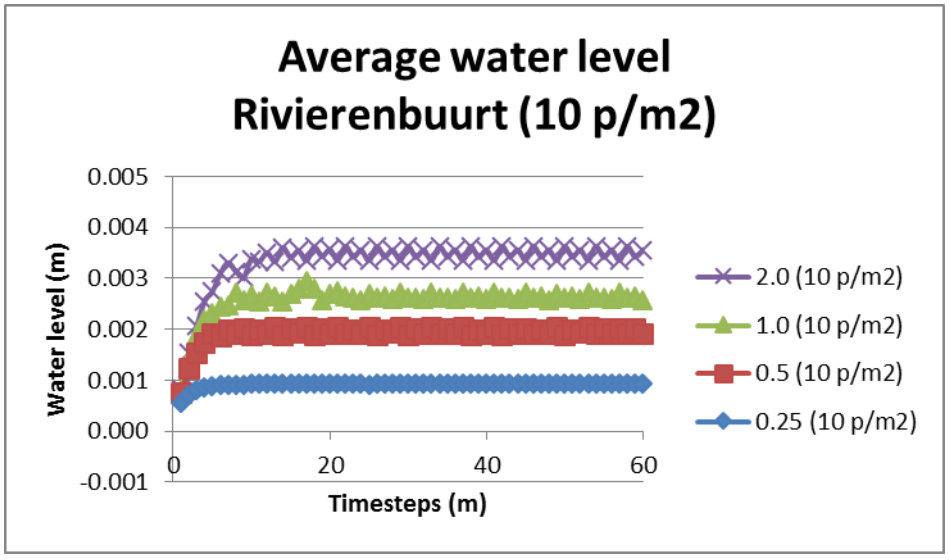

Figure B-2: Average water level in the Rivierenbuurt study site for SGM 10 p/m² DEMs

Table B-2: RMSE comparison of SGM 10 p/m² DEMs

Reference	Comparing	RMSE
0.25 (10 p/m²)	0.50 (10 p/m²)	0.00101
0.25 (10 p/m²)	1.0 (10 p/m²)	0.00167
0.25 (10 p/m²)	2.0 (10 p/m²)	0.00245
0.5 (10 p/m²)	1.0 (10 p/m²)	0.00066
0.5 (10 p/m²)	2.0 (10 p/m²)	0.00145
1.0 (10 p/m²)	2.0 (10 p/m²)	0.00080

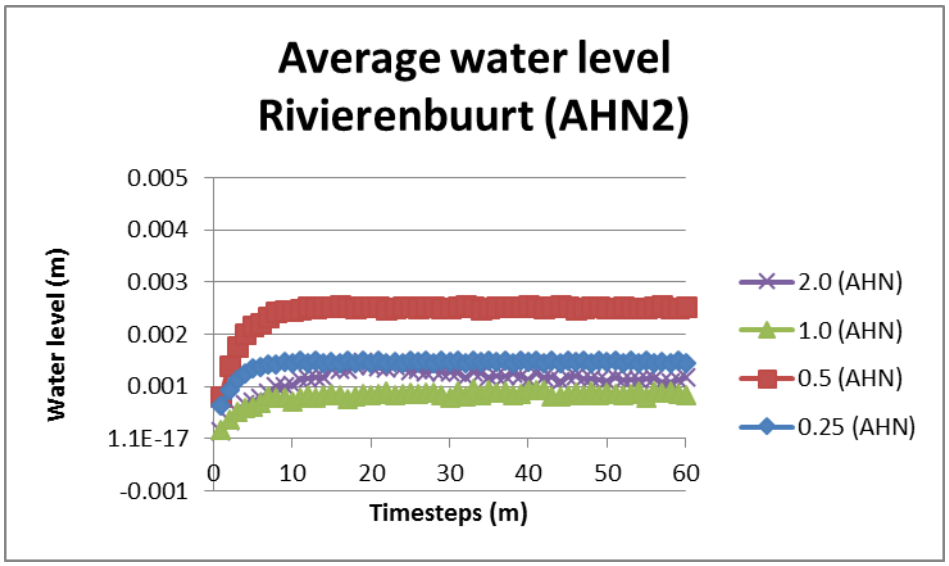

Figure B-3: Average water level in the Rivierenbuurt study site for AHN DEMs

Table B-3: RMSE comparison of AHN DEMs

Reference	Comparing	RMSE
0.25 AHN	0.50 AHN	0.00101
0.25 AHN	1.0 AHN	0.00062
0.25 AHN	2.0 AHN	0.00033
0.5 AHN	1.0 AHN	0.00163
0.5 AHN	2.0 AHN	0.00130
1.0 AHN	2.0 AHN	0.00036

Zuidas

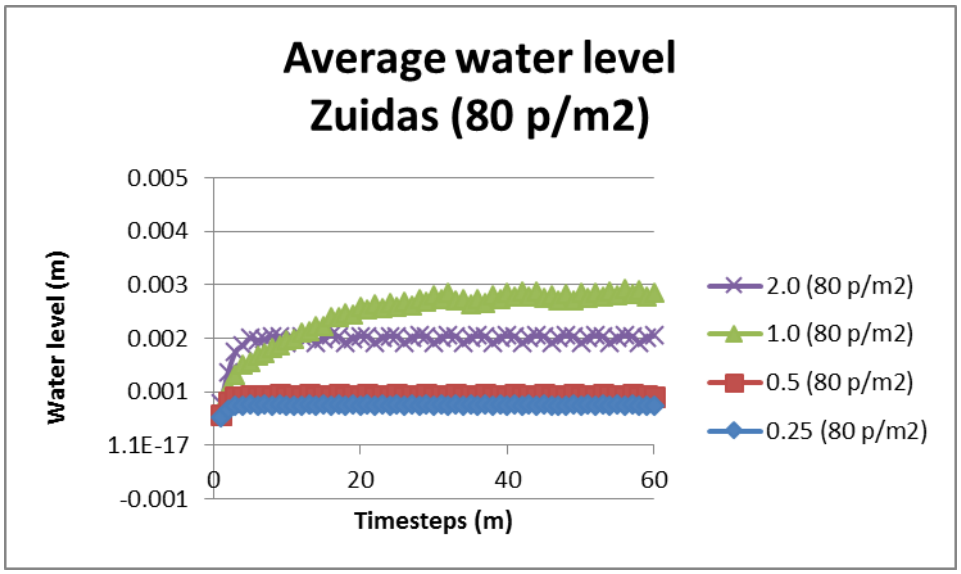

Figure B-4: Average water level in the Zuidas study site study site for SGM 80 p/m^2 DEMs

Table B-4: RMSE comparison of SGM 80 p/m^2 DEMs

Reference	Comparing	RMSE
0.25 (80 p/m^2)	0.50 (80 p/m^2)	0.0002
0.25 (80 p/m^2)	1.0 (80 p/m^2)	0.0018
0.25 (80 p/m^2)	2.0 (80 p/m^2)	0.0023
0.5 (80 p/m^2)	1.0 (80 p/m^2)	0.0016
0.5 (80 p/m^2)	2.0 (80 p/m^2)	0.0011
1.0 (80 p/m^2)	2.0 (80 p/m^2)	0.0006

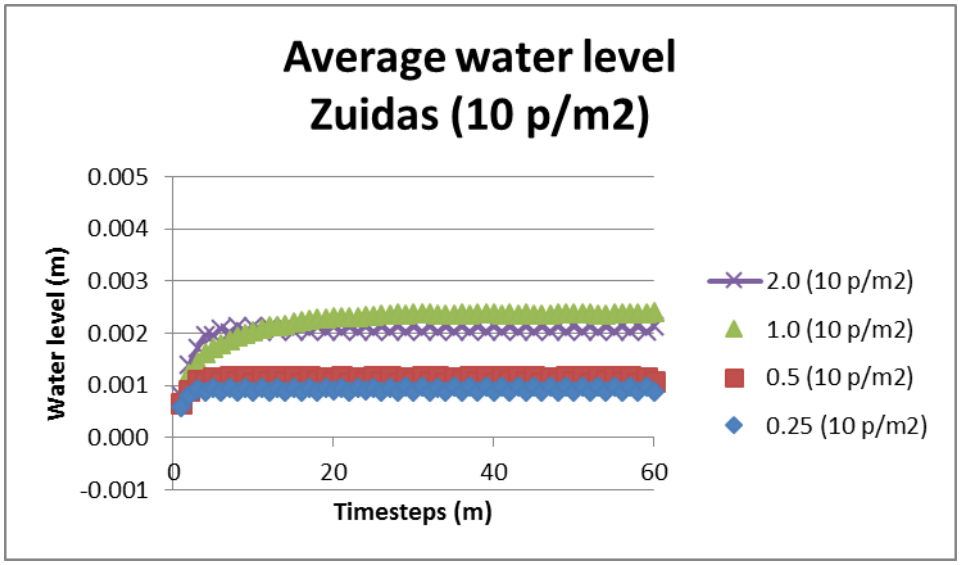

Figure B-5: Average water level in the Zuidas study site study site for SGM 10 p/m^2 DEMs

Table B-5: RMSE comparison of SGM 10 p/m^2 DEMs

Reference	Comparing	RMSE
0.25 (10 p/m^2)	0.50 (10 p/m^2)	0.0002
0.25 (10 p/m^2)	1.0 (10 p/m^2)	0.0013
0.25 (10 p/m^2)	2.0 (10 p/m^2)	0.0002
0.5 (10 p/m^2)	1.0 (10 p/m^2)	0.0011
0.5 (10 p/m^2)	2.0 (10 p/m^2)	0.0009
1.0 (10 p/m^2)	2.0 (10 p/m^2)	0.0003

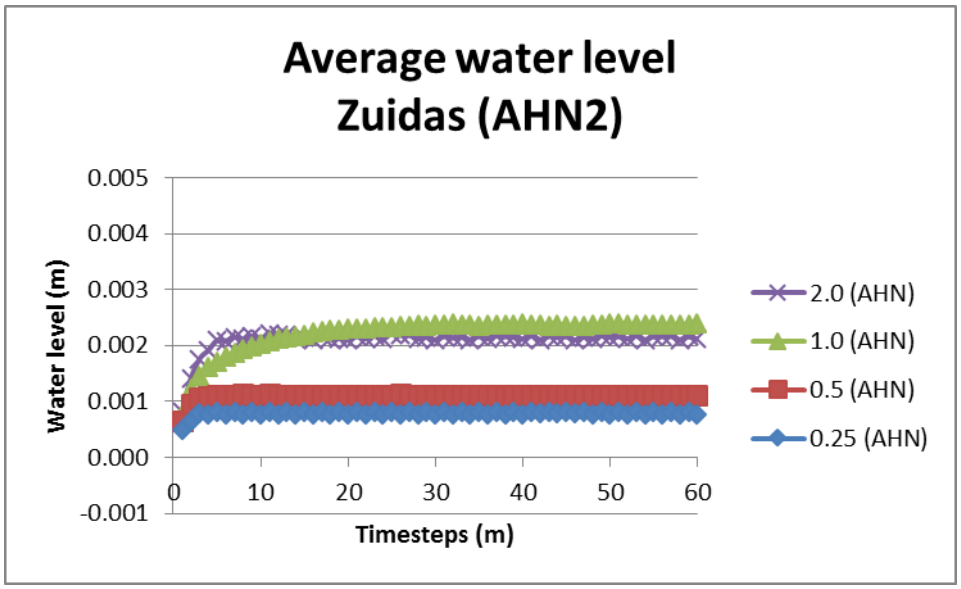

Figure B-6: Average water level in the Zuidas study site study site for AHN DEMs

Table B-6: RMSE comparison of AHN DEMs

Reference	Comparing	RMSE
0.25 AHN	0.50 AHN	0.0003
0.25 AHN	1.0 AHN	0.0015
0.25 AHN	2.0 AHN	0.0013
0.5 AHN	1.0 AHN	0.0011
0.5 AHN	2.0 AHN	0.0010
1.0 AHN	2.0 AHN	0.0002

APPENDIX C – MODEL OUTPUT (PONDED AREA)

Rivierenbuurt

Table C-1: F^2-statistic comparison of SGM 80 p/m²

Reference	Comparing	F^2 statistic
0.25 (80 p/m²)	0.50 (80 p/m²)	-0.11258
0.25 (80 p/m²)	1.0 (80 p/m²)	0.12255
0.25 (80 p/m²)	2.0 (80 p/m²)	0.14905
0.5 (80 p/m²)	1.0 (80 p/m²)	0.30126
0.5 (80 p/m²)	2.0 (80 p/m²)	0.30445
1.0 (80 p/m²)	2.0 (80 p/m²)	0.40808

Table C-2: F^2-statistic comparison of SGM 10 p/m²

Reference	Comparing	F^2 statistic
0.25 (10 p/m²)	0.50 (10 p/m²)	0.18971
0.25 (10 p/m²)	1.0 (10 p/m²)	0.14621
0.25 (10 p/m²)	2.0 (10 p/m²)	0.16243
0.5 (10 p/m²)	1.0 (10 p/m²)	0.22503
0.5 (10 p/m²)	2.0 (10 p/m²)	0.27856
1.0 (10 p/m²)	2.0 (10 p/m²)	0.36916

Table C-3: F^2-statistic comparison of AHN

Reference	Comparing	F^2 statistic
0.25 AHN	0.50 AHN	0.23297
0.25 AHN	1.0 AHN	0.27951
0.25 AHN	2.0 AHN	-0.00377
0.5 AHN	1.0 AHN	0.34781
0.5 AHN	2.0 AHN	0.42320
1.0 AHN	2.0 AHN	0.39436

Table C-4: F^2-statistic comparison of SGM 80 p/m² with SGM 10 p/m²

Reference	Comparing	F^2 statistic
0.25 (80 p/m²)	0.25 (10 p/m²)	-0.16334
0.50 (80 p/m²)	0.50 (10 p/m²)	0.11332
1.0 (80 p/m²)	1.0 (10 p/m²)	0.15563
2.0 (80 p/m²)	2.0 (10 p/m²)	0.41875

Table C-5: F^2-statistic comparison of AHN with SGM 80 p/m^2

Reference	Comparing	F^2 statistic
0.25 AHN	0.25 (80 p/m^2)	-0.35643
0.50 AHN	0.50 (80 p/m^2)	-0.02654
1.0 AHN	1.0 (80 p/m^2)	0.05927
2.0 AHN	2.0 (80 p/m^2)	0.46314

Table C-6: F^2-statistic comparison of AHN with SGM 10 p/m^2

Reference	Comparing	F^2 statistic
0.25 AHN	0.25 (10 p/m^2)	-0.26095
0.50 AHN	0.50 (10 p/m^2)	-0.04905
1.0 AHN	1.0 (10 p/m^2)	0.01204
2.0 AHN	2.0 (10 p/m^2)	0.35799

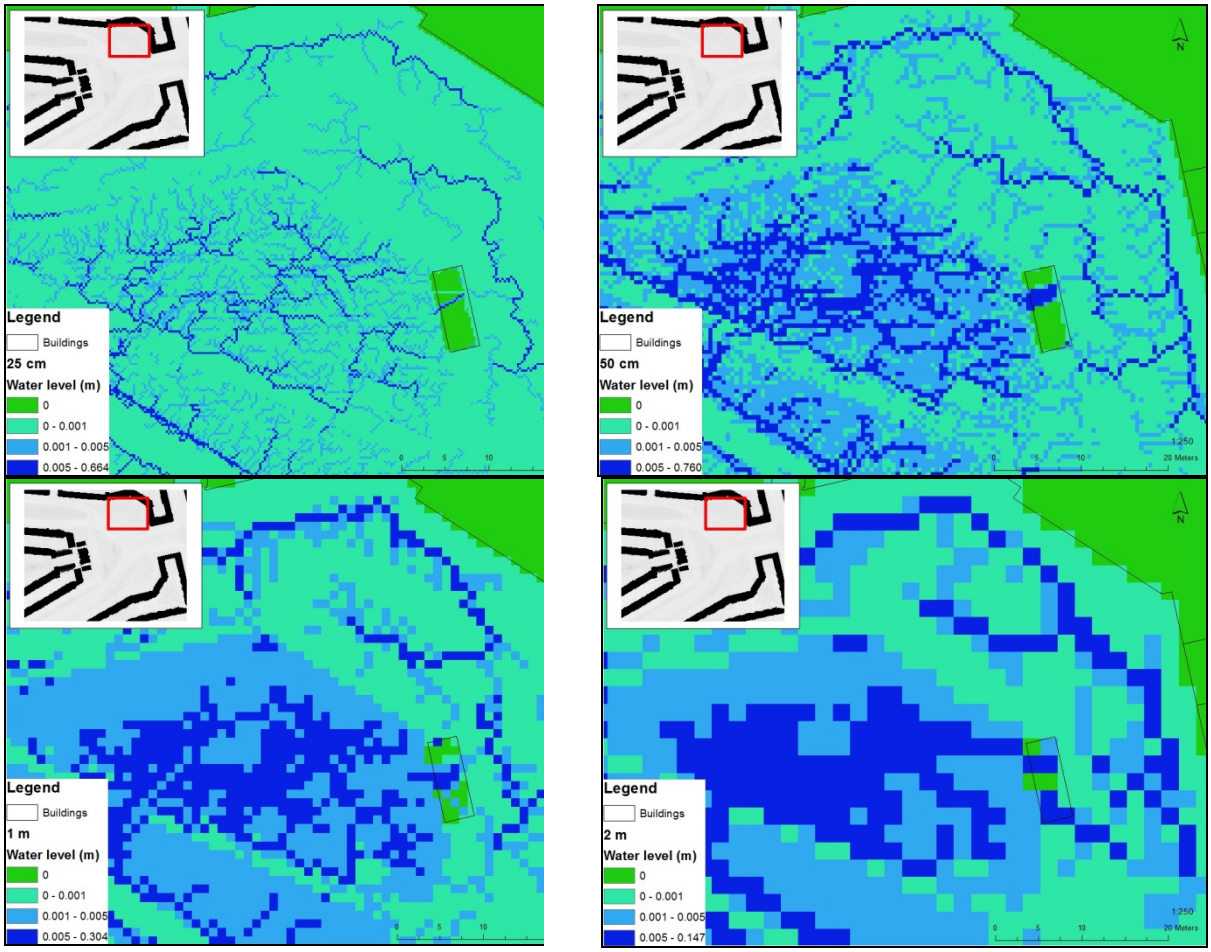

Figure C-1: A close-up to the study site Rivierenbuurt, here the four AHN resolutions are compared.

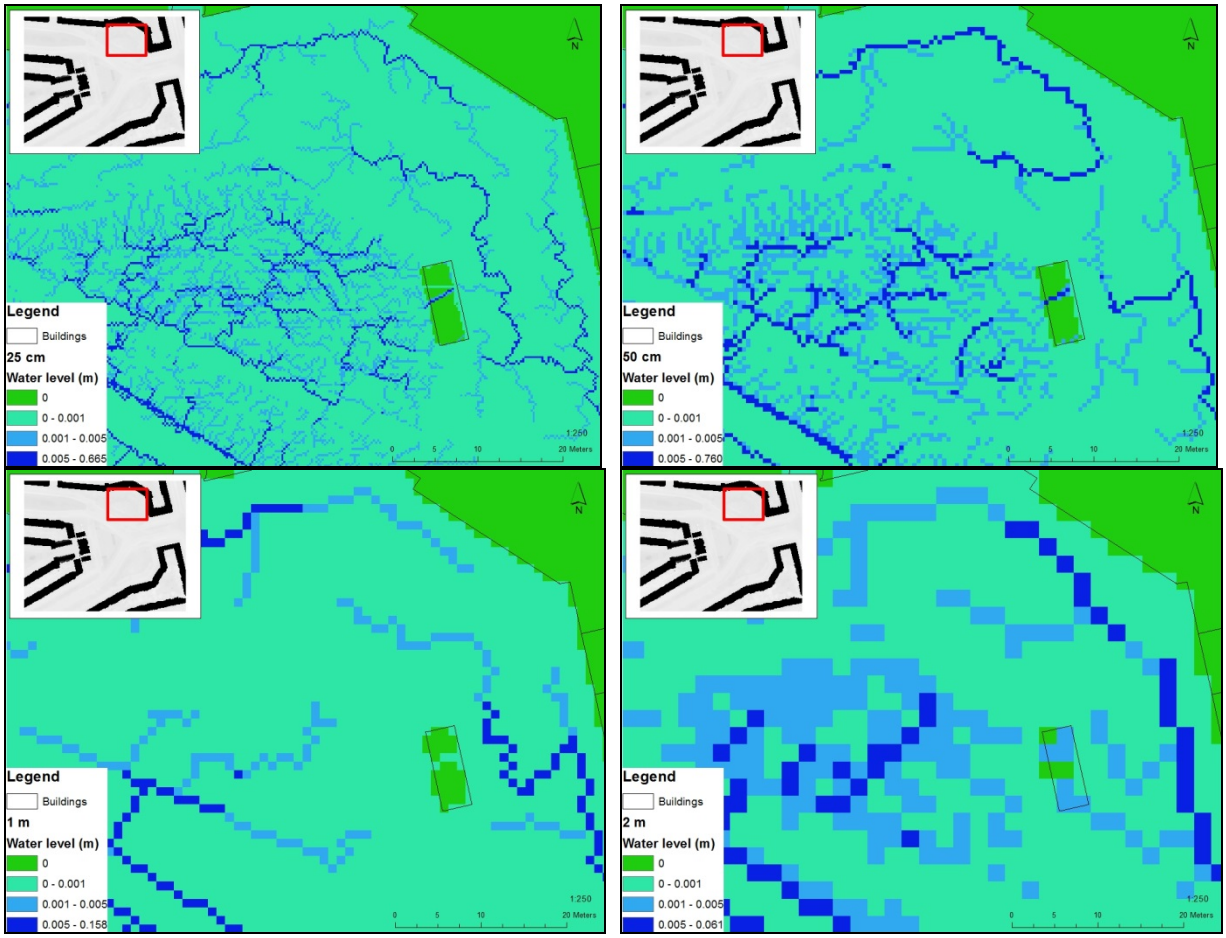

Figure C-2: Close up of the aggregated DEMS of the Rivierenbuurt study site.

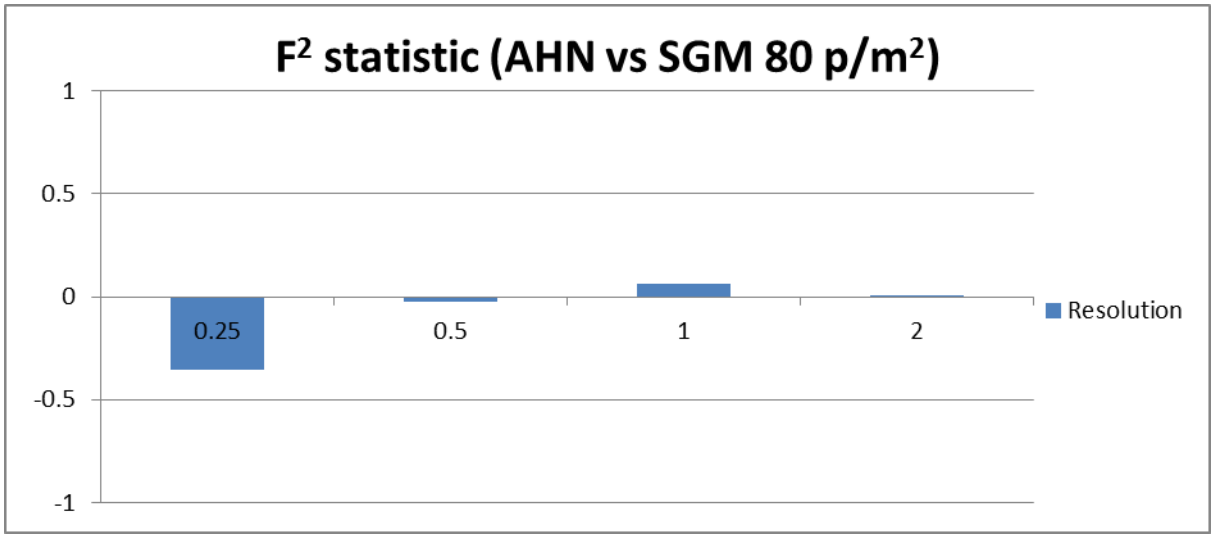

Figure C-3: F^2 statistic SGM 80 p/m^2 compared with the AHN in the Rivierenbuurt. 1 is perfect similarity between the DEM sources and -1 is no similarity.

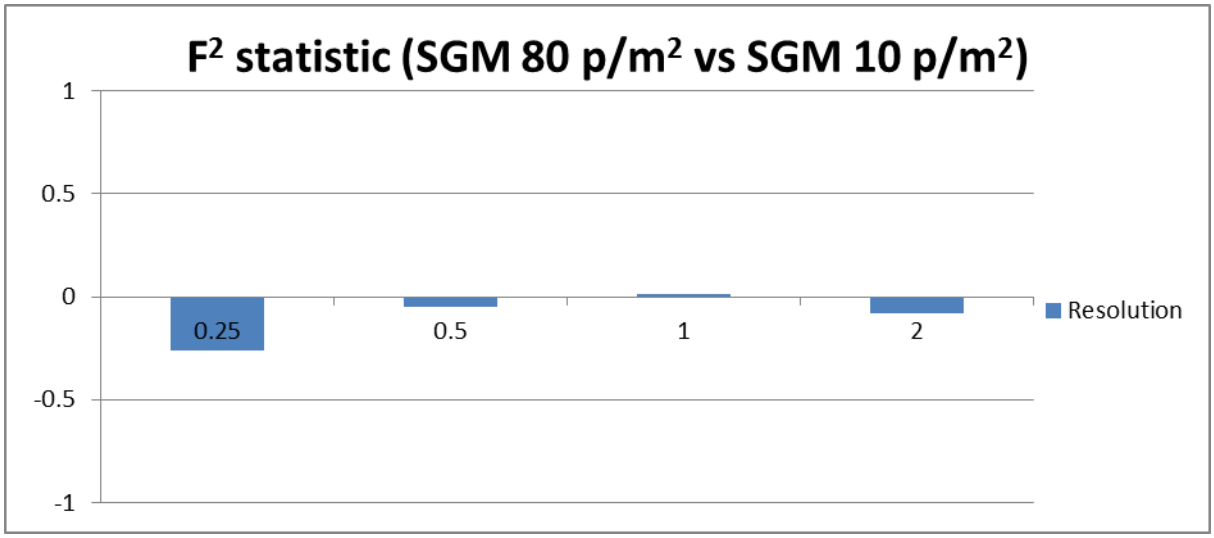

Figure C-455: F^2 statistic SGM 10 p/m^2 compared with the SGM 80 p/m^2 in the Rivierenbuurt. 1 is perfect similarity between the DEM sources and -1 is no similarity.

Zuidas

Table C-7: F^2-statistic comparison of SGM 80 p/m²

Reference	Comparing	F^2 statistic
0.25 (80 p/m²)	0.50 (80 p/m²)	-0.16199
0.25 (80 p/m²)	1.0 (80 p/m²)	-0.12569
0.25 (80 p/m²)	2.0 (80 p/m²)	-0.09785
0.5 (80 p/m²)	1.0 (80 p/m²)	0.016338
0.5 (80 p/m²)	2.0 (80 p/m²)	0.091903
1.0 (80 p/m²)	2.0 (80 p/m²)	0.143297

Table C-8: F^2-statistic comparison of SGM 10 p/m²

Reference	Comparing	F^2 statistic
0.25 (10 p/m²)	0.50 (10 p/m²)	-0.05721
0.25 (10 p/m²)	1.0 (10 p/m²)	-0.07228
0.25 (10 p/m²)	2.0 (10 p/m²)	0.028587
0.5 (10 p/m²)	1.0 (10 p/m²)	0.014383
0.5 (10 p/m²)	2.0 (10 p/m²)	0.067019
1.0 (10 p/m²)	2.0 (10 p/m²)	0.095983

Table C-9: F^2-statistic comparison of AHN

Reference	Comparing	F^2 statistic
0.25 AHN	0.50 AHN	-0.36861
0.25 AHN	1.0 AHN	-0.17878
0.25 AHN	2.0 AHN	-0.00249
0.5 AHN	1.0 AHN	-0.22602
0.5 AHN	2.0 AHN	-0.00363
1.0 AHN	2.0 AHN	0.045423

Table C-10: F^2-statistic comparison of SGM 80 p/m² with SGM 10 p/m²

Reference	Comparing	F^2 statistic
0.25 (80 p/m²)	0.25 (10 p/m²)	-0.22722
0.50 (80 p/m²)	0.50 (10 p/m²)	-0.08215
1.0 (80 p/m²)	1.0 (10 p/m²)	-0.03589
2.0 (80 p/m²)	2.0 (10 p/m²)	0.20881

Table C-11: F^2-statistic comparison of AHN with SGM 80 p/m²

Reference	Comparing	F^2 statistic
0.25 AHN	0.25 (80 p/m²)	-0.51092
0.50 AHN	0.50 (80 p/m²)	-0.44684
1.0 AHN	1.0 (80 p/m²)	-0.26476
2.0 AHN	2.0 (80 p/m²)	0.15592

Table C-12: F^2-statistic comparison of AHN with SGM 10 p/m^2

Reference	Comparing	F^2 statistic
0.25 AHN	0.25 (10 p/m^2)	-0.46163
0.50 AHN	0.50 (10 p/m^2)	-0.08215
1.0 AHN	1.0 (10 p/m^2)	-0.23812
2.0 AHN	2.0 (10 p/m^2)	-0.09679

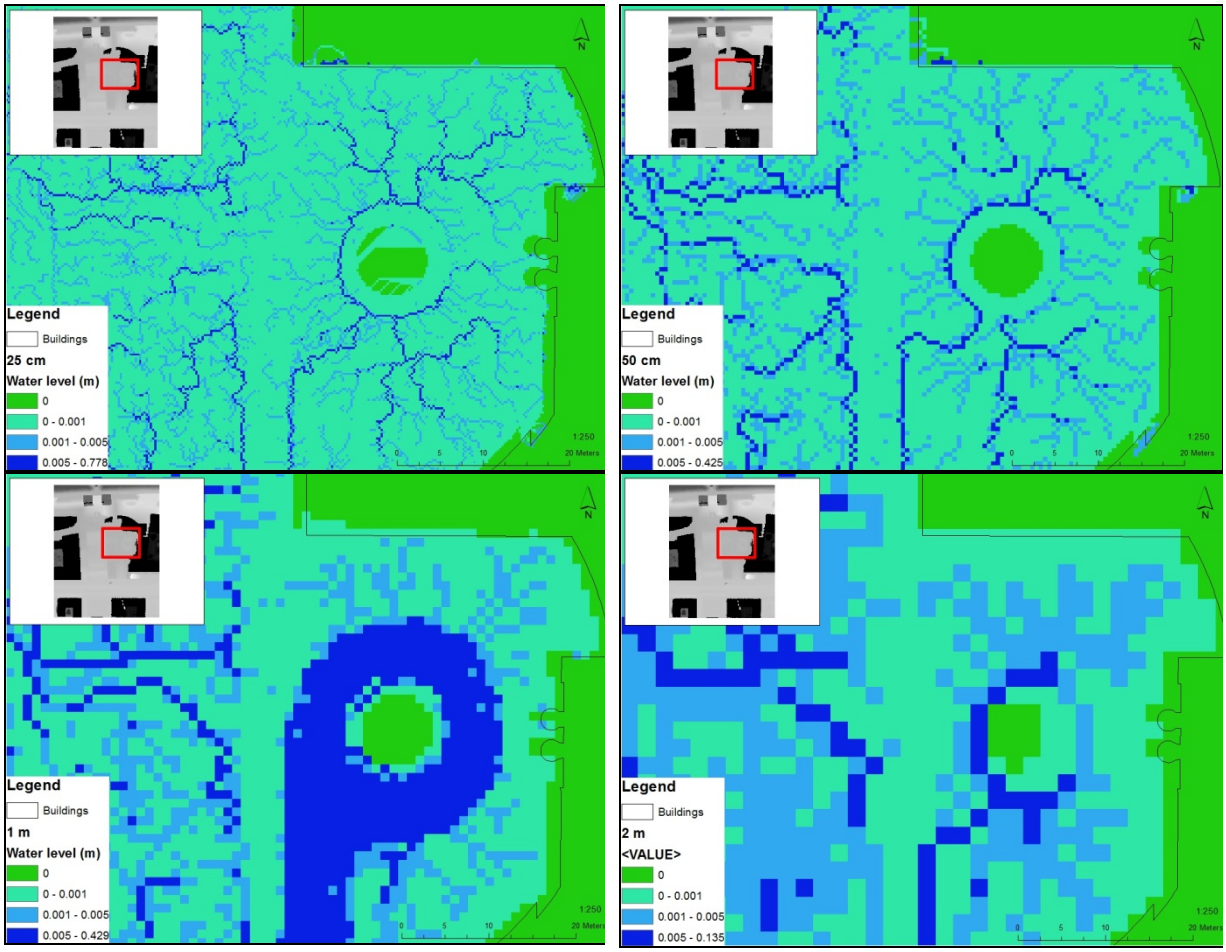

Figure C-5: A close-up to the study site Zuidas, here the four AHN resolutions are compared.

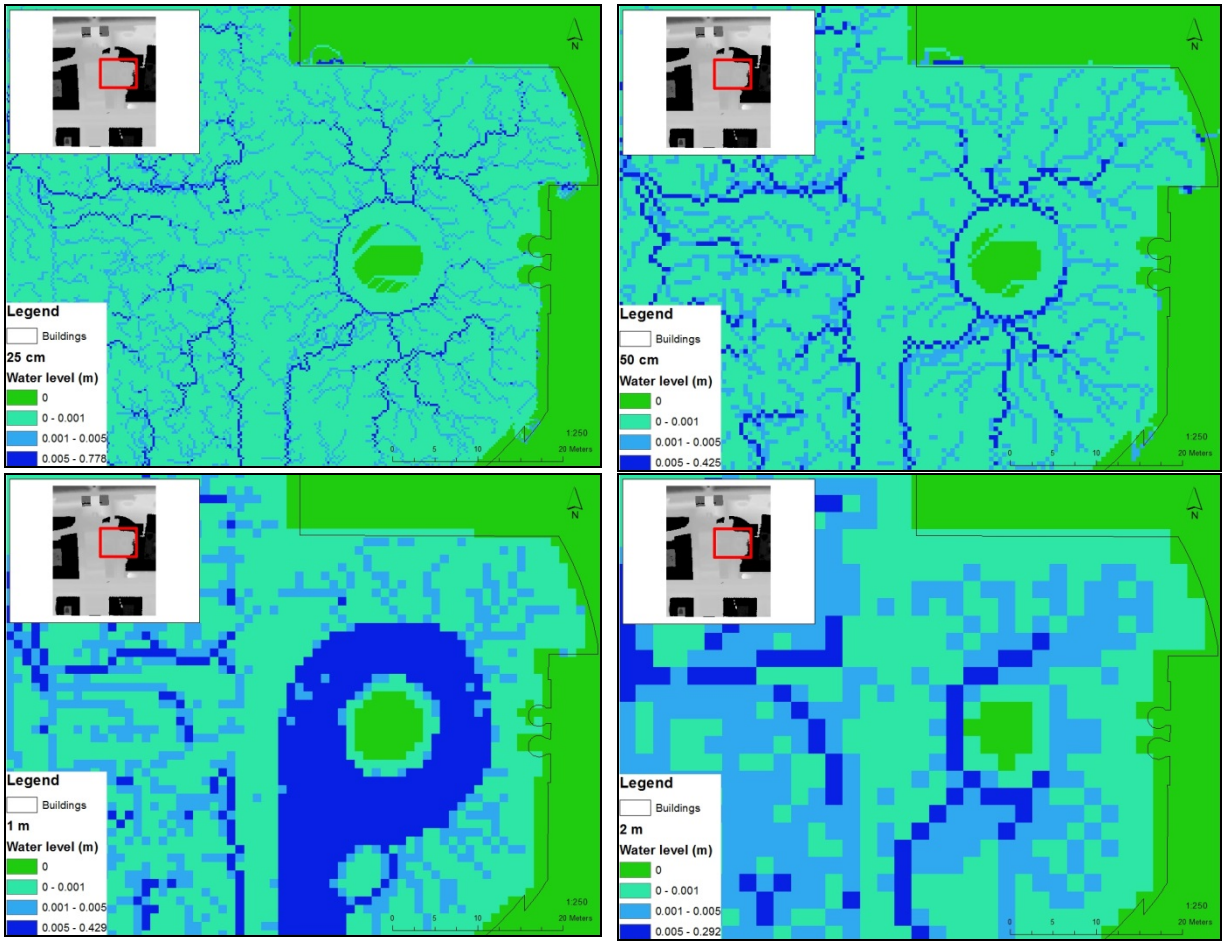

Figure C-6: Close up of the aggregated DEMS of the Zuidas study site.

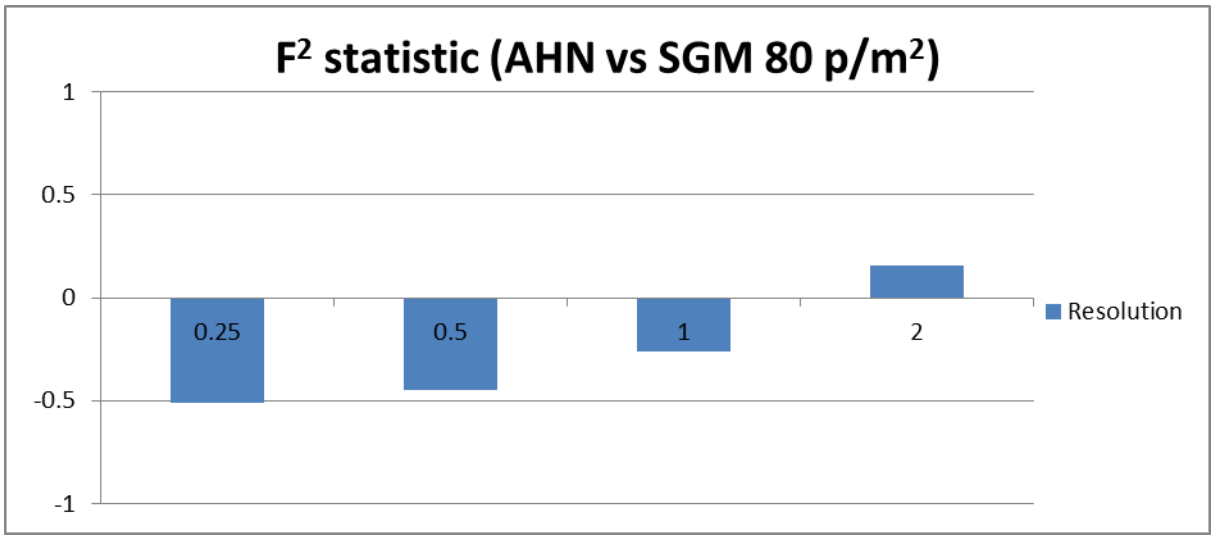

Figure C-7: F^2 statistic SGM 80 p/m^2 compared with the AHN in the Zuidas. 1 is perfect similarity between the DEM sources and -1 is no similarity.

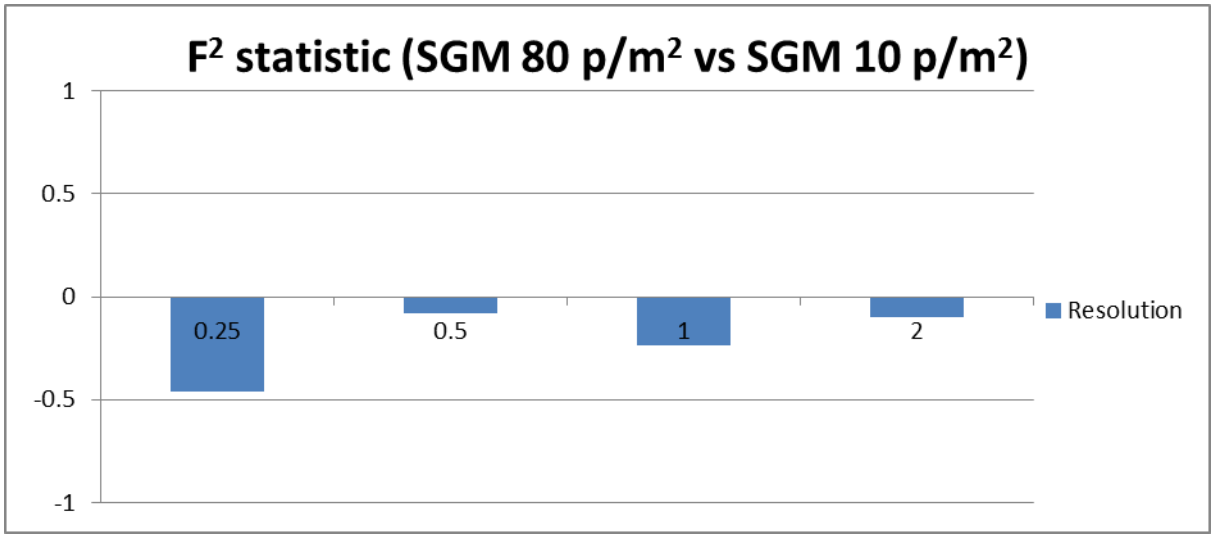

Figure C-8: F^2 statistic SGM 10 p/m^2 compared with the SGM 80 p/m^2 in the Rivierenbuurt. 1 is perfect similarity between the DEM sources and -1 is no similarity.

APPENDIX D – LITERATURE OVERVIEW

Table D-1: Overview of urban hydrological modeling research and usability.

Author	Topic	Model	Main interests/outcomes/usability
Blanc et al. (2012)	River-rainfall flooding	Infoworks	Rainfall estimates are important in understanding flood risk. Computational expense is a limiting factor when using a high-resolution DEM.
Chen et al. (2012)	River flooding	Urban Inundation Model	Used a different manner of coarse grid resampling by adding building coverage ratio (BCR). This reduced the computation time, but kept the model efficiency. DEM used in the research is mesh grid.
Dottori et al. (2013)	Urban hydrological model comparison	-	Sewage and drainage system is never optimal in real world situations, this should be reflected in model. Computation time is a limiting factor when using a high-resolution DEM. Urban situation should be reflected in model resolution choice. More complexity, means necessity for a higher resolution DEM.
Fewtrell et al. (2008)	River flooding	LISFLOOD-FP	Used high-resolution DEM comparison. Optimal model grid cell should be the minimum distance between objects. Resampling technique for DEMs is less important than grid size choice.
Fewtrell et al. (2011)	River flooding	LISFLOOD-FP	Used high-resolution DEM comparison. Maximum adequate resolution is 2 m. Was unable to use grid size smaller than 50 cm because of computing time.
Gallegos et al. (2009)	Dam break flooding	BreZo – finite volume model	Used high-resolution DEM. Optimal model grid should have at least three cells for street width, otherwise flow cannot be adequately modeled.
Krebs et al. (2014)	Rainfall runoff - Impact of land surface change on water balance	SWMM	Used small-scale case sites to study parameter values for high-resolution DEMs. Regionalization effects are (almost) not present, thus parameters values are usable in large-scale sites. Volume runoff is not affected by grid size, while peak flow is.
Maksimovic et al. (2009)	Rainfall flooding	SIPSON 1D/1D	Effect of flooding on drainage systems using a 1D surface flow network. 1D is not usable for ponding effects.
Mason et al. (2007)	River flooding	Horritt simple finite volume (SFV) model	Different use of DEM with implementation of small vegetation (<1 m) as friction. Combination of Lidar data and land use map for Manning's n assessment.
Mitasova & Mitas (2001)	Soil erosion simulations	Grass (Qgis)	Non-urban model, but implements GIS functionality. Also usable in urban situations.
Ozdemir et al. (2013)	River Flooding	LISFLOOD-FP	Evaluated scale and roughness effects in urban flooding. Using high resolution Lidar derived DEM

			ranging from 10 cm to 1 m. Concludes that micro scale terrain features are more important to the water level height than flow equations.
Rumman et al. (2005)	Infiltration modeling	HEC-GeoHMS	Confirmation that spatial parameters can be easier assessed from DEMs than from manual measurements (slope, aspect). Also obtaining watersheds from DEMs was possible. Uses a land use map for Manning's n assessment.
Sampson et al. (2013)	Rainfall flooding	LISFLOOD-FP	Used ponding effect in model. Restricted flow velocity to simulate the water behavior. Further simplification of the model, by assuming rooftops flow directly to drainage systems. Computation time is reduced by limiting the routes were water can flow to, thus reducing the number of cells which have to compute the flow equations.
Schubert et al. (2008)	River flooding	BreZo – finite volume model	Mesh grid model comparison with no-building and building. The no-building model output was comparable with building-model output. Construction of grids with building-hole or building-block method.
Skotnicki & Sowinski (2013)	Rainfall flooding	SWMM (v5)	Simulates rainfall-runoff in a urban setting. Influence of depression storage is very limited to overall model.
Yu & Lane (2006)	River flooding	Mesh grid diffusion-wave model	Comparison of mesh grid and raster grid model. Mesh grid model was sensitive to spatial resolutions. Roughness parameters can compensate for the effects of coarser resolution.